# STUDIES ON THE FUNCTION AND MECHANISM OF ACTION OF ATTRACTIN

by

Ruth Erin Thomas

A DISSERTATION

Presented to the Neuroscience Graduate Program
and the Oregon Health and Science University
School of Medicine
in partial fulfillment of
the requirements for the degree of Doctor of Philosophy
August 2005

School of Medicine

Oregon Health and Sciences University

---

# CERTIFICATE OF APPROVAL

---

This certifies that the Ph.D. dissertation of

Ruth Erin Thomas

has been approved

[redacted]

Mentor/Advisor

[redacted]

Member

[redacted]

Member

[redacted]

Member

[redacted]

Member

# TABLE OF CONTENTS

TABLE OF CONTENTS ....................................................................i

LIST OF FIGURES ....................................................................iv

LIST OF ABBREVIATIONS ....................................................................vi

ACKNOWLEDGEMENTS ....................................................................x

ABSTRACT ....................................................................xi

**CHAPTER 1. INTRODUCTION** ....................................................................1

1. THE ATTRACTIN FAMILY ....................................................................2

2. THE RELATIONSHIP BETWEEN THE ATTRACTIN FAMILY AND THE MELANOCORTIN SYSTEM ....................................................................5

3. ATTRACTIN AND NEURODEGENERATION ....................................................................8

4. MOLECULAR ROLES FOR ATTRACTIN ....................................................................10

5. *MAHOGANOID* MUTATIONS PRODUCE PHENOTYPES REMARKABLY SIMILAR TO MUTATIONS IN ATTRACTIN ....................................................................14

6. THE ROLE OF UBIQUITIN CONJUGATING ENZYME 13 ....................................................................17

7. SPECIFIC AIMS AND OUTLINE OF THESIS ....................................................................21

CHAPTER 2. IDENTIFICATION OF PROTEINS THAT CAN INTERACT WITH THE INTRACELLULAR TAIL OF ATTRACTIN ........................................23

ABSTRACT ........................................24

INTRODUCTION ........................................25

MATERIALS AND METHODS ........................................26

RESULTS ........................................27

DISCUSSION ........................................28

CHAPTER 3. CHARACTERIZATION OF DISTRACTED, THE *DROSOPHILA* HOMOLOGUE OF ATTRACTIN ........................................35

ABSTRACT ........................................36

INTRODUCTION ........................................37

MATERIALS AND METHODS ........................................39

RESULTS ........................................43

DISCUSSION ........................................48

CHAPTER FOUR. THE *DROSOPHILA* HOMOLOGUE OF ATTRACTIN INTERACTS WITH UBC13/BENDLESS TO INFLUENCE PHOTORECEPTOR PATHFINDING AND NEURONAL DEGENERATION ........................................58

ABSTRACT ........................................59

INTRODUCTION ....................................................................60

MATERIALS AND METHODS ........................................................63

RESULTS ............................................................................66

DISCUSSION ........................................................................73

**SUMMARY AND CONCLUSIONS** ...............................................87

**REFERENCES** ...................................................................95

**Appendix** ........................................................................103

A1. *Attractin* tissue and developmental RT-PCR ...............................103

A2. Creation of *dsd* Deletion alleles ...............................................104

A3. Melanocortin 5 receptor papers ................................................105

A3.1 Melanocortin 5 receptor deficiency promotes defensive behavior in male mice ...............................................................................105

A3.2 Melanocortin 5 receptor deficiency reduces a pheromonal signal for aggression in male mice .......................................................................111

## LIST OF FIGURES

### CHAPTER ONE

**FIGURE 1.** AMINO ACID COMPARISON OF THE INTRACELLULAR TAILS OF MOUSE ATTRACTIN (ATRN), *DROSOPHILA MELANOGASTER* DISTRACTED (DSD), AND *C. ELEGANS* F33C8.1/ATTRACTIN (F33C8.1) ..............................4

### CHAPTER TWO

**TABLE 1.** THE TITER FOR THE MATING OF THE ATRN BAIT IN PJ69-2A YEAST TO THE PRETRANSFORMED ADULT MOUSE BRAIN LIBRARY IN Y187 YEAST ..........................................................................................33

**TABLE 2.** THE LIST OF ATRN INTRACELLULAR INTERACTING CANDIDATES, SPLIT INTO CATEGORIES BASED ON FUNCTION ........................................34

### CHAPTER THREE

**FIGURE 1.** COMPARISON OF ATTRACTIN, ATTRACTIN-LIKE PROTEIN, AND DISTRACTED PROTEINS ...............................................................52

**FIGURE 2.** THE 5' UNTRANSLATED REGION OF *DISTRACTED* (*DSD*) AND DEVELOPMENTAL EXPRESSION OF *DSD* ............................................53

**FIGURE 3.** IN SITU HYBRIDIZATION OF EMBRYOS WITH *DISTRACTED* ANTISENSE AND SENSE PROBES ..................................................54

**FIGURE 4.** DISTRACTED EXPRESSION IN THE THIRD INSTAR CNS ............55

**FIGURE 5.** TRANSPOSABLE ELEMENT INSERTIONS CREATE HYPOMORPHIC

*DISTRACTED* ALLELES AND USE OF THE DROSDEL INSERTIONS CREATED THE DEFICIENCY *DF(3R)ED6274* ....................................................56

**FIGURE 6.** PHOTORECEPTOR AXONAL PROJECTIONS IN *DISTRACTED*$^{P}$ MUTANTS ....................................................57

## CHAPTER FOUR

**FIGURE 1.** CONFIRMATION OF THE BIOCHEMICAL INTERACTION BETWEEN DISTRACTED (DSD) AND BENDLESS (BEN) ........................................81

**FIGURE 2.** ASSESSMENT OF PHOTORECEPTOR AXONAL PROJECTIONS IN *BEN*$^{1}$, *DSD*$^{P}$, AND *BEN*$^{1}$;*DSD*$^{P}$ MUTANTS ........................................82

**FIGURE 3.** FAILURE OF R2-R5 PHOTORECEPTOR AXONS TO RESPOND TO THE LAMINA GLIA AND TERMINATE APPROPRIATELY IN MUTANTS ..........83

**FIGURE 4.** THE BORDER OF THE INNER PROLIFERATION CENTER (IPC) WAS NOT COMPROMISED IN THE MUTANTS ........................................84

**FIGURE 5.** ADULT BRAIN ARCHITECTURAL DEFECTS AND AGE-DEPENDENT NEURAL DEGENERATION IN ADULT FLIES ........................................85

**FIGURE 6.** QUANTIFICATION OF THE ANTENNAL LOBE VACUOLES ..........86

## APPENDIX

**FIGURE A1.** THE EXPRESSION OF MOUSE *ATTRACTIN* (*ATRN*) IN MULTIPLE TISSUES AND AT DIFFERENT EMBRYONIC STAGES WAS DETERMINED BY RT-PCR ....................................................103

## LIST OF ABBREVIATIONS

| | |
|---|---|
| AD | activation domain |
| AGRP | Agouti related protein |
| ALP | Attractin-like protein |
| Atrn | Attractin |
| *A*$^{y}$ | *Lethal yellow* mouse |
| Ben | Bendless |
| *ben*$^{1}$ | Hypomorphic *bendless* mutation |
| β-gal | β-Galactosidase |
| CNS | Central nervous system |
| CS | Canton S |
| Ctbp1 | C-terminal binding protein 1 |
| C-terminus | Carboxy-terminal domain |
| CUB | Complement subcomponents Clr/Cls, Uegf, Bmp1 domain |
| Df | Deficiency |
| DNA-BD | DNA binding domain |
| Dsd | Distracted |
| *dsd*$^{P}$ | Hypomorphic *distracted* alleles caused by insertion of P-elements |
| dUEVIA | *Drosophila* UEV1A |
| E1 | Ubiquitin activating enzyme |
| E2 | Ubiquitin conjugating enzyme |
| E3 | Ubiquitin ligase |
| E14 DRG | Embryonic day 14 dorsal root ganglion |

| | |
|---|---|
| EGF | Epidermal growth factor |
| eIF-3s10 | Eukaryotic translation initiation factor subunit 10 |
| ERK | MAP kinase |
| Fas III | Fasciclin III |
| GAP-43 | Growth associated protein-43 |
| GCK | Germinal center kinase |
| GEF-2 | Rho/rac guanine nucleotide exchange factor 2 |
| GST | Glutathione S transferase |
| IKK | IκB kinase |
| IL-1β | Interleukin-1beta |
| Imd | Immune deficiency pathway in *Drosophila* |
| IPC | Inner proliferation center |
| Jab1/CSN5 | C-Jun activation domain binding protein 1/COP9 subunit 5 |
| JIP3 | JNK interacting protein 3 |
| JNK | C-jun kinase |
| K48 | Lysine 48 of ubiquitin |
| K63 | Lysine 63 of ubiquitin |
| lacZ | β-galactosidase |
| LC | Light chain of MAP1A or MAP1B |
| MAP1A | Microtubule associated protein 1A |
| MAP1B | Microtubule associated protein 1B |
| MBP | Maltose binding protein |
| $mg^{3J}$ | Attractin null allele at *mahogany* locus in mice |

| | |
|---|---|
| *mg* | Hypomorphic allele at *mahogany* locus in mice |
| $mg^L$ | Weakest hypomorphic allele at *mahogany* locus in mice |
| $md^{nc}$ | Null allele at *mahoganoid* locus in mice |
| *md* | *Mahoganoid* locus |
| MC1R | Melanocortin 1 receptor |
| MC4R | Melanocortin 4 receptor |
| NF-kappaB | Nuclear factor-kappaB |
| N-terminus | Amino-terminal domain |
| PAI-1 | Plasminogen activator inhibitor type 1 |
| PBS | Phosphate buffered Saline |
| PCM1 | Pericentriolar material 1 |
| PCNA | Proliferating cell nuclear antigen |
| PCR | Polymerase Chain Reaction |
| Pin1 | Proline isomerase1 |
| polyUb | Polyubiquitin |
| R1-R8 | Labels for the eight photoreceptors in a ommatidia of *Drosophila* |
| RING | Really interesting new gene domain |
| RIP | Receptor interacting protein |
| RP49 | Ribosomal protein 49 |
| RT-PCR | Reverse transcription polymerase chain reaction |
| SOD | Superoxide dismutase |
| TAB2 | TAK1-binding protein 2 |
| TAK1 | Transforming growth factor beta activated kinase1 |

| | |
|---|---|
| TCR | T-cell receptor |
| TLR | Toll like receptor |
| TNF-α | Tumor necrosis factor alpha |
| TRAF2 | Tumor necrosis factor receptor associated factor |
| TRAF6 | Tumor necrosis factor receptor associated factor |
| Ub | Ubiquitin |
| UBC13 | Ubiquitin conjugating enzyme 13 |
| UEV1A | Ubiquitin enzyme variant 1A |
| UTR | Untranslated region |

# ACKNOWLEDGEMENTS

I would like to thank Roger D. Cone for his trust and encouragement to pursue the characterization of Attractin in *Drosophila* when this model system was not used by the rest of the laboratory.

I thank Michael Forte for his guidance, support and collaboration while I pursued my thesis research. I am indebted to members of his laboratory for their expertise, time, skills, and participation, particularly William Wolfgang, Catherine Clay, and Jacqueline Parker.

I thank Sarah Smolik for sharing her expertise in genetics and Doris Kretzschmar for sharing her expertise in *Drosophila* neurodegeneration. I would also like to thank Doris for the use of her laboratory space and equipment to characterize the adult fly brains.

My appreciation goes to Malcolm Low for serving on my thesis committee and to Philip Copenhaver for his advice on immunohistochemistry in insects. I also thank Aurelie Snyder for her help capturing the confocal images.

I thank all members, past and present, of the Cone laboratory for their interest and stimulating discussions. I would like to especially thanks Daniela Dinulescu for the many great discussions we had and for our preliminary work on axonal guidance in *Attractin* mutant mice that lead to my pursuit of the UBC13 interaction in flies. I would also like to thank Patricia Rene for many interesting discussions and shared struggle.

Finally, I would like to thank all my family for their support, especially my mother, Dorothy G. Thomas, and my second sister, Sara L. Thomas, for their time helping me type in and edit this dissertation.

# ABSTRACT

Disrupted expression of Attractin (Atrn), a single pass transmembrane protein, leads to darker pigmentation, leanness, neurodegeneration, and hypomyelination in rodents. Atrn has also been implicated in immune function as release of the extracellular region of Atrn by activated human T-cells causes changes in macrophage morphology and the clustering of T-cells around the macrophage. Atrn's extracellular structure, including a CUB domain and four epidermal growth factor (EGF) related domains, is suggestive of roles in cell-cell interaction, guidance and signaling. Indeed, studies of the pigmentary phenotype of Atrn deficient mice show Atrn is necessary for the actions of agouti, an endogenous antagonist for the melanocortin 1 receptor. However, the molecular mechanism by which Atrn acts is unclear, both in pigmentation and in the other systems impacted by loss of Atrn. The studies presented herein identify potential Atrn intracellular interactors, characterize the *Drosophila* homologue of Atrn, Distracted (Dsd), and confirm one interactor, ubiquitin conjugating enzyme 13 (UBC13)/Bendless (Ben), as important to the molecular mechanism of Atrn/Dsd, particularly to photoreceptor pathfinding and neurodegeneration in *Drosophila*. These studies therefore identify UBC13/Ben as having a role in neurodegeneration in addition to the already established roles for UBC13 in DNA repair and immune response and establish another role for the Attractin family in axonal pathfinding, particularly in the developing *Drosophila* visual system. The interaction between UBC13/Ben and Atrn/Dsd is the first direct insight into a molecular mechanism of Atrn action and provides the means by which to begin to explain the pleiotropic actions of Atrn deficiency.

# CHAPTER ONE

# INTRODUCTION

## 1. THE ATTRACTIN FAMILY

The structure of the Attractin family is suggestive of roles in cell guidance, interaction, and signaling. Indeed, the first member of the Attractin family cloned was from human T-cells where Attractin modulates the immune cell interaction of T-cells and macrophages (25, 27). Mutations in Attractin have been identified in rats, mice, and hamsters and lead to darker pigmentation, leanness, hypomyelination, and neurodegeneration (49, 54). The Attractin family is conserved from *C. elegans* to human with one homologue in *C. elegans* and *Drosophila* and two homologues in mammals. The two members of the mammalian Attractin family are Attractin (Atrn) and Attractin-like protein (ALP), both single pass transmembrane proteins. Both Atrn and ALP have extracellular regions containing a Complement subcomponents Clr/Cls, Uegf, Bmp1 (CUB) domain flanked by epidermal growth factor (EGF) domains which are followed by plexin repeats, a C-lectin domain, and two laminin-like EGF domains (25, 40). The CUB domain is found on other developmentally dynamic proteins, such as neuropilin and bone morphogenic protein (BMP) (5). The CUB domain in neuropilin has been shown to be essential to neuropilin activity in axonal guidance (35). The CUB domain is also important to the function of BMP, which is involved not only in bone formation but brain development as well (65). The EGF and laminin-like EGF domains have been implicated in protein-protein interaction and cell adhesion (72) and the C-lectin domain binds carbohydrates (104). Finally, the plexin repeats are found in plexins, another group of proteins involved in axonal pathfinding (73). The conserved cystines in Atrn from human to *C. elegans* suggest conserved three dimensional structure as well (25).

Whereas the extracellular portion of Atrn and ALP has conserved domains, which predict roles for the Atrn family in guidance and cell-cell interaction, only ALP has a known signaling motif in its intracellular domain. At the C-terminus of ALP is a PDZ binding motif (33). Atrn on the other hand has no known motifs in its intracellular domain (71). However, there are several evolutionarily conserved clusters of amino acids in the intracellular tail, which suggest the importance of these residues to downstream protein interaction and signaling (Fig. 1). However the function of these motifs has yet to be established.

Both Atrn and ALP are expressed widely throughout the body (37, 40, 71). The highest levels of expression are in the brain, heart, kidney, lung and liver. Lowest levels are seen in the skeletal muscle and spleen. Within the brain, the highest levels of both Atrn and ALP are seen in the hippocampus, piriform cortex, cerebellum and midbrain (40, 60). While Atrn and ALP are expressed in many of the same places in the rodent brain, there are differences. As the in situs for ALP were done in mice and for Atrn in rat, the differences may be species related. However, overlap and differences in expression would be expected as seen with other protein families.

**Figure 1.** Amino acid comparison of the intracellular tails of mouse Attractin (Atrn), *Drosophila melanogaster* Distracted (Dsd), and *C. elegans* F33C8.1/Attractin (F33C8.1). The black bars represent the complete conservation of residues between all three Attractin family proteins as identified by BLAST comparison. The individual overall conservation between Atrn and Dsd was 45% and between Atrn and F33C8.1/Atrn was 36%.

```
    Atrn KIKQSCWASRRREQLLREMQQMASRPFASVNVALE---------TDEEPPDLIGGSIKTV
     Dsd KIKQKYDMFRRRQRLFVEMEQMASRPFSQVLVDIENRESIDLSLTLEGIGHLSKKRKKEC
F33C8.1 MIKVRIEAYRRNQRRIDEIEHMASRPFAST---------------KMELSMLSQFSSAGG

    Atrn PKPIALEPCFGNKAAVLSVFVRLPRGLGGIPPPGQS-GLAVASALVDI-SQQMPIVYKEK
     Dsd PSPIALEPCSGNRAAVLSLLVRLPTGGLSQAPSGQSAGLAVASALVTLGNPRRPSIDQHP
F33C8.1 PTPLSIEPCSNYRAGVFTLAVRLPTGGKAVTPSGTS-GLAVASSLCLLTPQQVGVLQAQD

    Atrn SGAVRN-RKQQPP--------AQPGTCI
     Dsd KEPKSK-RKQS----------QHPDSCT
F33C8.1 NGESNSGRKSNFRNLLRLTIRQRPNNND
```

## 2. THE RELATIONSHIP BETWEEN THE ATTRACTIN FAMILY AND THE MELANOCORTIN SYSTEM.

The melanocortin system, which has five known receptors, is involved in pigmentation, adrenal response, naturesis, energy homeostasis, and exocrine gland function (100). For the purposes of Atrn, only two are relevant, melanocortin 1 receptor (MC1R) and melanocortin 4 receptor (MC4R). The MC1R is expressed in melanocytes and regulates pigmentation and MC4R is expressed in the brain and regulates energy homeostasis. In the lethal yellow ($A^y$) and viable yellow ($A^{vy}$) mice, a promoter rearrangement causes agouti, the endogenous antagonist for MC1R, to be expressed everywhere in the body (67). This results in a mouse that is yellow due to antagonism of MC1R and obese due to antagonism of MC4R in the brain (29). The normal endogenous antagonist for MC4R in the brain is agouti related protein (AGRP) (79).

In mice, recessive mutations in Atrn are called *mahogany* (*mg*) due to the darker pigmentation phenotype of the mutants (67). The *mg* mutations had been isolated based on the darker pigmentation phenotype only before the mutated gene had been identified. Three alleles of mahogany have been identified, $mg^{3J}$, *mg*, and $mg^L$, in descending order of strength, the $mg^{3J}$ identified as a null allele (36). The other two alleles are caused by 5 kb insertions of the intracisternal A particle (IAP) element in introns of the *Atrn* gene. When the $A^y$ mutants are crossed to *mg* mutants, both the yellow pigmentation and obesity of the $A^y$ mutants are suppressed (23, 67). Whether mg mutations would block the $A^{vy}$ phenotype has not been reported. However, it seems clear from the blockade of the $A^y$

phenotype that agouti requires the presence of Atrn to function as an antagonist at both MC1R and MC4R.

Atrn has therefore been postulated to be a low affinity co-receptor for agouti. The biochemical evidence that agouti but not AGRP binds to Atrn (43), at a very low affinity, does not rule out the possibility that, rather than being a co-receptor, Atrn acts in some way to modulate the melanocortin receptors directly or acts in cell adhesion as proposed in Dinulescu and Cone 2000 (22). The interaction of Atrn with agouti but not AGRP does fit however with the observation that the *mg* mutations cannot suppress the obesity caused by AGRP overexpression (43).

The other member of the Attractin family, ALP, has recently been shown to interact with MC4R through yeast two-hybrid assay and GST-pulldown (40). The interaction takes place between the C-termini of ALP and MC4R. ALP and Atrn are 67% identical and the region in the C-terminus of ALP with which MC4R interacts contains one conserved and one highly divergent cluster of amino acids compared to Atrn. As a control, the C-terminus of Atrn is shown not to interact with the C-terminus of MC4R. The area in MC4R with which ALP interacts is involved in membrane trafficking of MC4R. This interaction provides more evidence of an important relationship between the Attractin family and the melanocortin system though the functional relevance of this interaction remains to be elucidated.

However, since agouti is normally only expressed in skin (22) and Atrn is expressed in both the skin and the brain, Atrn must have functions other than serving as a co-receptor for agouti, if indeed this is Atrn's role in the skin. Even in the skin, the pigmentation phenotype of *Atrn* mutants has a component independent of the agouti-mediated pigmentation switch (36). The *mg* mice also have changes in energy homeostasis independent of agouti (23). The *mg* mice are lean and hypermetabolic. The leanness and hypermetabolism are associated with the two alleles of *mahogany*, $mg^{3J}$ and *mg*, which also cause significant neurodegeneration (36). This observation led to the supposition that the energy homeostasis changes seen in *mahogany* mice are secondary to defects in neuronal survival. However, the energy homeostasis changes seen with the *mg* allele occur before significant neurodegeneration can be observed (36). This result could reflect defective wiring of the nervous system or predegenerative changes in cell-cell interaction. The neurodegeneration will be discussed in more detail in the following section. An independent function for Atrn is also supported by the fact that *C. elegans* and *Drosophila* have Atrn homologues but no direct agouti or melanocortin receptor homologues (42).

## 3. ATTRACTIN AND NEURODEGENERATION.

*Atrn* mutations have been identified in rats, mice and hamsters, *zitter* (*zi*), *mahogany* (*mg*) and *black tremor* respectively (37, 54, 55). In all cases *Atrn* mutations cause darker pigmentation and age-progressive neurodegeneration and hypomyelination (10, 36, 54, 55). A tremor also develops which results in flaccid paresis in *zitter* rats at 6 months of age (54). No Atrn mutations have been identified in humans as yet, so the impact of Atrn deficiency on human neurodegeneration is not known.

At birth, the gross anatomical structures of the central nervous system are normal in *Atrn* mutants. Vacuoles appear 3 to 4 weeks after birth in *zi* and $mg^{3J}$ animals, both null mutations of Atrn (36, 54). In the moderate *mg* mutation in mice, vacuoles only appear after 8 to 16 weeks (36). In *zitter* rats, the most thoroughly studied *Atrn* mutant, the vacuoles begin in the pons and outer thalamus then extend to the hippocampus, deep cortex, cervical spinal gray matter, and cerebellum, all sites of Atrn expression. Swollen astrocytic processes accompany the vacuoles. The overall spongy degeneration seen in *Atrn* mutants is similar to that seen in prion disease but without changes in protease sensitivity of the prion protein (34).

The progression of hypomyelination in the *Atrn* mutants follows a similar timeline to the progression of neurodegeneration (54). The initiation and formation of the myelin sheaths is normal as is expression of the biochemical components of myelin such as myelin basic protein. However, as the Atrn deficient animals age, the density of myelinated fibers and number of myelin lamellae decreases and is accompanied by aberrant or elongated myelin sheath formation (3, 54, 57). So while Atrn does not appear to be needed for the myelin formation, it does appear necessary for the maintenance of myelin over time.

The link between Atrn deficiency and neurodegeneration is clear but not well understood biologically or molecularly. The neurodegeneration and hypomyelination seen in *Atrn* mutants has been proposed to be due to abnormal or lost cell-cell interaction (3, 22), developmental defects, or decreased resistance to oxidative stress (70). The role of Atrn in responding to oxidative stress will be addressed in more detail in the following section as will the evidence for Atrn's role in mediating cell-cell interaction in the immune system.

## 4. MOLECULAR ROLES FOR ATTRACTIN.

Atrn was first identified and studied in the human immune system where a secreted form of Atrn, representing the extracellular domain, is released by activated T-cells (25). The expression of Atrn at the mRNA level does not change upon T-cell activation. However, the surface expression of Atrn is upregulated at 24 hrs and the secreted form is released by 48 hrs with Atrn levels starting to fall by 72 hrs (26). The secreted Atrn enhances the proliferative responses of peripheral blood mononuclear cells (PBMC) to recall antigens and modulates the interaction of macrophages and T-cells, inducing macrophages to spread out and T-cells to cluster around the macrophage. This induction of interaction and morphological changes only occurred when both T-cells and macrophages were together in culture (25).

T-cells activate in response to both innate and adaptive antigen presentation (75). Macrophages consume and present the antigen to the T-cell which then activates cytokine production and proliferation. Atrn's ability to facilitate the interaction between macrophages and T-cells could therefore theoretically be beneficial to the response of the immune system by strengthening the specific response to pathogens.

In some patients with common variable immune deficiency (CVID) the proliferative responses of their T-cells is low (85). T-cells from the CVID patients respond with normal signaling responses to the T-cell receptor (TCR) stimulation. However, CD3 crosslinking stimulation of T-cells from the CVID patients results in upregulation of CD26 and CD25 but no upregulation of Atrn. In addition, Atrn enhances the proliferation of PMBC cells to suboptimal doses of IL-2 (85). Together, these results indicate that one of the T-cell immune defects in CVID patients is the lack of Atrn upregulation upon T-cell activation.

The secreted form of Atrn in the immune system has only been described in humans. Although rats have been also shown to express the secreted form of Atrn (54), no studies to date have demonstrated the same role for Atrn in the rat immune system as seen in humans. The secreted form of Atrn arises from a splice variant resulting in a shorter transcript of 4.5 kb. This shorter transcript is only expressed in the periphery in humans, not in the nervous system (93, 94). The longer 9.0 kb transmembrane Atrn mRNA is expressed in the human brain and in the periphery.

However, since the secreted form of Atrn is only found in rats and humans, the transmembrane form must be important. Indeed, in transgenic rescue experiments in rats, only the transmembrane form of Atrn rescued the pigmentation, neurodegeneration, and hypomyelination phenotypes of Atrn deficient rats (54). Even overexpression of the secreted form of Atrn would not rescue the neurodegeneration or hypomyelination. This result suggests that the intracellular domain of Atrn has an as yet unknown critical role in signaling to downstream effectors.

One potential role for the Atrn protein as a whole is in oxidative stress, suggested from the study of the *zitter* rats (70). The Atrn deficient rats show increased expression of superoxide dismutase (SOD) and decreased catalase activity. Fibroblasts isolated from *zitter* rats show increased sensitivity to $H_2O_2$ treatment that is rescued back to wild type sensitivity by reintroduction of transmembrane Atrn to the Atrn deficient fibroblasts. Incubation with the antioxidant $\alpha$-tocopherol also protected Atrn deficient fibroblasts from death when exposed to $H_2O_2$. The ERK phosphorylation usually seen upon exposure to $H_2O_2$ is reduced in Atrn deficient cells and in the protein extracts from the brains of *zitter* rats (70). Cortical neurons from wild type and *zitter* rats had similar elaborations the first 5-7 days in culture. Then after 14 days in culture the Atrn deficient neurons began to show degenerative phenotypes with changes in cell shape and decreased viability. This degenerative phenotype is rescued by inclusion of the antioxidants α-tocopherol or catalase. This result suggests that Atrn deficiency cripples the endogenous antioxidant response to normal environmental oxidative stress. Involvement of Atrn in the cellular response to oxidative stress could underlie the neurodegeneration seen in Atrn mutants but no experiments to date have tested this theory in vivo.

Another role for Atrn may be in neurite outgrowth. The HCN-1A human cortical neuron cell line has been used to show the effect of exogenous Atrn on neurite outgrowth (93). This cortical cell line acquires a mature neuronal phenotype over 48 to 72 hours after differentiation media is applied. Incubation of the differentiating neurons with human serum causes inhibition of neurite outgrowth, inhibition that is not seen with serum cleared of Atrn. Additionally, incubation of the differentiating neurons with the recombinant extracellular domain of Atrn also causes inhibition of neurite outgrowth by 48 hours. So, while the primary cortical neurons from Atrn deficient *zitter* rats appeared to grow out normally in the study above (70), incubation of soluble Atrn, which is normally excluded from the brain, with the differentiating cortical cell line neurons inhibits their outgrowth (93). Direct comparison of these studies, given the different cells used, is not feasible but a possible explanation for the differences could be due to ALP compensating for Atrn loss in the *zitter* neurons or that by 5-7 days in culture the *zitter* neurons catch up to the wild type.

A study of spinal cord injury gives additional evidence that Atrn is involved in neurite outgrowth and thus potentially axonal pathfinding (21). One day after a spinal cord injury, Atrn, along with neuritin and microtubule associated protein 1A (MAP1A), is downregulated. After 14 days, Atrn, neuritin and MAPIA are back to previous levels and co-expressed with GAP-43, a regeneration and plasticity associated protein. Embryonic day 14 dorsal root ganglion (E14 DRG) neurons show upregulation of both Atrn and MAP1A after two weeks in culture. The neurite length of the E14 DRG neurons did not change when either Atrn or MAP1A light chain 2 (LC2) is overexpressed alone. When co-overexpressed however, the neurite length of the E14 DRG neurons increases by 30%. When neuritin is also co-overexpressed with Atrn and MAPIA, the neurite length of the E14 DRG neurons increased by 94%. Neuritin by itself increased neurite length by 42%. This study reports also that the LC2 of MAP1A and Atrn interacted physically (21). This results fits with our yeast two hybrid screening results, showing both light chains of MAP1A and MAP1B as potential partners for Atrn. MAPIB is the earliest expressed microtubule binding protein and has been shown to be involved in axon growth cone turning (7, 61). MAPIA is involved in stabilization and maintenance of microtubules (76). It is expressed in brain regions where neurite growth persists in the adult and robustly expressed during CNS myelination (21, 76, 80). The importance of these proteins in neurite outgrowth and axonal guidance would further support the same role for Atrn if these interactions are borne out.

## 5. *MAHOGANOID* MUTATIONS PRODUCE PHENOTYPES REMARKABLY SIMILAR TO MUTATIONS IN ATTRACTIN.

The *mahoganoid* (*md*) mutations cause darker pigmentation and block the yellow pigmentation and obesity of $A^y$ mice similar to the *mg* mutations in Atrn (67). Also, independent of the suppression of the $A^y$ phenotype, the *md* mice show increased food intake (23). Additionally, the $md^{nc}$ null allele produces neurodegeneration that shares many features with the neurodegeneration seen in Atrn deficient animals (spongy and accompanied by astrocytosis) (44). The neurodegeneration starts in the hippocampus and later extends to other regions. The neurodegeneration occurs only in the null $md^{nc}$ mice, not with the hypomorphic *md* alleles, and is delayed, compared to the $Atrn^{mg3J}$ null, not starting until 2 months of age. The delay in the onset of neurodegeneration in $md^{nc}$ mice may be due to redundancy as, similar perhaps to Atrn having ALP, there exists a closely related gene to the one mutant in *md* mice (44). While the neurodegenerative phenotypes of the *md* and *mg* mice are closely matched, it is the blockade of agouti signaling by both mutations that leads to the postulation that the protein mutated in *md* mice is involved in Atrn signaling.

The gene mutated in *mahoganoid* codes for an E3 ubiquitin ligase (44, 82), which has been named Mahogunin. Like *Atrn*, *mahogunin* mRNA is expressed both peripherally and centrally (82). It is expressed in the brain, heart, kidneys, and lungs. Within the brain the highest sites of *mahogunin* expression are in the hippocampus, cortex and cerebellum, again similar to *Atrn* (44). Mahogunin is also highly conserved. Homologues for Mahogunin exist in *C. elegans* and *Drosophila*, the homology at 37% and 43% respectively (82). Neither mutations in *Atrn* or *mahogunin* alter the expression levels of the other in mice and overexpression of Atrn does not rescue the *md* phenotype (44). No report has yet been given on whether Mahogunin overexpression would rescue the *mg* phenotype. These results suggest that Mahogunin is downstream of Atrn both in pigmentation and neurodegeneration. As yet though, the molecular nature of the link between Atrn and Mahogunin is not known.

The identity of Mahogunin as an E3 ubiquitin ligase comes from the presence of a RING (really interesting new gene) domain, which is common to many E3 ubiquitin ligases and necessary for their actions as ubiquitin ligases (50, 83). E3 ubiquitin ligases generally specify the substrates to be ubiquitinated by an E2 ubiquitin conjugating enzyme, which is charged with ubiquitin from the E1 activating enzyme. E3s can also serve as a substrate for the E2 ubiquitin conjugating enzyme. This ubiquitination of the E3 by the E2 is referred to as autoubiquitination. Of the E2s tested in vitro with Mahogunin, ubiquitin conjugating enzyme 5 (UBC5), an E2 involved in stress response, generates the so-called autoubiquitination of Mahogunin (44). Another E2, UBC3, which is involved in cell cycle control, did not produce the same laddering of ubiquitin-modified Mahogunin seen with UCB5. Mahogunin lacking the RING domain is not modified by either UBC.

Ubiquitin modification has generally been associated with the degradation of proteins (83, 84). This degradation is important for signaling cascade activation, termination and for clearing of malformed or damaged proteins. The prevention of ubiquitin-mediated degradation has been associated with several neurodegenerative diseases such as Alzheimer's and Parkinson's (81). One cause of familial forms of Parkinson's is the loss of another E3 ligase, parkin (58). So, as Atrn protein levels are not affected by *md* mutations (44), it would seem unlikely that Atrn is the target for ubiquitin modification facilitated by Mahogunin. Rather, somehow through Atrn, Mahogunin directs ubiquitination of a yet-to-be identified downstream target, leading to either degradation of the target or the activation of downstream signaling cascades, depending on the type of ubiquitin linkage facilitated by Mahogunin.

## 6. THE ROLE OF UBIQUITIN CONJUGATING ENZYME 13

Ubiquitin conjugating enzyme 13 (UBC13) is found from yeast to humans (83). In yeast, UBC13, with its catalytically inactive partner Mms2, is necessary for error-free DNA repair (64). In mammals, UBC13, with the non-catalytic ubiquitin enzyme variant 1A (UEV1A ), participates in multiple signaling cascades within the immune response (89, 92, 103). These include the response of TNF-α receptor, IL-1β receptor, Toll-like receptors (TLR) and T-cell receptor (TCR).

Ubiquitin has seven lysines that can serve as the linkage point between ubiquitins (84). The unique aspect of UBC13 and its partner UEV1A is that rather than conjugate ubiquitin through the usual lysine 48 (K48), UBC13/UEV1A conjugates ubiquitin through lysine 63 (K63) (46). No other proteins besides UBC13 and Mms2 or UEV1A are needed to specify the K63 linkage versus K48 (63, 64). This specific linkage is conferred by the ubiquitin binding pocket of Mms2 and how it positions Ub relative to UBC13 (63, 64, 101), as seen in the crystal structure of the human heterodimers (68). However, an E3 ubiquitin ligase would be necessary to specify the target for Ub modification. K63 linkage has been demonstrated to activate kinase cascades and K48 linkage to target modified substrate for degradation by the proteosome (84). The K63 polyubiquitin (polyUb) chains have been shown to take on a different conformation than K48 linked polyUb chains (102). This different conformation leads to different binding partners and would therefore likely play into the differences between K63 and K48 modification. However, one K63 polyUb binding protein, p62, actually leads to degradation of the modified substrate, tau (2). Tau is a microtubule binding protein found in aggregates associated with neurodegeneration (56). Additionally, loss of the E3 ubiquitin ligase parkin is one cause of familial Parkinson's disease and parkin facilitates both K48 and K63 linkage of synphilin-1, K48 modification leading to degradation and K63 modification leading to accumulation (58). Clearly, all the consequences of K63 polyUb chain modification are only beginning to be elucidated.

In yeast, UBC13 is needed to respond to UV damage or cellular stress, which leads to DNA damage (11, 45). UBC13 is essential to the error-free DNA lesion bypass pathway. UBC13 uses K63-linked polyUb to modify the DNA-polymerase processivity factor PCNA and this modification promotes the error-free DNA lesion bypass pathway (45). The participating E3 ubiquitin is RAD5 (45), which contains a RING domain similar to the Mahogunin E3 ligase mentioned previously and the E3 ligases that will be presented below. Whether the role for UBC13 in DNA damage tolerance described in yeast also holds in mammals has not been shown, but, as RAD5 and other components of the pathway are conserved in mammals, it seems possible.

The UBC13/UEVIA heterodimer in mammals has been demonstrated to be involved in innate and adaptive immunity. TNF-α, IL-1β, TLR and TCR receptors all use UBC13 to polyubiquitinate components of their pathways and activate downstream kinases (38, 92, 103, 110). Most common to these receptor pathways are tumor necrosis factor receptor associated factors 2 and 6 (TRAF2 and TRAF6). Both TRAFs are E3 ubiquitin ligases containing RING domains and are crucial to immunity and to the development of several tissues including the brain (106, 108). Both TRAF2 and TRAF6 can be polyubiquitinated by UBC13/UEV1A in response to receptor signaling. For example, when the TNF-αreceptor is activated, UBC13/UEVIA polyubiquitinates TRAF2 (87). TRAF2 then transfers the K63-linking polyUb to RIP. The K63-

ubiquitinated RIP will now bind TAB2, which causes the activation of Transforming growth factor beta activated kinase (TAK1), the kinase upstream of IκB kinase (IKK) activation. IKK then phosphorylates IκB, the inhibitor of NF-κB, leading to the K48 ubiquitination of IκB and subsequent degradation thus allowing NF-κB translocation to the nucleus. TRAF2 K63 polyubiquitination also leads to germinal center kinase related (GCKR) activation which leads to activation of JNK kinase (89). Something similar happens with TRAF6, albeit with different intermediate effectors (92, 103). TRAF6 has been shown to bind directly to UBC13 through its RING domain (105) and TRAF6 oligermization leads to K63 linked polyUb modification and activation of TAK1, and subsequently IKK and NF-κB (28). TRAF6 modification also leads to germinal center kinase (GCK) activation and JNK activation (109).

In *Drosophila*, innate immunity depends on the Toll and immune deficiency (Imd) signaling pathway, which are homologous to the mammalian TLR and TNF signaling pathways respectively (95). The UBC13 orthologue in *Drosophila* is encoded by the *bendless* (*ben*) gene. In cell culture, Ben and dUEVIA are needed to mount a sufficient response to lipopolysaccharide (LPS) which activates Imd and, indeed, flies with the hypomorphic *ben*$^1$ mutation show defects in their antibacterial response (111). Other components downstream of UBC13/Ben such as TAK1 and NF-κB (Relish) are also conserved in function in *Drosophila* (95).

The *ben*$^1$ mutation, however, had been identified first to affect neuronal connectivity (69, 78). The name *bendless* comes from the phenotype of the giant fiber axon, which, though it reaches its target area, fails to make its final bend to connect to the downstream motor neuron. Additionally, the *ben*$^1$ mutation affects photoreceptor pathfinding. Normally, photoreceptors in the *Drosophila* eye develop in groups of eight neurons called ommatidia (97). These eight cells are labeled R1-R8 and project axons to the optic lobe with R1-R6 stopping in the lamina and R7-8 projecting past into the medulla. These projections need to be precise in order to correctly convey visual information. In the *ben*$^{1}$ flies however, this does not occur, with uneven spacing and gaps seen in the projections as the photoreceptors differentiate and send their axons into the brain of third instar larvae (69, 78). Thus in *Drosophila*, UBC13/Ben has a role not only in innate immunity but in photoreceptor pathfinding as well.

## 7. SPECIFIC AIMS AND OUTLINE OF THESIS.

As can be seen from the data summarized in the introduction, Atrn appears important to many systems, including pigmentation, myelination, neurodegeneration and immunity. However, while hints existed as to potential signaling downstream of Atrn, no direct molecular data had yet to be presented.

Therefore, the initial goal of my thesis was to provide insight into the molecular mechanism of Attractin's action. To this end, a yeast two-hybrid screen of an adult mouse cDNA library was performed with the C-terminus of mouse Atrn as bait.

One of the candidate positive interacting partners was the N-terminus of UBC13. Though biochemical and cellular methods could have been used to characterize the interaction of the mammalian proteins, too little was known about the role of UBC13 and Atrn in the mammalian brain to make this an attractive option and Mahogunin had yet to be cloned. Since *Drosophila* has the only available UBC13 mutant, *bendless*$^{1}$, I decided to turn to *Drosophila* as a model system in which to begin characterizing a molecular role for Atrn in the nervous system by characterizing the *Drosophila* homologue of Atrn, named Distracted (Dsd), and its interaction with UBC13/Ben.

Therefore, the goals of this research were to determine:

1. With what proteins does the intracellular tail of mouse Attractin interact with? The results of a yeast two hybrid screen with the intracellular tail of Atrn as bait are presented in chapter 2.

2. When and where is *distracted* expressed? In *Drosophila* there is only one Atrn and ALP homologue, which has been named Distracted (Dsd). The expression of *dsd* and the Dsd protein is presented in chapter 3.

3. What is the consequence of hypomorphic mutations in *distracted*? Two lines of flies with transposable P-elements inserted just upstream of the predicted *dsd* start codon were available from the Bloomington stock center. Characterization of these alleles and their consequences in photoreceptor pathfinding is presented in chapter 3 and 4.

4. Do Dsd and Ben interact physically? Since the initial interaction was found using the mammalian proteins, confirmation of the *Drosophila* Dsd and Ben physical interaction is presented in chapter 4.

5. Do *ben* and *dsd* hypomorphic mutations show genetic interaction? As the *ben*$^1$ mutation has already been demonstrated to affect photoreceptor pathfinding, the effects of both the single mutants and double homozygous mutants on photoreceptor pathfinding were examined. Additionally, *Drosophila* has emerged as an excellent model system for study of neurodegenerative diseases. Given the phenotype of neurodegeneration in Atrn deficient animals, the adult flies, single and double homozygous for *ben*$^1$ and the *dsd*$^P$ alleles, were examined for neurodegeneration. The findings from these studies are presented in chapter 4.

The goal of my thesis research was to discover and characterize a molecular mechanism for Atrn's pleiotropic actions. To this end I identified UBC13/Ben as a molecular partner for Atrn. Using the *Drosophila* model system, I showed that this interaction has functional consequences in both photoreceptor pathfinding and neurodegeneration.

# CHAPTER TWO

# IDENTIFICATION OF PROTEINS THAT CAN INTERACT WITH THE INTRACELLULAR TAIL OF ATTRACTIN.

Ruth E. Thomas and Roger D. Cone

Vollum Institute, Oregon Health and Science University, 3106 SW Sam Jackson Park Rd, Portland OR, 97239.

## ABSTRACT

Mutations in Attractin (Atrn) cause neurodegeneration, hypomyelination, leanness, and darker pigmentation. Also, Atrn has been implicated in immune cell interactions and oxidative stress response. However, there have been no clear molecular functions ascribed to Atrn as yet. To this end, we performed a yeast two-hybrid screen of an adult mouse cDNA brain library using the intracellular tail of Atrn as bait. Of the 20 candidate interactors identified, six were involved in cytoskeletal regulation, ten in various signaling pathways, two in housekeeping enzymatic pathways, and two were of unknown function. A common thread of the proteins with known function is an impact on JNK and NF-κB activation and cytoskeletal regulation. These interactors would seem to support involvement of Atrn in cell migration, guidance, and signaling and provide areas for further study and definition of the molecular mechanism of Atrn action.

# INTRODUCTION

The GAL4 based yeast two-hybrid system uses the GAL4 transcription factor, split into its DNA binding domain (DNA-BD) and its activation domain (AD). The bait protein is fused to the DNA-BD and the library cDNA expressed as fusions with the AD. When the DNA-BD-bait protein interacts with a library-AD fusion, the DNA-BD and AD are brought into proximity and activate the transcription of reporter genes. This system allows for the identification of novel protein interactions and confirmation of these interactions (9).

The Attractin (Atrn) protein is a single pass transmembrane protein, which has known motifs extracellularly but no known motifs within the intracellular domain (37). The extracellular structure of Atrn with epidermal growth factor (EGF) domains and a CUB domain suggest a role for Atrn in cell signaling and interaction (3). Indeed, Atrn had been first identified in the human immune system (25). The extracellular region is secreted by activated T-cells and modulates the interaction between macrophages and T-cells. Also, the transmembrane form has been implicated in the cellular response to oxidative stress (70). However, the direct molecular mechanism behind these actions is not known. The intracellular tail of Atrn does have conserved motifs from *C. elegans* to humans and has been demonstrated to be essential to Atrn function as only transgenes encoding the transmembrane form of Atrn rescue the phenotype of *Atrn* mutants (54). So identifying proteins that interact with the intracellular tail of Atrn would give insight into the molecular function of Atrn with regards to pigmentation, neurodegeneration, hypomyelination and possible insight into other roles for Atrn, potentially in cell guidance and signaling.

# MATERIALS AND METHODS

Yeast two-hybrid screens were based in the generation of "bait" constructs in pGBKT7 (Clontech) representing the C-terminus of mouse *Attractin* (coding for 1301 to 1428 a.a.) fused to the GAL4 DNA binding domain. This construct was transformed into the yeast strain PJ69-2A and then mated to the pretransformed library from Clontech according to the manufacturer's instructions and selected for interaction. The library was an adult mouse brain cDNA library cloned into pACT2 (Clontech). The cDNA came from male mice 9-12 weeks old. It came pretransformed into the Y187 yeast strain and ready to be used to mate to the Atrn bait construct.

Briefly, interaction was selected for by plates lacking adenine and histidine. The DNA-BD vector and library vectors were selected by leaving out leucine and tryptophan. Once the positive clones grew, a β-galactosidase assay was performed to evaluate the strength of the interaction and confirm the interaction activated all three reporter genes. Glycerol stocks were made for all positives that activated all three reporter genes. Plasmids were isolated using the CPG yeast plasmid extraction kit. PCR was performed on the plasmids and PCR products digested with the frequent cutter Hae III or Alu I to determine duplicate positives. The plasmids were electroporated into DH5α E.coli and isolated from E. coli cultures. The plasmids were sequenced with a 5' primer within the pACT2 library vector. BLAST searches (www.ncbi.nlm.nih.gov/BLAST/) for both the nucleotide and translated protein sequence were performed. Only those positives that matched identities in both nucleotide and translated protein were considered as true potential interactors for Atrn.

# RESULTS

Once the DNA-BD-Atrn tail fusion was shown not to self-activate the reporter genes, a culture of PJ69-2A yeast transformed with the Atrn bait was mated with the pretransformed library of adult mouse brain. The potential positive interactors were selected by plating this mating on plates lacking leucine and tryptophan to select for the DNA-BD and AD vectors and also lacking adenine and histidine to select for interaction. The titer for the mating was calculated by plating a small amount of the mating culture, on –leu, -trp, and –leu-trp plates only. Based on the colony forming units (cfu) per ml of the library, bait, and diploid formation (Table 1), the number of clones screened in our yeast two hybrid mating was $2.76 \times 10^6$, more than sufficient to encompass the entire transcriptome captured in the library. This titer result would suggest that the positives we isolated represent the majority of interaction for Atrn in the adult mouse brain.

From the interaction selection based on the absence of histidine and adenine, 212 colonies grew on the selection plates. A β-galactosidase (β-gal) assay was performed on all 212 positives. Of the 212 originally selected colonies, 100 turned blue in the β-gal assay. Of those 100, 41 turned strongly blue, 31 turned mid-level blue and 28 turned weakly blue. Plasmids were isolated from these positives colonies and transformed into E. coli for harvest. Once purified library plasmid was obtained, sequencing was done in the 5' direction from the AD into the insert. The sequences were BLAST compared to the nucleotide database. Also, the nucleotide sequence was translated into the predicted fusion protein based on the AD reading frame and this protein sequence BLAST compared to the protein database. Positives were disregarded if their DNA sequence matched genomic DNA or matched the 3' UTR of a cDNA. Positives were also disregarded if the protein translation of the DNA sequence did not match the cDNA identity.

These criteria left 23 positives. Three of these were not good candidates as one was mitochondrial, cytochrome c oxidase subunit II, and two were extracellular proteins unlikely therefore to interact with an intracellular domain. The two extracellular proteins were transtherytin/prealbumin and the extracellular domain of the VPS Sorc receptor. So, disregarding these three, that left 20 positives as good candidates to interact with the Atrn tail. These 20 proteins fell into three general categories, cytoskeletal regulation, signaling pathways, and enymatic activity (Table 2). The most frequently identified positives were microtubule associated protein 1B and 1A (MAP1B and MAP1A). Seven colonies had MAP1A as the interactor and 11 had MAP1B as an interactor. The smallest inserts for MAP1B and MAP1A corresponded to the light chains (LC) that are cleaved from the C-terminus of the MAPs and mediate the interaction with microtubules (76). Other positives include ones regulating actin, such as Filamin, ones involved in c-jun kinase (JNK) and nuclear factor κB (NF-κB) activation and two involved in ubiquitin signaling, Ubx4 and UBC13.

## DISCUSSION

The extracellular region of Atrn has a structure that suggests molecular roles in cell guidance, migration, or signaling (25). However, the means by which Atrn would mediate these potential functions require protein interaction within the interior of the cell. The C-terminal tail of Atrn is short at 128 a.a. and has no known signaling motifs (71). It does however have conserved clusters of amino acids, which could be the points of contact with important downstream partners that underlie Atrn's molecular function. To identify these partners, a yeast two hybrid screen of an adult mouse brain library has been performed using the Atrn tail as bait.

Prior to this screening, the only two molecular functions for Atrn with data had been in neurite outgrowth and in cellular oxidative stress response. Of these two, the oxidative stress response has the most molecular information. In Atrn deficient cells, the response to hydrogen peroxide is blunted with the normal activation of ERK reduced (70). Additionally, superoxide dismutase (SOD) levels are down and catalase levels are up in the brains of *Atrn* mutants. These findings suggest Atrn is involved in the activation of ERK in response to oxidative stress but not how Atrn is likely to accomplish this activation.

Of the two studies showing Atrn's involvement in neurite outgrowth (21, 93), only one identifies a molecular interaction for Atrn. Embryonic day 14 dorsal root ganglion (E14 DRG) neurons cultured in differentiation medium show induction of Atrn and MAP1A message with a peak for Atrn at two weeks in culture (21). Overexpression of either protein alone in the E14 DRG neurons does not change the neurite length. When co-overexpressed however, Atrn and MAP1A LC2 increase the length of the neurite by 30% and direct physical interaction between Atrn and LC2 had been identified in yeast.

The interaction between the intracellular tail of Atrn and the LC of MAP1A has also been identified in our current study. MAP1A is present in seven positive colonies as is the closely related MAP1B LC in eleven positive colonies. Both MAPs are known to be involved in regulation of microtubule stability and MAP1B has been shown to be important to the turning of axon growth cones during axonal pathfinding (7, 15, 61, 76, 80).

The other candidates from our screen that have been identified to be involved with cytoskeletal regulation are Filamin, Pericentriolar material 1 (PCM1), rho/rac guanine nucleotide exchange factor 2 (GEF-2), and Translokin. Filamin crosslinks actin and links the cytoskeleton to the cell membrane, serving as a scaffold for signaling and trafficking molecules (30, 52). PCM1 recruits proteins to the centrosome and is necessary for the organization or anchoring of microtubules at the centrosome (51). GEF-2 has not been studied directly but family members have been shown to mediate the regulation of the actin cytoskeleton by microtubules (53). Translokin colocalizes with the microtubule network and is responsible for the intracellular trafficking of fibroblast growth factor-2 to the nucleus (6).

The signaling category of the Atrn interactors, into which GEF-2 and Translokin could also fit, includes C-terminal binding protein 1 (CtBP1), Eukaryotic translation initiation factor subunit 10 (eIF-3s10), nucleostemin, PAI-1 mRNA binding protein related, Mcp2, Ubx4, Jab1/CSN5, JNK interacting protein 3 (JIP3), proline isomerase1 (Pin1), and Ubiquitin conjugating enzyme 13 (UBC13). Of these candidates, the most interesting at this time are JIP3, Pin1, Jab1/CSN5, and UBC13 for the following reasons.

JIP3 is involved in the trafficking of vesicles and is known as Sunday driver in *Drosophila* (8, 14). JIP3 also participates in various aspects of JNK activation such as lipopolysaccharide (LPS) mediated JNK activation (62). This result implicates JIP3 in immune function, which could fit with Atrn's involvement in immune cell interaction and response.

Pin1 functions in multiple signaling pathways, including those responding to DNA damage, growth factors, and cytokines (p53, JNK, and NF-κB respectively) (59). Pin1 expression is also decreased in Alzheimer's disease (39, 59). This finding might therefore play into the neurodegeneration seen in *Atrn* mutants if the Pin1 interaction is found to be functionally relevant.

The next candidate, Jab1/CSN5, is part of the COP9 signalosome. Specifically, Jab1/CSN5 has been shown to be critical to the cleavage of ubiquitin-like Nedd8 from the Cul1 subunit of SCF ubiquitin ligases (18). In *Drosophila*, dJab1/CSN5 disruption causes photoreceptor pathfinding defects due in part to the reduction of laminal glia migration in these mutants (91). Both functions would fit with Atrn having a role in cell migration. However, the potential Jab1/CSN5 interaction could very likely be a false positive as one study shows that Jab1/CSN5 interacts directly with the GAL4 DNA binding domain (77). But as the function of Jab1/CSN5 fits with the rest of the interactors, it has been left in as a potential Atrn interactor.

The final candidate, UBC13, is critical to DNA damage repair in yeast (11, 45) and to immune response in mammals, specifically the activation of JNK and NF-κB (28, 38). In *Drosophila*, the UBC13 orthologue Bendless has also been shown to be involved in fly innate immunity (111) and to affect photoreceptor pathfinding (69, 78). Thus UBC13 represents a molecule covering the signaling aspects that seem common to the candidate Atrn interactors, namely cytoskeletal regulation (implicated by the photoreceptor pathfinding defects) and signaling (JNK and NF-κB activation).

The candidate Atrn interactors identified in our screen of an adult mouse brain library fall into two main categories, cytoskeletal regulation and signaling pathways particularly those leading to JNK and NF-κB activation. Also three candidates, Ubx4, Jab1/CSN5, and UBC13 have links to the ubiquitin system. Taken together, the candidates that have been identified in the yeast two hybrid screen lend credence to the prediction that Atrn acts molecularly to modulate cell guidance, interaction, and signaling, possibly through the regulation of the cytoskeleton and activation of NF-κB and JNK. Future studies will confirm whether all of the candidates do indeed form a functional partnership with Atrn and underlie the molecular mechanism of action of Atrn.

**Table 1.** The titer for the mating of the Atrn bait in PJ69-2A yeast to the Pretransformed adult mouse brain library in Y187 yeast was calculated according to the manufacturer's instructions. For the library, the number of colonies that grew on plates lacking only leucine (-leu) was used. For the Atrn bait, the number of colonies that grew on plates lacking only tryptophan (-trp) was used. For the diploid formation, the number of colonies that grew on plates lacking both leucine and tryptophan (-leu-trp) was used. The titer of the diploids was multiplied by the total volume of the mating culture, 11.5 mls, to calculate the number of clones screened. cfu = colony forming units

| | Titer |
|---|---|
| Library (-leu) | $2.36 \times 10^7$ cfu/ml |
| Atrn bait (-trp) | $1.07 \times 10^8$ cfu/ml |
| Diploid (-leu-trp) | $2.40 \times 10^5$ cfu/ml |
| **Number of clones screened** | ($2.40 \times 10^5$ cfu/ml diploid) x 11.5 mls=<br>**$2.76 \times 10^6$ clones screened** |

**Table 2.** The list of Atrn intracellular interacting candidates, split into categories based on function. The amino acid residues of the candidates are indicated if the positive clone only encoded part of the candidate protein. Otherwise, the full length protein was encoded in the positive clone. For microtubule associated protein 1A and 1B (MAP1A and MAP1B), only their light chains were listed as this represented the smallest of the numerous clones isolated for these two candidates. The number listed is the number of colonies that contained the candidate interactor in frame with the activation domain. The function listed is only the most prominent or salient feature of the candidates' functions and the references for such are in the discussion. N/A = not applicable.

| Categories | Positive Candidate | Number | Function |
|---|---|---|---|
| Cytoskeletal regulation | Filamin (63-121 a.a.) | 2 | Actin crosslinking |
| | MAP1A light chain 2 (LC2) | 7 | Microtubule stability, neurite outgrowth |
| | MAP1B light chain 1 (LC1) | 11 | Axon growth cone turning |
| | Pericentriolar material 1 (PCM1) | 1 | Organization of centrosome |
| | Rho/rac guanine nucleotide exchange factor (GEF-2) (1-759 a.a.) | 1 | Family member mediate actin regulation by microtubules |
| | Translokin | 1 | Trafficking of FGF-2 |
| Signaling molecules | C-terminal binding protein 1 (CtBP1) (1-87 a.a.) | 1 | Transcriptional corepressor |
| | Eukaryotic translation initiation factor subunit 10 (eIF-3s10) | 1 | Initiation of mRNA translation |
| | Jun coactivator Jab1/ COP9 signalosome subunit 5 (CSN5) | 1 | Deneddylation of theSCF E3 ubiqutin ligase and cell migration (*Drosophila*) |
| | JNK interacting protein 3 (JIP3) | 1 | c-Jun NH2-terminal kinase (JNK) scaffold and adapter protein vescicle transport |
| | Mcp2/cbx4 (461-538 a.a.) | 2 | Homeobox transcriptional repressor |
| | Nucleostemin | 1 | Promotes stem cell maintainence |
| | PAI-1 mRNA-binding protein related | 1 | Possibly mRNA binding and regulation |
| | Proline isomerase 1 (Pin1) | 1 | Cell cycle control and reduced activity in Alzheimer's disease state |
| | Ubiquitin conjugating enzyme 13 (UBC13) (1-63 a.a.) | 1 | Innate and adaptive immunity, photoreceptor axonal pathfinding (*Drosophila*) |
| | Ubx4 (contains domain of ubiquitin-regulatory proteins) (4-180 a.a.) | 1 | Unknown directly though a homologue in flies affects eye morphology |
| Housekeeping enzymes | glutamate oxaloacetate transaminase1 | 2 | Glutamate metabolism |
| | UMP-CMP kinase homologue | 1 | Nucleotide metabolism |
| Unknown function | cDNA C030044B11 gene | 1 | N/A |
| | FL10378/1700108L22 gene | 1 | N/A |

# CHAPTER THREE

# CHARACTERIZATION OF DISTRACTED, THE *DROSOPHILA* HOMOLOGUE OF ATTRACTIN.

Ruth E. Thomas, Jacqueline Parker, Michael A. Forte, Roger D. Cone

Vollum Institute, Oregon Health and Science University, 3106 SW Sam Jackson Park Road, Portland OR, 97239.

# ABSTRACT

The mammalian Attractin family, consisting of Attractin (Atrn) and Attractin-like protein (ALP), has been implicated in neurodegeneration, pigmentation, and immune function. Two previous reports point to Atrn involvement in neurite outgrowth but no evidence of Atrn involvement in axonal guidance has been presented although the structure of Atrn and ALP is suggestive of such a role. In *Drosophila*, one homologue of Atrn and ALP exists, CG5634, hereafter referred to as *distracted* (*dsd*). The Dsd protein was found to be 36% and 34% identical to Atrn and ALP respectively. The expression pattern of *dsd* was temporally dynamic throughout *Drosophila* development and continued in the adult head. Staining for Dsd protein showed strong expression in the eye-antennal disc of third instar larvae and colocalization with a marker for photoreceptors. Two transposable P-element insertions 0.3 kb upstream of the *dsd* start codon resulted in hypomorphic expression of *dsd*. A deficiency was generated using the stocks from the DrosDel collection as the *dsd* locus is not covered by any available deficiency. The *dsd*$^{P1}$ and *dsd*$^{P2}$ mutations were viable and the mutants showed disruption in photoreceptor pathfinding either as transheterozygotes or over the deficiency. This finding illustrates that the Atrn family is involved in influencing axonal guidance and sets up *Drosophila* as a model system in which to study the evolutionarily conserved molecular role of the Atrn family.

# INTRODUCTION

Mutations in Atrn have been identified in rats, mice and hamsters. In all cases Atrn mutations lead to changes in pigmentation and the appearance of neurodegeneration and hypomyelination (36, 54, 55). The structure of Atrn is suggestive of roles in cell-cell interaction and guidance (25). Atrn is a single pass, transmembrane protein with a CUB domain flanked by two EGF domains followed by a C-lectin domain, plexin repeats and two laminin-like EGF domains (37, 54). The intracellular tail of Atrn has no known signaling motifs but does have clusters of amino acids that are conserved from *C. elegans* to human (71). Other than this conservation, very little is known about the molecular mechanism by which Atrn might act.

The first recognized role for Atrn came from genetic studies with dominant agouti alleles such as lethal yellow ($A^y$) and viable yellow ($A^{vy}$). The $A^y$ and $A^{vy}$ mice overexpress agouti, an endogenous antagonist of melanocortin 1 receptor (MC1R) (22, 23, 67). The agouti antagonism of MC1R causes a switch from black/brown pigment production to yellow pigment production. The $A^y$ and $A^{vy}$ mice are completely yellow and are also obese. The obesity comes from agouti antagonism of melanocortin 4 receptor (MC4R) in the brain (29). In the presence of mutations in Atrn however, the $A^y$ mice are no longer yellow and obese but black and lean, showing that Atrn is necessary to the actions of agouti (22, 67). Atrn binds agouti, but not agouti related protein (AGRP), giving rise to the hypothesis that Atrn acts as a low affinity co-receptor for agouti in the skin where agouti is normally expressed (43).

The skin however is not the only site of Atrn expression. Both Atrn and ALP are widely expressed throughout the rodent, notably in the brain, heart, kidneys, liver and lungs with low expression in the spleen and skeletal muscle (37, 40, 71). Within the brain, the hippocampus and piriform cortex have the highest mRNA expression (40, 60). Similar expression of Atrn is seen in human tissue with the transmembrane form the only form expressed in the human brain (93). As agouti is normally restricted to the skin, being a co-receptor for agouti is unlikely to be Atrn's primary function, especially given the neurodegenerative phenotype of Atrn deficient animals (36, 54).

A splice variant only found in humans and rats produces the extracellular domain of Atrn as a secreted protein (54, 94) and the first biological role for Atrn came from studies of this secreted form within human T-cells (25). Atrn is secreted upon T-cell activation and modulates the interaction of monocytes and T-cells. However, only the transmembrane form of Atrn is found in mice and only the transmembrane form will rescue the neurodegeneration and hypomyelination phenotypes of Atrn deficient rats (54).

Incubation of cultured cortical neurons with the extracellular Atrn domain results in inhibition of neurite outgrowth (93). Upon spinal cord injury, Atrn, along with neuritin and microtubule associated protein 1A (MAP1A), is downregulated (21). After 14 days, Atrn, neuritin and MAPIA are back to previous levels and co-expressed with GAP-43, a regeneration and plasticity associated protein. When Atrn and MAP1A light chain 2 (LC2) are co-overexpressed in E14 dorsal root ganglion (DRG) cultured neurons, neurite length increases by 30%. When neuritin is also co-overexpressed with Atrn and MAPIA, the neurite length increased by 94%. Both these reports indicate that Atrn is involved in neurite outgrowth, a hallmark of proteins potentially involved in axonal guidance.

Another indictation that Atrn has other molecular roles other than its necessity in agouti action is that Atrn is conserved from *C. elegans* to humans whereas agouti and the melanocortin system are not. The *C. elegans* homologue of Atrn, F33C8.l, has the same extracellular domain structure except that it is missing the C-lectin domain present in mammalian Atrn and ALP (94). C-lectin is a domain associated with binding to carbohydrates (104). The intracellular domain of F33C8.1 also has conserved amino acids (71). However, little to nothing is known about the function of Atrn homologues in *C. elegans* or in *Drosophila*. This study aims to characterize the expression and role of the *Drosophila* homologue of Atrn and ALP.

## MATERIALS AND METHODS

### Fly stocks and genetics

Fly stocks were kept at room temperature (20°C) and crossed at 25°C on standard fly medium. Canton S were used as wild type controls. The *EP(3)3400* (*dsd*$^{P1}$) and *EP(3)3030* (*dsd*$^{P2}$) lines were obtained from the Bloomington stock center. To create a deficiency covering the *dsd* locus two lines were obtained from the DrosDel collection of RS insertion lines at Szeged stock center, *CB-0262-3* and *5SZ-3265* positioned at scaffold bp 23407072 and 23731698 on the right arm of the third chromosome. These lines were crossed to *y*$^{1}$*w*$^{1}$*hsFlp70;TM2, Ubx/TM6, Sb* females. Male progeny from this cross were backcrossed to *y*$^{1}$*w*$^{1}$*hsFlp70;TM2, Ubx/TM6, Sb* females to produce *y*$^{1}$*w*$^{1}$*hsFlp70; RS(CB-0262-3* or *5SZ-3265)/TM6, Sb* males or females. The *y*$^{1}$*w*$^{1}$*hsFlp70; CB-0262-3 /TM6, Sb* and *y*$^{1}$*w*$^{1}$*hsFlp70;5SZ-3265/TM6, Sb* flies were crossed and the progeny heat shocked 48 hours and 96 hours after egg laying by incubation for 1 hr at 37°C. The male non-stubble progeny from this cross were crossed to *w*$^{1}$*;TM3, Sb/TM6, Dr* females and individual progeny from this cross that were red eyed (a marker for creation of the deficiency) were crossed to *w*$^1$;*TM3, Sb*/*TM6, Dr* to create *w*$^1$; *Df* /*TM6, Dr* stocks. The creation of the deficiency was confirmed by PCR using AccuTaq LA (Sigma) using primers CB-forward 5' GGCAAC-TGTGGCGATATTTTT 3' and 5SZ-reverse 5' GAACTCCGATGGACAGAAGG 3'. In accordance with the Szeged stock center protocols this deficiency has been assigned as *Df(3R)ED6274*.

### Cloning of *distracted* cDNA

The cDNA clone for *dsd* was purchased from Research Genetics, clone LD38671 in the pOT2 vector. The clone was sequenced using vector and gene specific primers and found to have a ~5.2 kb insert. The cDNA source was 0-24 hr embryos.

To clone the entire 5' end of the *dsd* cDNA, mRNA was isolated from adult Canton S (C.S.) flies using the Promega PolyATract mRNA Isolation System IV. The mRNA was then subjected to reverse transcription using Powerscript Reverse Transcriptase from Clontech, which adds poly-cystines when it reaches the end of an mRNA (see Clontech SMART technical information). Included in the reaction were the oligoT primer and my polyG primer, 5' CATAGTACTAATTCCCTAGGGGG 3'. The oligoT primer alone was incubated for 60 min at 42°C, then the polyG primer was added to the reaction with a further 45 minute incubation at 42°C followed by termination by heat inactivation. For the RT-PCR, the forward primer was the same as the polyG primer except missing the Gs at the 3'end, giving a sequence of 5' CATAGTACTGAA-TTCCCTAG 3'. The reverse primer was gene specific for *dsd*, nestR 5' TCACCG-AATAGTTGCCCCATC 3'. The resultant bands were gel purified and cloned using

TOPOXL kit (Invitrogen). Resultant clones were sequenced and compared to the embryonic LD38671 *dsd* cDNA and *dsd* genomic sequence.

**In situ hybridization**

Dechoronitated C.S. embryos 0 to 22 hours old were incubated with either sense or antisense *dsd* probes labeled with digoxygenin essentially as described (96). The probes represented the coding sequence for the *dsd* C-terminal tail.

**Antibody generation**

Dsd antibodies where generated through the services of Pocono Rabbit Farm. Guinea pigs were initially injected with polyacrylamide gel slices containing a maltose binding protein (MBP) fusion with the Dsd tail protein, isolated from bacteria transformed with pMAL-c2E (New England Biolabs) carrying the Dsd tail coding sequence inserted in frame. These injections were followed by subsequent injections with GST-Dsd tail fusion protein, the *dsd* tail cloned in frame to the pGEX-KG vector (gift from the R. Goodman lab). Both the MBP and GST fusion proteins were purified using the recommended protocols from the respective sources (New England Biolabs and Sigma respectively). Antibodies were affinity purified from the terminal bleeds by Pocono Rabbit Farm using 6xHis-tagged Dsd C-terminal tail, the tail coding sequence cloned in frame into the pet15b vector (Novagen). This protein was purified under denatured conditions according to the protocol recommended by Qiagen, the makers of the Ni-NTA suspension used. The 6xHis-tagged Dsd Cterminal tail was covalently linked to Affinity Matrices by Pocono Rabbit Farm and the affinity-purified antibodies tested for specificity by the company as well.

## Immunohistochemistry

Brains from C.S. third instar larvae were dissected and fixed in 4% paraformaldehyde in PBS, then washed one hour in 10% normal goat serum PBST (0.6% Triton) before primary antibody was applied. The affinity-purified guinea pig anti-Dsd antibody was used at 1:200 and incubated for 48 hrs at 4°C. Dsd antibodies were blocked by incubating the diluted antibodies with 5 μg MBP or MBP-Dsd tail or GST or GST-Dsd tail for an hour at room temperature before being put onto the third instar brains. For the blockade using GST, Glutathione sepharose 4B (Amersham) was used to pull out the GST and bound antibodies before application to the tissue. 24B10, used at 1:100 and 8D12 anti-repo, used at 1:10, came from the Developmental Hybridoma Bank. The secondary antibodies were used at 1:1000 and 1:500, goat anti-guinea pig Alexa 568 and goat anti-mouse Alexa 647 (Molecular Probes) respectively. The brains were mounted in Gel/Mount (Biomeda) and pictures taken with the confocal microscope Icon TE300 BioRad Scanning Laser 1024 at 20-40x. For the DAB staining of 24B10 staining of C.S. and the *dsd*$^{P}$ mutants, 10% normal horse serum in PBST (0.3% Triton) was used with the secondary the biotinylated horse anti-mouse (1:200) from Vector and ABC solution made using the kit from Vector. The optic lobes with attached eye discs were whole mounted in 50% glycerol and pictures taken at three focal planes, and then overlaid in Adobe Photoshop.

## Real-time PCR

Total RNA was extracted from C.S., *dsd*$^{P1}$, and *dsd*$^{P2}$ flies and 1 μg subjected to reverse transcription using oligoT primer according to manufacturer's instructions (MBI Fermentas). The reactions were diluted to 100 μl and stored at –80C, with 3 μl used as template per individual PCR reaction. Real-time PCR was performed on the Opticon machine (MJ Research) using SyBR Green I (Molecular Probes) at 0.5X as the detecting reagent and Hotstart NovaTaq (Novagen) as the amplifying polymerase. The primers used were as follows: for actin 5C 5'-CGAAGAAGTTGCTGCTCTGGT-3' and 5'-CACAATCGATGGGAAGACGGC-3' and for dsd 5'-TGGAACAGATGGCGAGTCG-ACCGT-3' and 5'-TGCCCTCCAGCGTCAGACTCAGAT-3'. The PCR was performed 4 times and in each PCR the samples from each genotype were measured in triplicate for *actin* and *dsd*. Standards for *actin* and *dsd* were done in duplicate. Triplicate values estimated from the standard curves were averaged and the average *dsd* value divided by the *actin* value. These ratios were normalized to the C.S. ratio and values from the 4 PCRs combined.

## RESULTS

### The *Drosophila* homologue of Attractin is encoded by the *distracted* gene

One predicted gene in *Drosophila*, CG5634, encoded for a protein 36% identical to Atrn and 34% identical to ALP, now referred to as *distracted* (*dsd*). The Dsd protein had the same domain structure as Atrn and ALP (Fig. 1A). The extracellular region contained two EGF domains flanking a CUB domain and these domains were followed by plexin repeats and two laminin like EGF domains (Fig. 1 B). The only domain not present was the C-lectin domain, which is also not present in the *C. elegans* F33C8.1 homologue of Atrn (94). The conservation of the intracellular tail of Dsd was 45% and 44% respectively for Dsd to Atrn and ALP. To confirm the actual sequence of the *dsd* mRNA, a cDNA clone was obtained from Research Genetics and sequenced. This clone stopped 7 bps before the predicted ATG. In order to determine if the predicted ATG was indeed the actual start codon of *dsd* and that there were no other ATG's upstream of this one, the 5' end of the *dsd* mRNA was cloned from the adult fly using the SMART schematic developed by Clontech. This scheme uses the activity of the Clontech reverse transcriptase that adds poly-cystines residues to the end of the reverse transcript once the reverse transcriptase reached the 5' end of the mRNA (112). The clone thus derived contains the entire 5' end of the transcript. The *dsd* 5' UTR encompassed 276 bps upstream of the predicted ATG (Fig. 2A). The predicted ATG was the only ATG in frame with the ORF of *dsd*. However, after the ATG, the codons for 57 amino acids (a.a. 2 to 59 from the embryonic clone) were missing, indicating a possible splicing difference between adult and embryonic *dsd*. The last 7 amino acids missing represent the beginning of the first EGF domain.

### Expression of *distracted*

We next determined the relative levels of expression of the *dsd* gene throughout *Drosophila* development. By RT-PCR, *dsd* was expressed at 0-4 and 4-8 hrs of post-fertilization (Fig. 2B). Then the level of *dsd* decreased and remained low until the third instar larval stage. The expression of *dsd* persisted into adulthood, appearing in the adult heads.

Since one period with the strongest expressions of *dsd* appeared to be very early in embryogenesis, in situ hybridization was done to see if there were any spatial clues as to the function of *dsd* in embryogenesis (Fig. 3). *Drosophila* embryogenesis take approximately 22 hours at 25°C (13, 41). The first fourteen divisions of the nucleus lead to approximately 5000 nuclei that migrate to the edge of the egg. In late stage 4, at about one and a half hours post-fertilization, the nuclei have reached the edge of the egg and the cell walls begin to form. The expression of *dsd* was very high during stage 4, both early (data not shown) and late (Fig. 3A), though the expression did not show any dorsal-ventral or anterior-posterior expression pattern. The fully cellularized blastoderm forms at stage 5, two and a half hours post-fertilization. Stage 5 embryos showed *dsd* expression in the newly formed cells and at the interface between the cells and the yolk sack (Fig. 3 B).

After gastrulation during stage 6 and 7, the germband elongation begins, encompassing stages 8 through 11 and lasting from three to seven and half hours post-fertilization (13, 41). Expression of *dsd* was seen in stage 8 when the germ band rapidly elongates (Fig. 3 C). In stages 9 through 11, during the slow phase of germ band elongation, *dsd* expression was low, the antisense embryos appearing no different than the sense embryos (Fig. 3D,D'). By eight hours, at stage 12, the germ band begins to retract and the rudimentary nervous system has formed. Expression of *dsd* was seen during stage 12, with broad expression throughout the embryo, no stronger in the ventral nerve cord than elsewhere (Fig. 3E). Both stage 8 and stage 12 are times of rapid cell movement. After stage 12, in agreement with the RT-PCR results, little difference was seen between the sense and antisense embryos (data not shown).

Since very little spatial distinction was seen in embryonic *dsd* expression, these results gave us few clues about Dsd function. However, the RT-PCR data showed that *dsd* appeared to be most strongly expressed in the head not the body of adult flies. As the brains of third instar larvae are more accessible than adults, we examined the expression of Dsd protein at this stage. Antibodies were generated to the intracellular tail of Dsd and affinity purified. Using these antibodies, the highest expression of Dsd in the brains of third instar larvae was shown in the eye-antennal disc, with lower expression in the optic lobe and ventral nerve cord (Fig. 4A). This Dsd stain was specific as preincubation with the antigen, the C-terminal tail of Dsd, abolished most of the signal (Fig. 4B).

The strong expression of Dsd in the eye-antennal disc led us to ask if Dsd expression would colocalize with a marker for photoreceptors, the monoclonal antibody 24B10 (12, 74, 91). Indeed, we found that 24B10 and Dsd staining colocalize, though the photoreceptors were clearly not the only cells expressing Dsd (Fig. 4D-E). We also determined whether Dsd colocalized with a marker for mature glia, Repo (86, 107). Dsd expression did colocalize with Repo in the eye disc but elsewhere, in the optic lobe and ventral nerve cord, the colocalization was not pronounced (Fig. 4F-H). This result fits with Atrn expression, which is primarily in neurons within the brain rather than glia (60).

### Identification of *dsd* hypomorphic alleles and creation of a deficiency covering *dsd*.

Examination of genomic databases indicated that two existing fly lines contained insertions of the EP transposable element in opposite orientations [*EP(3)3400* and *EP(3)3030*, now referred to as *dsd*$^{P1}$ and *dsd*$^{P2}$, respectively], each 303 bp from the start codon of the Dsd protein (Fig. 5A). Real-time PCR analysis revealed that these P insertions resulted in reductions in the expression of *dsd* mRNA in flies homozygous for each insertion: in *dsd*$^{P1}$ and *dsd*$^{P2}$ flies, *dsd* expression was decreased to 70% and 38% of wild-type Canton S (C.S.) levels, respectively (Fig. 5B). These hypomorphic mutations allowed us to examine the consequences of reduced *dsd* expression, particularly with respect to processes like photoreceptor pathfinding given the coexpression of Dsd and 24B10.

Additionally, since both P-element insertions came from the Rorth collection and therefore had the same genetic background, it was crucial to control for any secondary site mutations that might confound our analysis of the *dsd* mutant phenotype. As no previous deficiency covered the *dsd* locus, a deficiency was generated covering the *dsd* locus by use of the RS element insertions mapped for the DrosDel project (www.drosdel.org). In accordance with the Szeged stock center protocols, this deficiency has been assigned as *Df(3R)ED6274*. This deficiency deletes approximately 324 kb of DNA from 98A7 to 98B5, beginning one gene 5' upstream of *dsd*, which is located at 98A12. The deletion was confirmed by PCR which with primers on either side of the RS insertions gave a ~8kb band which was not present in either parent strain or in the balancer stock (Fig. 5C).

### Photoreceptor pathfinding defects in *dsd* mutants

The *Drosophila* eye is composed of ~800 ommatidia, groups of eight photoreceptors, all of which must project their axons to the optic lobe (97). The optic lobe is composed of a series of ganglia (lamina, medulla, lobula and lobula plate). During eye development in third instar larvae, the axons of photoreceptor neurons R1-R6 project to the lamina, where they will eventually synapse with the laminal interneurons. In contrast, axons of the R7 and R8 photoreceptors pass through the lamina and project to specific neuropil layers within the medulla. Normally, photoreceptor axons fasciculate into distinct bundles and display highly ordered trajectories to and through the lamina (17). In the *dsd*$^P$ mutants however, disorganized and unevenly spaced bundles of photoreceptor axons exited the optic stalk to the lamina (Fig. 6B-D). The R1-R6 projections no longer terminated in the lamina in a connected curve, instead having gaps and dips along the laminal extent (Fig. 6B). The R7 and R8 projections were also disorganized compared to wild-type flies, with shorter and unevenly spaced projections, which appeared to terminate in inappropriate levels within the medulla. Defects were also observed in Bolwig's nerve the projection from the larval photosensing organ (47), which in mutant larvae had sometimes projected inappropriately to the thoracic ganglion (Fig. 6C). When present, this defect greatly affected the R8 and R7 projections to the medulla as they seemed to use the Bolwig's nerve as a guidepost. The mistargeting of Bolwig's nerve was not always present and did not seem to overtly affect the lamina formation. The same phenotypes were observed when $dsd^{P1}$ and $dsd^{P2}$ were over the deficiency (Fig. 6D).

## DISCUSSION

Distracted is the *Drosophila* homologue of Atrn and ALP. Dsd is 36% and 34% identical to Atrn and ALP respectively. Dsd has the same domain structure as Atrn and ALP, only missing the C-lectin domain, which is also not present in the *C. elegans* Atrn homologue (25, 37). The homology of the intracellular tail of Dsd goes up to 45% and 44% respectively with Atrn and ALP. It could be argued then that any important intracellular signaling produced by Atrn or ALP would be conserved in *Drosophila*, making *Drosophila* an attractive model system in which to understand the molecular mechanism by which the Atrn family acts.

The expression of *dsd* occurs very early in development from 1 to 8 hours post fertilization. From the embryonic in situs, *dsd* is expressed during cellularization, thus maternally contributed, and also at the beginning of germ band elongation and the beginning of germ band retraction (13, 41). The embryonic expression of *dsd* is not neural specific, rather appearing to be expressed in most tissues. The expression wanes after 8 hours, agreeing with the RT-RCR data. The broad expression of *dsd* is perhaps not unexpected given that both *Atrn* and *ALP* transcripts are expressed in the brain and in many peripheral tissues such as the heart, kidneys and lungs (37, 40). In the brain, the hippocampus and cortex have the highest levels of expression (40, 60).

The Dsd protein shows expression in the eye-antennal disc of third instar larvae and, albeit lower, in the optic lobe and ventral nerve cord. The strong expression of Dsd protein in the eye antennal disc suggests roles for Dsd in head formation, including the eyes and antennae (24). While no gross morphological defects have been observed in the heads of *dsd* mutants, more subtle changes in cell-cell interaction or morphogenesis during adult development are possible. The expression of Dsd in the optic lobe and ventral nerve cord of third instar larvae allow for other roles in brain development. Additionally, as *dsd* expression is seen by RT-PCR in the adult head, roles for Dsd in neurodegeneration are possible, which would be in keeping with the neurodegeneration seen in *Atrn* mutants where the formation of the gross anatomical structure is normal in *Atrn* mutants with the neurodegeneration only appearing as the animals age (36, 54, 55).

The insertion of EP transposable elements 0.3 kb upstream of the *dsd* start codon reduced the expression of *dsd* to 70% and 38% for the $dsd^{P1}$ and $dsd^{P2}$ alleles respectively. The only difference between these alleles is the orientation of the P-element. The $dsd^{P2}$ allele has the P-element in the wrong orientation for driving expression of *dsd* with GAL4. The greater reduction in *dsd* expression seen with this insertion fits with other observations showing that attempts to drive a gene with GAL4 when the UAS promoter is in the wrong orientation will actually silence the gene though no mechanism for this phenomenon has been proven (90).

Since there was no available deficiency covering the *dsd* locus, one was made; *Df(3R)ED6274* covers from scaffold base pair 23407072 to 23731698, cytogenically 98A7 to 98B5, a deletion of 324,626 kb. This deficiency facilitated the analysis of the *dsd*$^{P}$ mutants as it helped control for any secondary site mutations.

As Dsd coexpressses with 24B10, a marker for photoreceptors (12, 74, 91), we examined the photoreceptor pathfinding in *dsd*$^{P}$ and *dsd*$^{P}$/Df third instar larvae. We find that the photoreceptor axons are unevenly spaced as they exit the optic stock and that the lamina, where R1-R6 axons should stop, is often uneven with gaps and dips along its length. Additionally, the R8 and R7 projections to the medulla tend to clump toward the middle, toward the Bolwig's nerve. Bolwig's nerve, the projection of the larval photosensing organ (47), is also sometimes observed to project past the optic lobe and into the ventral nerve cord. This defect seemed to cause the medullary projections of the R8 and R7 photoreceptors to follow, clustering around the Bolwig's nerve. This phenotype for Bolwig's nerve has not been described previously for any other mutant. However, defects in the Bolwig's nerve projection did not seem to greatly affect the lamina formation. The defects in lamina formation are similar to those seen in *off-track* (a tyrosine kinase) (12), *Jabl/CSN5* (a component of the COP9 signalosome) (91), and *bendless* (the *Drosophila* ubiquitin conjugating enzyme 13 homologue) (69, 78). These similarities suggest a permissive rather than instructive role of Dsd in photoreceptor pathfinding.

Distracted, the *Drosophila* homologue of mammalian Atrn and ALP, shares the same domain structure and has conserved intracellular amino acid clusters. The expression of *dsd* is broad during the initial embryogenesis and the expression of Dsd protein is high in the eye antennal disc of third instar larvae. The finding that hypomorphic mutations in *dsd* lead to photoreceptor pathfinding defects illustrates another role for the Atrn family in axon guidance and builds a foundation on which to study the molecular mechanism of Atrn action in a genetically accessible model (4).

**Figure 1.** Comparison of Attractin, Attractin-like protein, and Distracted proteins. (A) Amino acid comparison of *Drosophila* Distracted (Dsd) and mouse Attractin (Atrn) and Attractin-like protein (ALP). The overall homology between Dsd and Atrn is 36% and between Dsd and ALP is 34% while the homology in intracellular domains is 45% and 44% respectively. The residues in black represent identical residues in Dsd and the Attractin family members. (B) The domain structure of Dsd and Atrn. Dsd and Atrn share essentially the identical domain structures, except that Dsd lacks one plexin repeat and the lectin C-type domain found in Atrn.

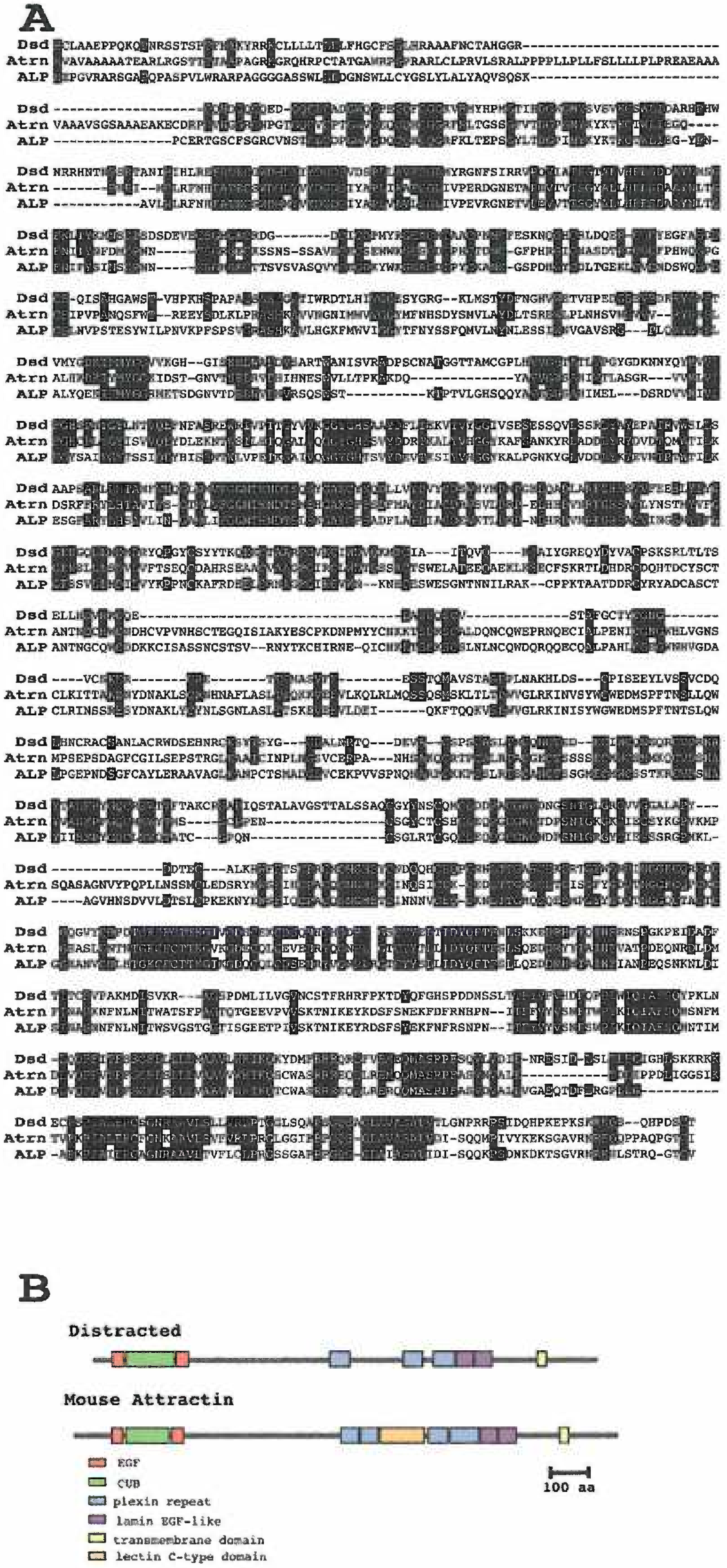
A
Dsd
Atrn
ALP
B
Distracted
Mouse Attractin
EGF
CUB
plexin repeat
lamin EGF-like
transmembrane domain
lectin C-type domain
100 aa

**Figure 2.** The 5' untranslated region of *distracted* (*dsd*) and developmental expression of *dsd*. (A) A cartoon representation of the cloned 5' UTR of *dsd* from adult flies had 276 bp upstream of the predicted ATG start codon. Then the first 171 bp after the ATG were spliced out of the first exon in contrast to the embryonic clone of dsd. This splicing would result in the first 57 a.a. after the starting methione to be unexpressed, the last seven of these residues constituting the beginning of the first EGF domain. (B) RT-PCR from indicated developmental stages was performed with primers specific to the 3' UTR of *dsd* using the *Drosophila* Rapid Scan cDNA panel from Origene that is normalized to the expression of *Drosophila* ribosomal protein 49 (RP49). Photoreceptors begin to differentiate in late second instar larvae.

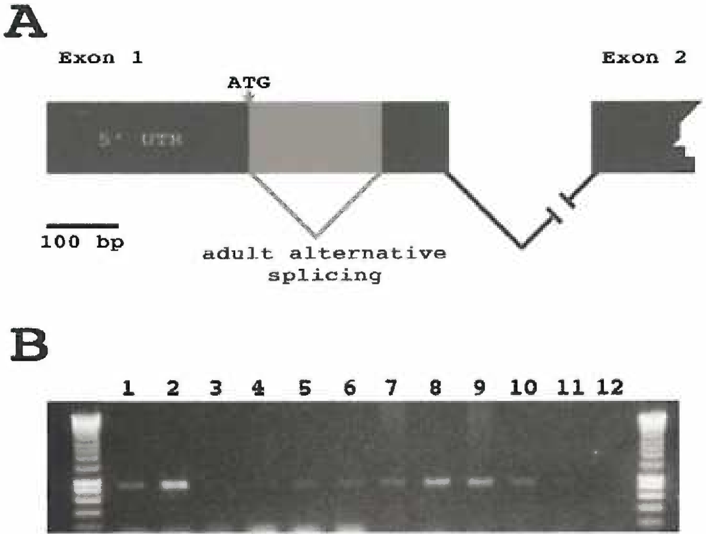

A
Exon 1
ATG
5' UTR
Exon 2
100 bp
adult alternative splicing
B
1 2 3 4 5 6 7 8 9 10 11 12

1. Embryo 0-4hrs
2. Embryo 4-8hrs
3. Embryo 8-12hrs
4. Embryo 12-24hrs
5. First instar
6. Second instar
7. Third instar
8. Pupae
9. Male head
10. Female head
11. Male body
12. Female body

**Figure 3.** In situ hybridization of embryos with *dsd* antisense (A-E) and sense (A'-E') probes. (A, A') Stage 4 embryos. The expression of *dsd* was high at this stage when the cell walls begin to form. Zygotic transcription has yet to begin. (B, B') Stage 5 embryos. The fully cellularized blastoderm showed high *dsd* expression in the cells and by the border between the cells and yolk. (C, C') Stage 8 embryos. The expression of *dsd* was seen in all tissues at this time of rapid germ band elongation. (D, D') Stage 9 embryos. No difference was seen between the antisense (D) and the sense (D') stage 9 embryos. Stage 10 and 11 showed similar results (data not shown). Stage 9-11 represents the period of slow germ band elongation. (E, E') Stage 12 embryos. The expression of *dsd* was apparent in all tissues at this time of rapid germ band retraction. Abbreviations: api amnioproctodeal invagination, cf cephalic furrow, cl clypeolabrum, nb neuroblasts, pl procephalic lobe, pNR procephalic neurogenic region, vnc ventral nerve cord.

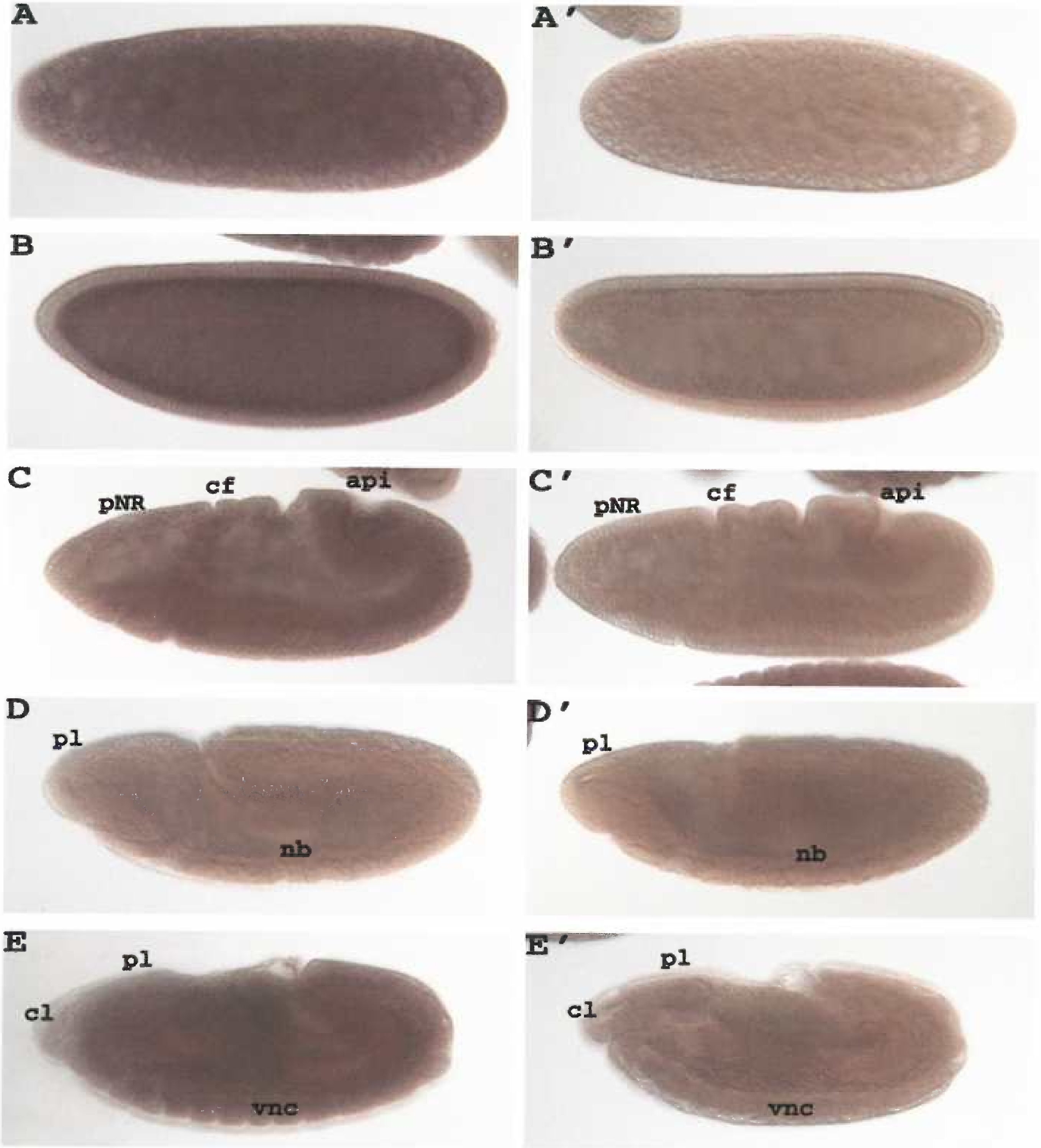
A
A′
B
B′
C
pNR
cf
api
C′
pNR
cf
api
D
pl
nb
D′
pl
nb
E
pl
cl
vnc
E′
pl
cl
vnc

**Figure 4.** Distracted expression in the third instar CNS. (A,B) Pre-incubation of anti-Dsd with GST fused to Dsd tail (B) but not GST alone (A) greatly reduced the staining of the eye-antennal disc and the optic lobe. Note that Dsd expression is strongest in the eye and antennal disc relative to the optic lobe (C-E) Dsd expression (red) colocalizes with 24B10 (blue), the photoreceptor marker. (F-H) Expression of Dsd in mature glial cells. (F) Location of glial cells as visualized by anti-Repo staining (blue). (G) Dsd expression in the thoracic ganglion (red). (H) The co-expression of Repo and Dsd appeared roughly equivalent in the visual system (arrow) and thoracic ganglion (arrowhead) glia. Eye disc (eye), antennal disc (ant), and optic lobe (opl). Scale bar; A, B = 40 μm; C-H = 20 μm.

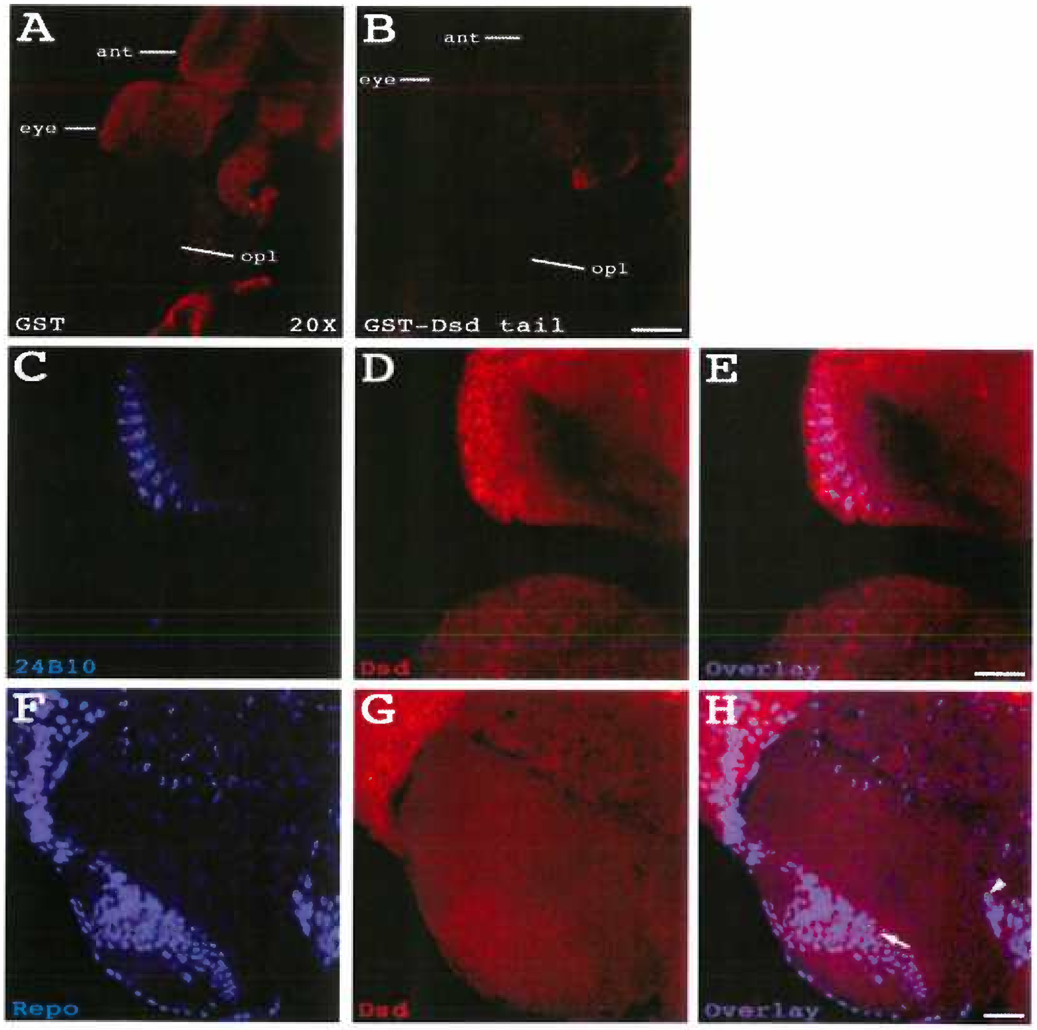
A
ant
eye
opl
GST
20X
B
ant
eye
opl
GST-Dsd tail
C
24B10
D
Dsd
E
Overlay
F
Repo
G
Dsd
H
Overlay

**Figure 5.** Transposable element insertions create hypomorphic *dsd* alleles and use of the DrosDel insertions created the deficiency *Df(3R)ED6274.* (A) Two lines, each carrying an insertion of a transposable EP-element in opposite orientations [*EP(3)3400* and *EP(3)3030*], 303 base pairs 5' to the *dsd* start codon were obtained from the Bloomington stock center. Both insertions are homozygously viable and have been renamed the *dsd*$^{P1}$ and *dsd*$^{P2}$ respectively. (B) Real-time PCR results for *dsd* expression level, normalized to actin 5C expression levels, from control (C.S.), *dsd*$^{P1}$, and *dsd*$^{P2}$ in cDNA prepared from adult flies. See Materials and Methods for details. (C) PCR on genomic DNA using primers outside the insertion sites for the parental RS elements CB-0262-3 and 5SZ-3265. The approximately 8 kb band only appeared in the lanes representing individual stocks of the created deficiency. The 1 kb ladder is from MBI Fermentas, top band of 10 kb.

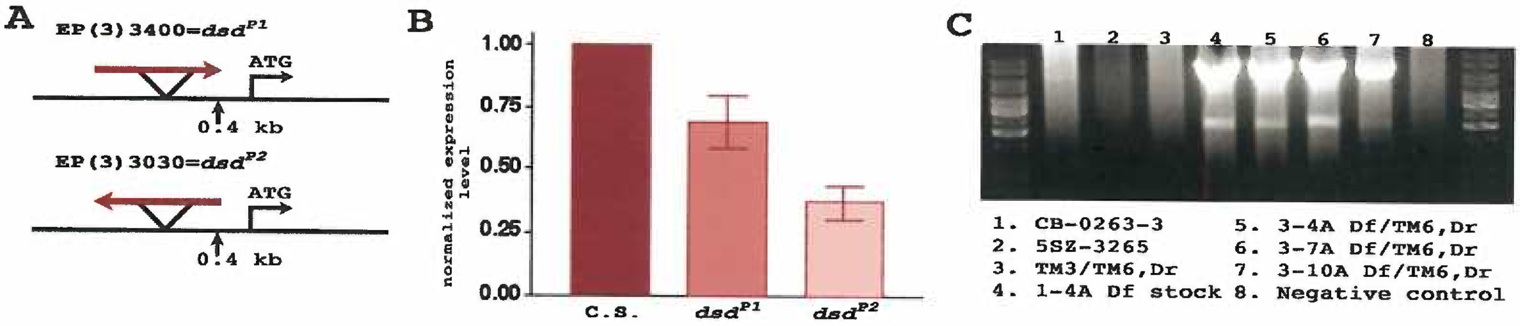
A
EP(3)3400=dsd^P1
ATG
0.4 kb
EP(3)3030=dsd^P2
ATG
0.4 kb
B
normalized expression level
1.00
0.75
0.50
0.25
0.00
C.S.
dsd^P1
dsd^P2
C
1
2
3
4
5
6
7
8
1. CB-0263-3
2. 5SZ-3265
3. TM3/TM6,Dr
4. 1-4A Df stock
5. 3-4A Df/TM6,Dr
6. 3-7A Df/TM6,Dr
7. 3-10A Df/TM6,Dr
8. Negative control

**Figure 6.** Photoreceptor axonal projections in *dsd*$^{P}$ mutants. (A-D) Optic lobes with attached eye discs from third instar larvae were immunostained with 24B10, a monoclonal antibody, which labels all photoreceptors and their axons. (A) Example of wild-type Canton S projections to the lamina (lam) by R1-R6 and the medulla (med) by R7 and R8. (B-D) Disrupted photoreceptor axon projections of *dsd*$^{P}$ and *dsd*$^{P}$/*Df* mutants. (B,C) The transheterozygous *dsd*$^{P1}$/*dsd*$^{P2}$ mutants showed disruption in the formation of the lamina and medulla. Arrowheads in (B) and (C) indicate gaps and dips in the lamina. In (C), the Bolwig's nerve (arrow) projected past the optic lobe and to the ventral nerve cord, shown by a longer view, including 327 more pixels in height, than in (A) and (B). (D) The projection of Bolwig's nerve (arrow) to the thoracic ganglion was also apparent in when the *dsd*$^{P}$ mutations were over the *Df* (*dsd*$^{P2}$/*Df* mutant representative), though not in all (data not shown).

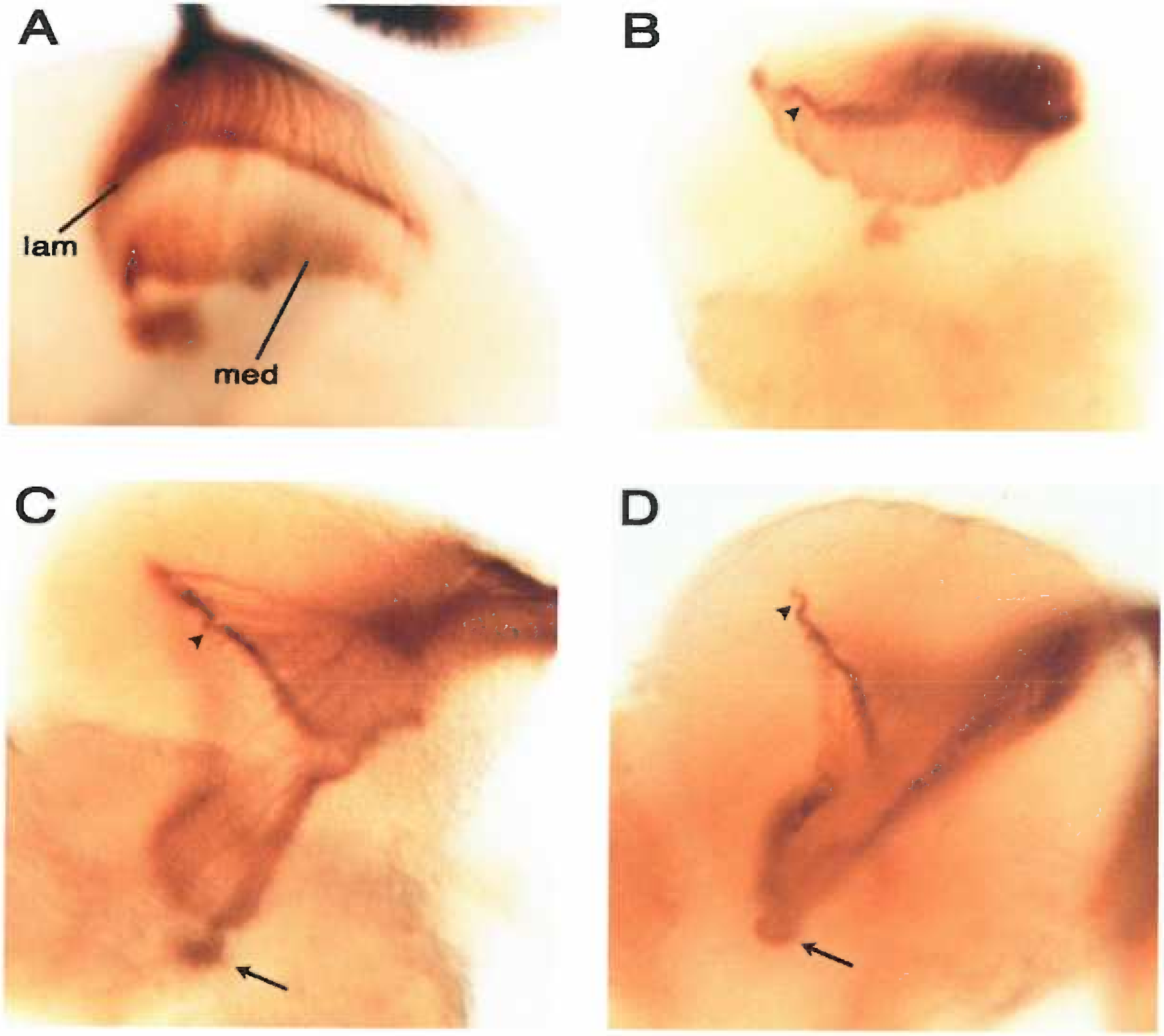
A
lam
med
B
C
D

# CHAPTER FOUR

## THE *DROSOPHILA* HOMOLOGUE OF ATTRACTIN INTERACTS WITH UBC13/BENDLESS TO INFLUENCE PHOTORECEPTOR PATHFINDING AND NEURONAL DEGENERATION.

Ruth E. Thomas, Jacqueline Parker, Michael A. Forte, Roger D. Cone

Vollum Institute, Oregon Health and Science University, 3106 SW Sam Jackson Park Road, Portland OR, 97239.

## ABSTRACT

Attractin (Atrn) is a single pass transmembrane protein containing extracellular epidermal growth factor (EGF), plexin, C-lectin, and CUB domains and a short cytoplasmic tail with no known signaling motifs. Studies in mammals have demonstrated that Atrn is involved in a wide array of biological processes, including immune cell interactions, pigmentation, energy homeostasis, myelination, and neuronal survival; however, the molecular mechanisms of Atrn action are unclear. Through two-hybrid analysis, we demonstrate that the C-terminal intracellular domain of Atrn interacts with the mammalian homolog of the yeast ubiquitin-conjugating enzyme 13 (UBC13), which is responsible for the generation of polyubiquitin chains through lysine 63 (K63) of ubiquitin. Furthermore, two-hybrid and biochemical assays show that the *Drosophila* Atrn homologue, which we have termed Distracted (Dsd), also directly interacts with the *Drosophila* orthologue of UBC13, Bendless (Ben). Genetic and morphological analyses in *Drosophila* show that the defects in photoreceptor pathfinding caused by hypomorphic mutations in *dsd* and *ben* are similar. Furthermore, these defects are accentuated in $ben^1;dsd^P$ double mutants, leading to structural abnormalities in the adult optic lobe. Additionally, age-dependent neurodegeneration is observed in the antennal lobes of both $ben^1$ and $dsd^P$ single mutants, a phenotype that is again amplified in $ben^1;dsd^P$ double mutants. These genetic and phenotypic results confirm the biochemical interactions observed between Ben and Dsd. Moreover, they establish roles for *dsd*, *ben*, and K63-linked protein ubiquitination both in axonal pathfinding within the developing *Drosophila* visual system and in neurodegeneration within the antennal lobe, providing the first insights into a molecular mechanism of Atrn action.

# INTRODUCTION

One of the earliest steps in the development of both the central and peripheral nervous system is the initiation of axon outgrowth from newly born neurons. Nascent axons then navigate towards their specific targets to establish the intricate network of connections found within the mature nervous system. In doing so, the growing axons must continually reassess their spatial environment and select a correct pathway among the maze of possible routes. A variety of molecular navigational systems governing axon pathfinding have now been identified, many involving the recognition of external cues by transmembrane receptors exposed by the axons and their growth cones (16, 99).

Roles in cell adhesion, guidance or signaling are all suggested by Atrn's structure (25). Atrn is a cell surface transmembrane protein that contains a CUB domain flanked by epidermal growth factor (EGF) domains and followed by four plexin repeats, a C-lectin domain, and two laminin-like EGF domains within its extracellular region, followed by a single transmembrane domain and a short intracellular C-terminal domain with no known signaling motifs (37, 71). Atrn was first identified and studied in the human immune system, where a secreted form of Atrn, representing the extracellular domain, is released by activated T-cells to modulate the interaction of activated T-cells and macrophages (27). Secreted forms of Atrn are generated by alternative splicing and appear to be only present in humans and rat (54, 94). Transmembrane forms of Atrn however are present in all metazoans and are structurally well conserved.

The transmembrane Atrn was first identified when the *mahogany* (*mg*) locus in mice was cloned and demonstrated to encode murine Atrn (37, 71). Recessive alleles at *mg* had been identified by virtue of their role as suppressors of yellow pigmentation and obesity, resulting from ectopic expression of the agouti protein in mouse strains containing dominant agouti alleles such as *lethal yellow* ($A^y$) (23, 67). Agouti is a paracrine factor secreted from dermal papilla cells, where it normally acts as an endogenous antagonist of the melanocortin 1 receptor (MC1R) expressed on melanocytes (22). When aberrantly expressed in the CNS, as in $A^y$ mice, agouti is also able to inhibit the central melanocortin 4 receptor (MC4R), resulting not only in pigment changes but also obesity (29). Another mouse mutation, *mahoganoid* (*md*), also suppresses pigmentation changes and obesity in $A^y$ mice (67). The protein encoded by the *md* gene, Mahogunin, is an E3 ubiquitin ligase (44, 82), suggesting an interaction between Atrn and ubiquitin-modification systems, although the details of this interaction remain to be precisely defined.

Roles for Atrn in neuronal development were initially demonstrated by the phenotypic analysis of *Atrn* gene mutations in mice, rats and hamsters (36, 54, 55). In each species, mutations in *Atrn* are characterized by progressive neural degeneration that first appears from 3 to 4 weeks of age in the case of strong mutant alleles, with vacuolization developing first in the brain stem, pons and outer thalamus and then extending into the deep cortex, hippocampus, and other areas. The initiation of myelination and the fundamental structures of the myelin sheaths are normal in the *Atrn* mutants, but significant deficits in the number of myelin lamellae and the number of myelinated fibers appear as *Atrn* mutants age and as neural degeneration develops. Pathologically, this progressive neurodegeneration and hypomyelination are also often accompanied by tremors and seizures. The studies also demonstrate the importance of the Atrn intracellular domain, since only transgenic expression of the transmembrane form of Atrn, not the secreted form, was able to rescue the neural degeneration and hypomyelination phenotypes present in mutant animals (54). Additional roles for Atrn in axonal outgrowth have been suggested by the observation that incubation of the extracellular domain of Atrn with cortical neurons inhibits neurite outgrowth (93). Atrn's role in neurite extension is possibly mediated through interaction with the microtubules. Following spinal cord injury, Atrn has been recently shown to be upregulated along with neuritin and microtubule associated protein 1a (MAP1A), overexpression of Atrn with neuritin and MAP1A in dorsal root ganglion (DRG) neurons from embryonic day 14 (E14) stimulates neurite outgrowth (21). However, the mechanisms by which Atrn regulates normal aspects of neuronal outgrowth and survival are still unclear.

To identify potential intracellular signaling pathways modulated by Atrn, we initially searched for proteins that interact with the intracellular, C-terminal domain of murine Atrn (residues 1301-1428) through a yeast two hybrid screen as described in chapter 2. One of the interactors identified in screens of an adult mouse brain library was a homologue of the yeast UBC13 protein. UBC13, with its partner Mms2 or UEV1A, conjugates ubiquitin onto substrates through lysine 63 (K63) (46, 103). In contrast to K48-linked chains, K63-linked polyubiquitin chains have been demonstrated not to result in the proteosomal degradation of modified substrates but, in contrast, initiate important regulatory cascades (28, 89, 92). A UBC13 orthologue has been characterized genetically in *Drosophila*, being encoded by the *bendless* (*ben*) gene. Previous analyses of *ben* mutations demonstrated that *ben* plays a key role in axonal pathfinding, particularly in the establishment of appropriate connections between photoreceptor cells and their targets in the CNS (69, 78). To test whether Atrn and UBC13 interact in vivo and to examine the putative role of Atrn-UBC13 interactions in the establishment of appropriate synaptic connections, we used the *distracted*$^{P}$ (*dsd*$^{P}$) hypomorphic mutations detailed in the previous chapter to examine photoreceptor development and neurodegeneration in *ben*, *dsd* and *ben;dsd* double mutants, to test the hypothesis that Dsd signals through Ben to regulate axonal pathfinding and neurodegeneration in vivo.

## MATERIALS AND METHODS

### Fly stocks and genetics

Fly stocks were kept at room temperature (20°C) and crossed at 25°C on standard fly medium. Canton S was used as wild type controls. The *EP(3)3400* (*dsd*$^{P1}$) and *EP(3)3030* (*dsd*$^{P2}$) lines were obtained from the Bloomington stock center. The *bendless*$^{1}$ line, gene on the X chromosome, was a gift from J. B. Thomas. *Ro-Tau-lacZ* line, insertion on the third chomosome, was a gift from U. Gaul. To create the deficiency covering 98A7 to 98B5, fly stocks *y*$^{1}$*w*$^{1}$*hsFlp70;TM2, Ubx/TM6, Sb*, *CB-0262-3*, and *5SZ-3265* were obtained from the Szeged stock center. Details on the crosses done are in chapter 2. In accordance with the Szeged stock center protocols this deficiency has been assigned as *Df(3R)ED6274*. The *Ro-Tau-lacZ* marker was recombined on to this chromosome for use in experiments examining R2-R6 axons in the *dsd*$^{P}$ mutants.

### Yeast two-hybrid

To confirm the interaction of homologous *Drosophila* proteins, the C-terminus of *distracted* (coding for 1187 to 1323 a.a.) and the N-terminus of *bendless* (1 to 68 a.a.) were cloned into the pGADT7 (AD) and pGBKT7 (DNA-BD) vectors respectively and co-transformed with each other or with empty or non-relevant vector constructs from Clontech. The p53/T-antigen fusions were used as a positive control.

### GST-pulldown

The full-length and N-terminus of Bendless was cloned into the pGEX-KG vector. GST-Ben fusion proteins were expressed as described in chapter 3. The Dsd tail along with the T7 epitope tag was cloned into the pMAL-c2E vector (New England Biolabs) and the maltose binding protein (MBP) fusion expressed according to manufacturer's instructions. Glutathione sepharose 4B (Amersham) was used to bind the GST proteins and buffer T (20mM Tris, 100mM KCL, 0.1 mM EDTA, 10% glycerol) used as the binding buffer for MBP-Dsd tail. The samples were run out on SDS-PAGE, transferred, and the MBP-Dsd tail protein detected by a monoclonal T7 antibody (Novagen).

### Immunohistochemistry

Optic lobes from third instar larvae were dissected and fixed in 4% paraformaldehyde for 1 hour, then washed with 10% HS-PBST (10% horse serum in phosphate buffered saline with Triton-X) and incubated overnight at 4° C in 1:100 24B10 (Developmental Studies Hybridoma Bank). The secondary was biotinylated horse anti-mouse (1:200) and ABC solution was made using the kit from Vector. DAB was used to visualize binding. Optic lobes were mounted in 50% glycerol and pictures taken at three focal planes, then overlaid in Adobe Photoshop. Scoring of mutant phenotypes was done with the original pictures. The phenotype of the third instar larval photoreceptor projections were scored blind to genotype and according to a qualitative 0-3 range score for lamina formation, medulla projections and overall shape of the photoreceptor projections. A score of 0 for the lamina represented a strait, connected curve; a score of 1 indicating that the curve was still connected but had some discontinuities (i.e., bumps) or became V-shaped rather than U-shaped; a score of 2 score indicating that the projections no longer terminated in a strait connected curve but had gaps, thickenings, or dips in the line; a score of 3 indicating that there was minimal to no laminal formation visible, usually accompanied by less spread. Wild-type C.S. laminar projections generally fell into the 0 and 1 scores while scores of 2 and 3 characterized disrupted lamina. Data was analyzed using the Kolmogorov-Smirnov test, available on-line at http://www.physics.csbsju.edu/stats/KS-test.hmtl, which tests for differences in the overall distribution of data between two groups

### Confocal imaging

For *Ro-Tau-lacZ*, rabbit anti-β–galactosidase (1:2000) (Carpel) was used with anti-Repo 8D12 (1:10) or anti-Fas III (1:50) (Developmental Studies Hybridoma Bank) and visualized with goat anti-rabbit Alexa 594 (1:500) and donkey anti-mouse Alexa 488 (1:500) secondary antibodies (Molecular Probes), using 10% normal donkey or goat serum in PBST (0.6% Triton). Brains were imaged using the Icon TE300 Byroad Scanning Laser 1024 at 40x.

### Paraffin embedding

Adult fly heads were embedded in paraffin and sectioned as described (19). Briefly, flies were loaded onto collars with control *sine oculis* (*so*) flies (eyeless) to separate the genotypes then fixed in Carnoy (60% ethanol: 30% chloroform:10% acetic acid) for 4 hrs. The collars were then washed in ethanol and put into methyl benzoate overnight at room temperature. The next day, the methyl benzoate was exchanged with paraffin over 4 hrs at 60°C. Collars were subsequently embedded in paraffin and the paraffin blocks containing the heads removed from the collars and sectioned serially at 8 μm. The sections were mounted on polylysine-coated slides and allowed to dry overnight in a dust-free environment. Sections were then cleared of paraffin using Safeclear (Fisher Scientific) and overlaid with coverslips. The antennal lobes anatomically comprised from where the antennal nerves entered the brain to where the round structure of the lobes flatten out. Vacuoles were counted from both lobes from each brain.

## RESULTS

### The *Drosophila* Attractin homologue Distracted interacts physically with Bendless

Using two different assays, we confirmed that, like their mammalian homologues, *Drosophila* Bendless (Ben) and the C-terminal tail of Distracted (Dsd) could interact. First, yeast two-hybrid assays were used to demonstrate an interaction between the C-terminal domain of Dsd (residues 1187-1323) and the N-terminus of Ben (residues 1-68) (Fig. 1A). In addition, GST-pulldown experiments confirmed the direct interaction of the C-terminal region of Dsd with this same N-terminal domain of Ben, although the interaction appeared to be stronger when full length Ben was used in these assays (Fig. 1B). Thus, the physical interaction between Atrn and UBC13 first observed in the context of mammalian proteins also occurs with their *Drosophila* homologues.

### Photoreceptor pathfinding defects in *dsd* mutants

Examination of genomic databases indicates that two existing fly lines contain insertions of the EP transposable element in opposite orientations, each 303 bp from the start codon of the Dsd protein. The initial characterization of these inserts, now referred to as $dsd^{P1}$ and $dsd^{P2}$, is presented in chapter 3. Briefly, real-time PCR analysis revealed that *dsd* expression is decreased in $dsd^{P1}$ and $dsd^{P2}$ flies to 70% and 38% of wild-type

Canton S (C.S.) levels, respectively. These *dsd*$^{P}$ mutations also affect photoreceptor pathfinding whether transheterozygous or over *Df(3R)ED6274*.

Drosophila have compound eyes composed of ~800 ommatidia, groups of eight photoreceptors, all of which must project their axons to the optic lobe, which is composed of a series of ganglia called the lamina, medulla, lobula and lobula plate (97). During the differentiation of the adult photoreceptors in the third instar larval stage, the axons of photoreceptor neurons R1-R6 project to the lamina, stopping between two layers of glia, which serve as an intermediate target for the axons. In contrast, axons of the R7 and R8 photoreceptors pass through the lamina and project to specific neuropil layers within the medulla (74). Normally, photoreceptor axons fasciculate into distinct bundles and display highly ordered trajectories to and through the lamina (17). In *ben*$^{1}$ mutants, many of the photoreceptor axons do not appear to be appropriately fasciculated into bundles, as previously noted (69). Furthermore, the photoreceptor axons entering the lamina from the retina are disordered and no longer evenly spaced when compared to wild-type larvae (78). In addition, the orderly arrangement of the R7 and R8 photoreceptor projections to the medulla is disrupted, with many R7 and R8 axons terminating in inappropriate positions within the medulla.

To compare the phenotypic consequences of hypomorphic *dsd* mutations during photoreceptor axonal projection, optic lobes with attached eye discs were dissected from the third instar larvae carrying individual *ben*$^{1}$ and *dsd*$^{P}$ mutations and immunostained with monoclonal antibody 24B10, which labels all photoreceptors and their axons. The *dsd*$^{P1}$ and *dsd*$^{P2}$ flies were also crossed to *ben*$^{1}$ flies, to determine whether a genetic interaction between *ben* and *dsd* could be demonstrated. Defects in photoreceptor projections were quantified by comparison of mutant to wild-type larvae (Fig. 2A). Optic lobes examined from the single *ben*$^1$ mutants typically displayed a phenotype similar to that seen in the *dsd*$^P$ mutants, whether transheterozygous or over a deficiency, with disorganized and unevenly spaced bundles of photoreceptor axons exiting the optic stalk to the lamina (Fig. 2B,C). Termination of the R1-R6 projections in the lamina no longer occurred in a connected curve, having instead gaps and dips along the laminal extent. The R7 and R8 protections were also disorganized compared to wild-type C.S. flies, with shorter and unevenly spaced projections, which appeared to terminate in inappropriate levels within the medulla. Defects were also occasionally observed in the larval photosensing nerve, Bolwig's nerve (47), which in mutant larvae had projected inappropriately to the thoracic ganglion (data not shown). In the double homozygous *ben*$^1$;*dsd*$^P$ mutants, either *ben*$^1$ flies transheterozygous for *dsd*$^P$ mutations or individual *dsd*$^P$ mutations over the deficiency, photoreceptor axon pathfinding defects were amplified beyond those observed in individual *dsd*$^P$ mutants or *ben*$^1$ mutants alone (Fig. 2D). Typically, the spacing between the bundles of the photoreceptors exiting the optic stalk were minimal and, at times, no longer present, with reductions in the extent of the axonal elaboration. R1-R6 photoreceptor axons produced minimal to no visible laminal line. R7 and R8 projections sometimes did not project past the lamina or could no longer be distinguished from the R1-R6 axons. These phenotypes were not fully penetrant; consequently, each optic lobe was scored separately for the formation of the lamina, medulla, and shape of the photoreceptor projections.

Defects were seen in all the genotypes but to determine whether there was a statistical difference between the scores given in each group, the Kolmogorov-Smirnov test was used. This test determines whether there is an overall significant difference in the distribution of the data in two groups and can be used to evaluate data that is not normally distributed. By the Kolmogorov-Smirnov test, the distribution of $dsd^{P1}$ laminal projection scores into the different categories was not statistically different from the distribution of C.S. laminal scores, $P= 0.661$ (Fig. 2 E). The $dsd^{P1}$ would be the weakest allele according to the RT-PCR analysis in the previous chapter. The scores of the $dsd^{P2}$ allele by itself though were statistically significant compared to C.S., $P= 0.026$ (Fig. 2F), as were the scores of the $ben^{1}$ single mutant, $P= 0.028$. The scores of the $dsd^{P1}/dsd^{P2}$ transheterozygous were also not significant from the C.S., $P= 0.190$. The $P$ values increased when the distributions of the $dsd^{P}/Df$ scores were compared to the C.S. scores. The $P$ value reached significance for $dsd^{P1}/Df$, P= 0.027, in contrast to $dsd^{P1}$ alone (Fig. 2E), and increased in significance for $dsd^{P2}/Df$, $P= 0.004$ (Fig. 2F). The $P$ value was not significant when the $dsd^{P1}$ was compared to $dsd^{P1}/Df$ ($P= 0.476$) or when $dsd^{P2}$ was compared to $dsd^{P2}/Df$ ($P= 0.999$). The double homozygous $ben^{1};dsd^{P}$ and $ben^{1};dsd^{P}/Df$ mutants (Fig. 2E, F) were all highly significantly different from the single $ben^{1}$ or $dsd^{P}$ mutants, $P\leq 0.001$, as were the $ben^{1};dsd^{P1}/dsd^{P2}$ scores from the $dsd^{P1}/dsd^{P2}$ scores.

The defects observed in laminar formation could reflect defects in glial cell migration to the lamina, as the photoreceptor axons induce the scaffold necessary for glial migration (20). Conversely, the laminar defects seen could reflect defects in the ability of the R1-R6 photoreceptor axons in the $ben^{1}$ and $dsd^{P}$ mutants to respond to cues provided by the lamina glia, as these cells represent the intermediate target for the R1-R6 axons during their projection to the lamina (97). Using a marker (*Ro-Tau-lacZ)* expressed in photoreceptors R2-R5, we examined the projection pattern of this subset of retinal cells in *ben*$^{1}$, *dsd*$^{P}$ and *ben*$^{1}$;*dsd*$^{P}$/*Df* double mutants, relative to the positioning of mature glia in these mutant backgrounds (as determined by immunostaining with antibodies to the glial cell marker, Repo) (107). In wild-type larvae, all R2-R5 photoreceptors terminated between the layers of lamina glia (Fig. 3A). In *ben* and *dsd* single mutants, a subset of the R2-R5 axons projected through the lamina glia and into the medulla (Fig. 3B,C). These projections past the lamina occurred even when the lamina did not have gaps, which would give the mutants a lower score according to the categories used for the 24B10 staining. The number of glia did not appear grossly different, indicating that differentiation and migration of glia was not overtly altered in the single mutants. In the double homozygous mutants, the dramatic disorganization of the photoreceptor projections made defining the presumptive lamina difficult. However, in those double homozygous optic lobes where a somewhat normal projection pattern was observed (Fig. 3D), glia appeared to migrate to roughly appropriate positions in the lamina but then seemed to follow the pattern of the photoreceptors rather than organize themselves into discrete layers in the lamina. Some thick bundles of R2-R5 photoreceptors could be clearly seen projecting past the lamina and into the medulla (Fig. 3D).

One cause of overshooting the lamina is the loss of compartmental boundaries between the inner proliferation center (IPC) and the lamina. This boundary loss and overshooting phenotype is seen in the *slit*$^{dui}$ hypomorphic mutants and in RNAi experiments knocking down expression of Robo1-3, the receptors for Slit (98). Slit and Robo are molecules extensively studied and shown to be involved in axonal pathfinding and cell migration.

To determine if the cause of overshooting the lamina in the *ben* and *dsd* mutants was due to disruption of the IPC border, Fasciclin III (Fas III) staining was used to visualize the IPC (98). In the *dsd*$^{P2}$*/Df* or *ben*$^{1}$ single mutants, no compromise of the compartmental boundary between the Fas III staining and the R2-R5 axons appeared to occur (Fig. 4B,C), though the photoreceptors showed uneven spacing compared to wild type (Fig. 4A). In the *ben*$^{1}$*;dsd*$^{P2}$*/Df* double homozygous, the IPC again appeared to be intact with no mixing of compartmental boundaries (Fig. 4D), though the spacing of the photoreceptor axons was even more uneven than that seen in the single mutants. These results indicated that the projection of the R2-R5 axons through the lamina seen in the single and double homozygous mutants was not due to compartmental boundary defects.

During the transition from the larval to adult visual system, photoreceptor axons in *Drosophila* induce the proliferation and differentiation of their secondary neurons in the optic lobe, the lamina precursor cells, as well as go through extensive morphogenic changes (20, 66, 97). To determine whether the pathfinding defects observed in *ben*$^{1}$, *dsd*$^{P}$ and *ben*$^{1}$*;dsd*$^{P}$ third instar larvae might impact the adult morphology, adult male heads were examined for visual system structural abnormalities (Fig. 5A-D). While no abnormalities in adult brain morphology were visible at this level of resolution in either of the single mutants, the double homozygous *ben*$^{1}$*;dsd*$^{P}$ flies showed marked structural abnormalities of the optic lobe at Day 1 post eclosion (Fig. 5D), with the lamina and medulla no longer separated and even derangement of the lobula shape. Thus, the photoreceptor pathfinding abnormalities of the double homozygous animals had striking consequences in the adult animal and indicated that the morphogenetic movements of the optic lobe compartments in the *ben*$^{1}$*:dsd*$^{P}$ double homozygous flies were compromised.

The genetic and biochemical data outlined above supports the critical role of the Dsd/Ben interaction during photoreceptor pathfinding. Data in the previous chapter shows that Dsd is expressed most highly throughout the eye and antennal discs with lower levels of staining in the optic lobes and thoracic ganglion. Dsd staining in the eye disc colocalizes with 24B10 staining, which identifies photoreceptor cells, although Dsd expression is not limited to these cells during eye development. Thus, Dsd is expressed in appropriate spacio/temporal pattern to have an impact on photoreceptor axon pathfinding, although its broad expression pattern suggests a permissive rather than instructive role for Dsd in this process.

### Neurodegeneration associated with *ben* and *dsd* mutations

Mutations in mammalian genes encoding Atrn result in progressive neurodegeneration, characterized by the age-dependent vacuolization of the CNS (36, 54). To determine if age-dependent neurodegeneration was also associated with mutations in *dsd* or *ben* in *Drosophila,* sections of adult heads were prepared from flies carrying *dsd*, *ben*, or both mutations and assessed for the presence of age-dependent CNS vacuoles. As the flies aged, vacuoles appeared in both the optic and antennal lobes of mutant but not wild-type flies (Fig. 5E-H). Since the degeneration present in optic lobes may have arisen from the photoreceptor pathfinding defects generated by these mutations (20, 31), age-dependent vacuolization of optic lobes was not quantified. However, since no gross morphological defects appeared to be initially present in the antennal lobes, we quantified vacuole formation in this region of the CNS as flies aged.

Vacuoles appeared in the antennal lobes of the double mutant animals three days post eclosion (Fig. 6A). The antennal lobes of *ben*$^1$ mutants also exhibited vacuolization at this time, although at reduced levels from double *ben*$^{1}$;*dsd*$^{P}$ mutants. Antennal lobe vacuoles were not present in *dsd* mutant flies at three days of age (data not shown). Vacuolization continued to increase in both *ben*$^{1}$ and *ben*$^{1}$;*dsd*$^{P}$ flies until Day 6. However, between Day 6 and Day 12, there was no additional significant increase in the number of vacuoles (Fig. 6A). Double mutant flies consistently survived up to twelve days post eclosion. Therefore, single and double mutants as well as wild-type controls were aged twelve days and the number of vacuoles present throughout the antennal lobes counted. After twelve days, *dsd*$^{P}$ mutants showed a small, though consistent, and significant increase in the number of antennal lobe vacuoles compared to controls (Fig. 6B), while *ben*$^{1}$ mutants showed much higher levels of antennal lobe vacuolization than the *dsd* mutants (note scale differences) (Fig. 6C). The double *ben*$^{1}$;*dsd*$^{P}$ mutants exhibited a synergistic increase in the number of antennal lobe vacuoles compared to *dsd*$^{P}$ and *ben*$^{1}$ mutants alone (Fig. 6C). These results demonstrated that mutations in the *Drosophila dsd* gene result in age-dependent neurodegeneration, as do mutations in the genes encoding Atrn in a variety of mammals. Furthermore, the genetic interaction between *dsd* and *ben* observed in photoreceptor axonal pathfinding was also reflected in the context of enhanced age-dependent neurodegeneration seen within the antennal lobes of the combined mutations of these two genes.

## DISCUSSION

The identification of UBC13/Ben as a partner for Atrn/Dsd allows greater insight into possible molecular functions of the Atrn family of proteins in the nervous system. Direct physical interaction between the *Drosophila* homologues of Atrn and UBC13, Dsd and Ben, has been demonstrated by yeast two-hybrid and GST pulldown assays, confirming the original results of yeast two-hybrid screens of an adult mouse brain library with the Atrn C-terminal tail. We have demonstrated that the interaction between Dsd and Ben is functionally relevant by characterizing the phenotypic interaction between *ben* and *dsd* mutant alleles during the establishment of the fly visual system. As previously noted, mutations in *ben* result in defects both in giant fiber and photoreceptor pathfinding (69, 78). Our characterization of the $dsd^{P}$ mutant flies has shown that $dsd^{P1}$ and $dsd^{P2}$, which have 70% and 38% expression levels of *dsd* transcript respectively, result in defects in photoreceptor axonal pathfinding very similar to those seen in $ben^{1}$ mutants; the spacing of the photoreceptor axons is uneven and lamina formation is aberrant. Additionally, the shape of the projection field and formation of the medulla is altered. The increase in *P* value when the $dsd^{P}$ alleles are over the deficiency would seem to indicate that they are indeed hypomorphic though the characterization of the wild-type *dsd* allele over the deficiency would be the true test. One reason perhaps that the $dsd^{P1}$ scores are not statistically different from the $dsd^{P1}/Df$ scores are that the categorization of the photoreceptor phenotype is too broad to differentiate the difference in single allele strength as the categorization used to quantify the photoreceptor phenotypes had to be necessarily broad in order to cover the range of phenotypes observed from C.S. to the $ben^{1};dsd^{P}$ double homozygous mutants.

In $ben^{1};dsd^{P}$ double mutant larvae, a greater percentage of the photoreceptor projections are aberrant, as would be expected if the direct physical interaction between the two gene products (established by the biochemical assays outlined above) play a functional role during the establishment of the fly visual system. The disruption of photoreceptor pathfinding is also more severe in the double $ben^{1};dsd^{P}$ mutants, with often no formation of a lamina or aberrant projections extending beyond the medulla. The normal array of the photoreceptor axons is also compromised, which fits with a previous study showing inhibition of neurite outgrowth when exogenous Atrn is incubated with a cell line of differentiating cortical neurons (93). Additionally, specific staining of the R2-R5 photoreceptors reveals that some of these axons do not stop at the lamina in the single mutants though glial migration is not grossly compromised. In the *ben*$^1$;*dsd*$^P$ double mutant larvae, the disruption of the photoreceptor pathfinding is much more severe but, again, the glial cells did appear to migrate appropriately, although they were not arranged in the ordered fashion observed in wild-type controls.

Photoreceptor axons have been shown to participate in both the guidance of glial migration and the differentiation of their secondary neurons in the optic lobe (20, 66, 97). Thus, the photoreceptor pathfinding defects that we observed may be due to defects in signaling within the axons themselves or in the failure of glial cells to respond to appropriate cues in mutant larvae. Further study of glial migration in mutant larvae by clonal analysis should help to define more precisely the key target cells and the mechanisms of action of the *dsd/ben* interaction, ultimately leading to the pathfinding defects observed.

Immunohistochemical analysis shows expression of Dsd protein in the eye-antennal disc and the brain of third instar larvae (see chapter three). Expression of Dsd coincided with sites of *ben* mRNA expression, which is seen in the eye-antennal disc along with abundant expression in the optic lobe and ventral nerve cord (69). The generalized presence of Dsd and *ben* in the developing CNS suggests that Dsd and Ben may have additional roles in the developmental and morphological changes that occur throughout pupation and formation of the adult brain. Still, both Dsd and Ben appear to be expressed in a correct spatio/temporal context to affect photoreceptor pathfinding, although our data suggest that they are likely serving a permissive rather than instructive role.

In adult *Drosophila*, severely aberrant morphology is present in the optic lobes of *ben*$^{1}$;*dsd*$^{P}$ double mutants. The morphogenetic failure of the lamina, medulla and even lobula suggest that the compartments of the optic lobe fail to move properly during pupation. We show that the IPC boundary is intact at the third instar stage in both single *ben*$^{1}$ and *dsd*$^{P}$ mutants and double *ben*$^{1}$;*dsd*$^{P}$ mutants. Therefore the loss of compartmental boundaries seems unlikely, though there may be defects in the differentiation of downstream neurons. Thus, the morphogenetic defects seen in the optic lobes of adult double homozygous *ben*$^{1}$;*dsd*$^{P}$ mutants seem most likely to arise during the morphogenetic events of pupation, perhaps due to failure of the lamina to twist properly. Nevertheless, these findings support the conclusion that *ben* and *dsd* participate in the same or parallel signaling pathways required for axonal pathfinding of *Drosophila* photoreceptors and, thus, the subsequent differentiation and organization of the optic lobe.

Besides the suppression of $A^{y}$-generated obesity (67), the most prominent phenotype of Atrn-deficient mammals is neurodegeneration and hypomyelination (36, 54). Neurodegeneration in *Atrn* mutants begins in the brain stem and then spreads throughout the nervous system. In *dsd*$^{P}$ and *ben*$^{1}$ single mutants and in *ben*$^{1}$;*dsd*$^{P}$ double mutants, age-dependent neurodegeneration, marked by the formation of vacuoles, is observed in the antennal and optic lobes, phenotypes analogous to the neurodegeneration observed in a variety of mammals carrying *Atrn* mutations. As the vacuoles in the optic lobes of the double homozygous *ben*$^{1}$;*dsd*$^{P}$ mutants could be due to the extremely aberrant morphology of this structure that occurs when both mutations are present, we focused on the vacuolization of the antennal lobe. In *dsd*$^{P}$ and *ben*$^{1}$ mutants, vacuoles appear in the antennal lobes at low levels, but in *ben*$^{1}$;*dsd*$^{P}$ double mutants, the number of vacuoles greatly increased compared to either mutant alone. The neurodegeneration observed in *ben*$^{1}$ mutants is a new finding. Indeed, the higher levels of vacuolization present in the *ben*$^{1}$ mutants compared to *dsd*$^{P}$ mutants perhaps suggests the existence of other targets for Ben-mediated ubiquitination that are required for neuronal cell survival besides those proteins that Dsd signaling would target. However, even in *ben*$^{1}$;*dsd*$^{P}$ double mutants, degeneration is confined to the antennal lobes and the optic lobes, despite the expression of both proteins in other areas of the CNS; this may reflect cell-specific sensitivity of visual and olfactory centers to reductions in the level of Dsd and Ben.

A similar selective neurodegeneration of the antennal lobe has been recently described in flies with hypomorphic alleles of *futsch*, the *Drosophila* MAP1B homologue, despite the widespread expression of *futsch* (19). MAP1B also plays a key role in meditating the turning of axons, and thus axonal pathfinding, by merit of its ability to link surface proteins to the cytoskeleton (7, 61, 76). Notably, Atrn has been reported to interact with a related isoform of MAP1B, MAP1A, and overexpression of Atrn with neuritin and MAP1A stimulates neurite outgrowth in E14 DRG neurons (21). Our yeast two-hybrid screen also identified both MAP1A and MAP1B as potential interacting partners. Therefore, the selective vacuolization of the antennal lobe in the *futsch* mutants provides an additional avenue to explore Dsd function and a good example of cell specific susceptibility to degeneration.

Cell specific susceptibility is a common theme in neurodegenerative diseases, as is the essential role of the immune system, both innate and adaptive (75). Atrn is expressed on the surface of activated T-cells, secreted by activated human T-cells, and modulates immune cell interactions (25). UBC13/Ben is essential to innate immunity in both mammals and *Drosophila*, and it plays a key role in adaptive immunity in mammals. Thus, although the mechanism by which vacuoles develop in the CNS of mammals lacking Atrn function or in *Drosophila* lacking Dsd or Ben function remains to be determined, a comparison with the actions of these proteins with respect to immune responses may ultimately provide insights into these degenerative mechanisms.

Protein ubiquitination involves the sequential action of an ubiquitin-activating enzyme (E1), a ubiquitin-conjugating enzyme (E2) (represented here by the UBC13/Ben protein), and a ubiquitin-protein ligase (E3) (83). E3s bind both E2 and substrate, thereby facilitating the transfer of ubiquitin molecules from the E2 to the target. UBC13 E2 function is mediated by a complex of the UBC13 protein and an obligate partner protein, UEV1A (46, 103). In this complex, the N-terminal domain of UBC13 is responsible for binding to the RING domain in downstream E3 ubiquitin ligases (63). However, in contrast to K48-dependent ubiquitination, which targets proteins for degradation by the proteosome, K63 ubiquitination, which is mediated by UBC13/UEV1A, shares common features with other forms of covalent modification (e.g., phosphorylation) and results in the activation of signaling cascades (84). For example, both are reversible; thus, part of the intracellular pathway involving Ben and Dsd is likely to involve a de-ubiquitination enzyme (87). In addition, both are highly specific and controlled by a diverse set of enzymes; both the fly and mammalian genomes encode tens of E2 enzymes and hundreds of different E3s. Thus, although many substrates are likely recognized by Ben and subject to K63 ubiquitination, target specification would be mediated by the appropriate E3 partner. Though the identity of the relevant E3 partner, or de-ubiquitination enzyme, has yet to be defined for Dsd, a potential E3 ligase in the case of mammalian Atrn has been proposed to be encoded by the *mahogunin* gene: *mahoganoid* mutations in the mouse *mahogunin* gene lead to phenotypes almost identical to *Atrn* mutations (44, 67). As might be predicted, the *Drosophila* genome contains a gene (CG9941) that encodes a protein with high similarity to the mouse Mahogunin, suggesting additional functional conservation in this signaling pathway.

Finally, in the case of the TNFα receptor, the best-characterized mammalian receptor that uses K63 ubiquitination for initiation of its intracellular cascade, the receptor protein itself is not subject to modification by K63-linked ubiquitins (87). Rather, key members of the complex assembled by the intracellular receptor domains are modified by this recruitment. TNFα receptor activation leads to the recruitment of a number of receptor-associated proteins to its intracellular domains, among them RIP and a K63 ubiquitin ligase, TRAF2. The K63 polyubiquitination by UBC13 of TRAF2 (and potentially TRAF2 of RIP) then appears to stimulate the binding of a kinase complex to RIP, thereby activating the TAK1 protein kinase, and ultimately resulting in the expression of NF-κB-dependent genes. In the case of Atrn/Dsd-activated signaling, it is tempting to speculate then that a similar cascade of modifications also exists, leading to the activation of transcriptional systems responsible for the recognition and response by photoreceptor axons to appropriate guidance cues and to the protection of the antennal lobe from neurodegeneration.

Our characterization of the physical and genetic interactions between *Drosophila* Dsd and Ben provides potential insight into the mechanisms underlying Atrn action: our data suggest a model whereby Atrn/Dsd activation (by a signal that remains to be identified) is transmitted through UBC13/Ben, resulting in K63 ubiquitination of a downstream target, which ultimately mediates appropriate axonal guidance and neuronal survival. Further studies will clarify the role that interactions between Dsd and Ben play in photoreceptor pathfinding, optic lobe morphology, neuronal survival, and the identity of downstream effectors in this pathway.

**Figure 1**. Confirmation of the biochemical interaction between Distracted (Dsd) and Bendless (Ben). (A) Yeast two-hybrid assay showing specific interaction between the Dsd C-terminal tail (residues 1187-1323) and the N-terminus of Ben (residues 1-68). Fusions were made to the GAL4 activation domain (AD) or DNA binding domain (DNA-BD) respectively and tested in combination with each other, with control proteins and the GAL4 domains alone. (B) GST pulldown assay demonstrates direct interaction between the Dsd C-terminal tail and both full-length Ben and N-terminal Ben. The MBP fused to Dsd-C-terminal domains was detected using a monoclonal antibody directed to the T7 epitope. The input represents 20% of the T7-tagged maltose binding protein (MBP) fused to the Dsd tail used in the pulldown assays.

**A**

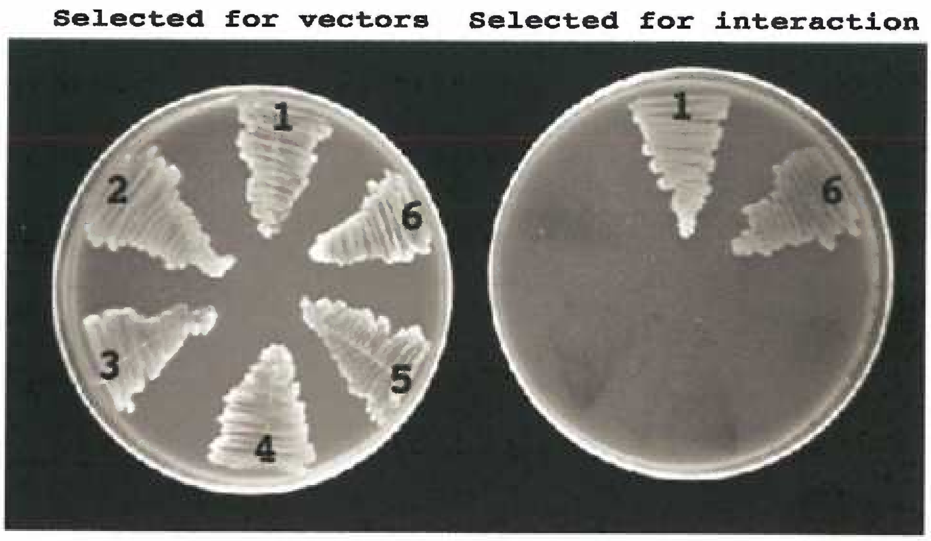
Selected for vectors
Selected for interaction
1
2
6
3
5
4
1
6

1. DNA-BD-p53/
   AD-T-antigen
2. DNA-BD/AD
3. DNA-BD-Lamin/
   AD-Dsd tail
4. DNA-BD/AD-Dsd tail
5. DNA-BD-N-term Ben/
   AD
6. DNA-BD-N-term Ben/
   AD-Dsd tail

**B**

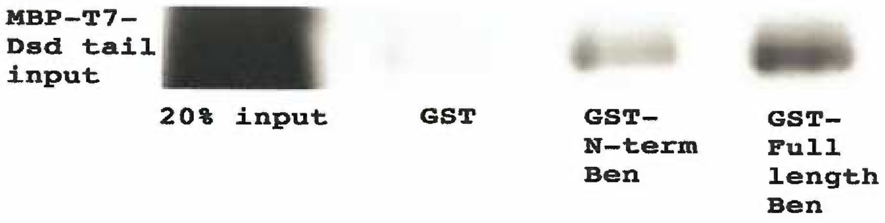
MBP-T7-
Dsd tail
input
20% input
GST
GST-
N-term
Ben
GST-
Full
length
Ben

**Figure 2.** Assessment of photoreceptor axonal projections in *ben*$^{1}$, *dsd*$^{P}$, and *ben*$^{1}$;*dsd*$^{P}$ mutants (A-D). Optic lobes with attached eye discs from third instar larvae were immunostained with the monoclonal antibody 24B10, which labels all photoreceptors and their axons. (A) Example of wild-type photoreceptor projections to the lamina (R1-R6; lam) and medulla (R7 and R8; med). (B-D) Disrupted photoreceptor axon projections and lamina formation in individual *ben* and *dsd*$^{P}$ mutants and in double *ben*$^{1}$;*dsd*$^{P}$ mutants. Arrowhead in (B) and (C) indicates gaps or dips in lamina. Defects in the medulla projections and overall shape of the photoreceptor projections are also apparent. (E-F) Graphic representation of phenotype distribution of disrupted laminal projections. Each optic lobe was scored separately. (E) The percentage distribution into categories of laminal projection formation for the *dsd*$^{P1}$ allele by itself, over *Df(3R)ED6274* (*Df*), and in the presence of the *ben*$^{1}$ for the double homozygous *ben*$^{1}$;*dsd*$^{P1}$ or *ben*$^{1}$;*dsd*$^{P1}$/*Df*. *ben*$^{1}$ (n=38), *dsd*$^{P1}$ (n=34), *dsd*$^{P1}$/*Df* (n=18), *ben*$^{1}$;*dsd*$^{P1}$ (n=36), *ben*$^{1}$;*dsd*$^{P1}$/*Df* (n=41), (F) The percentage distribution into categories of laminal projection formation for the *dsd*$^{P2}$ allele by itself, over *Df*, and in the presence of the *ben*$^{1}$ for the double homozygous *ben*$^{1}$;*dsd*$^{P2}$ or *ben*$^{1}$;*dsd*$^{P2}$/*Df*. *ben*$^{1}$ (n=38), *dsd*$^{P2}$ (n=32), *dsd*$^{P2}$/*Df* (n=29), *ben*$^{1}$; *dsd*$^{P2}$ (n=32), *ben*$^{1}$; *dsd*$^{P2}$/*Df* (n=25). The single *ben*$^{1}$ allele distributions are represented in both graphs. Scores for C.S. (n=40), *dsd*$^{P1}$/*dsd*$^{P2}$ (n=21), *ben*$^{1}$; *dsd*$^{P1}$/*dsd*$^{P2}$ (n=32) were also recoreded (data not shown). Defects in medulla projections and the overall spread and shape of the photoreceptor projections were also seen with more derangement present when the *dsd*$^{P}$ mutants or the *dsd*$^{P}$ mutants over the *Df* were combined with *ben*$^{1}$.

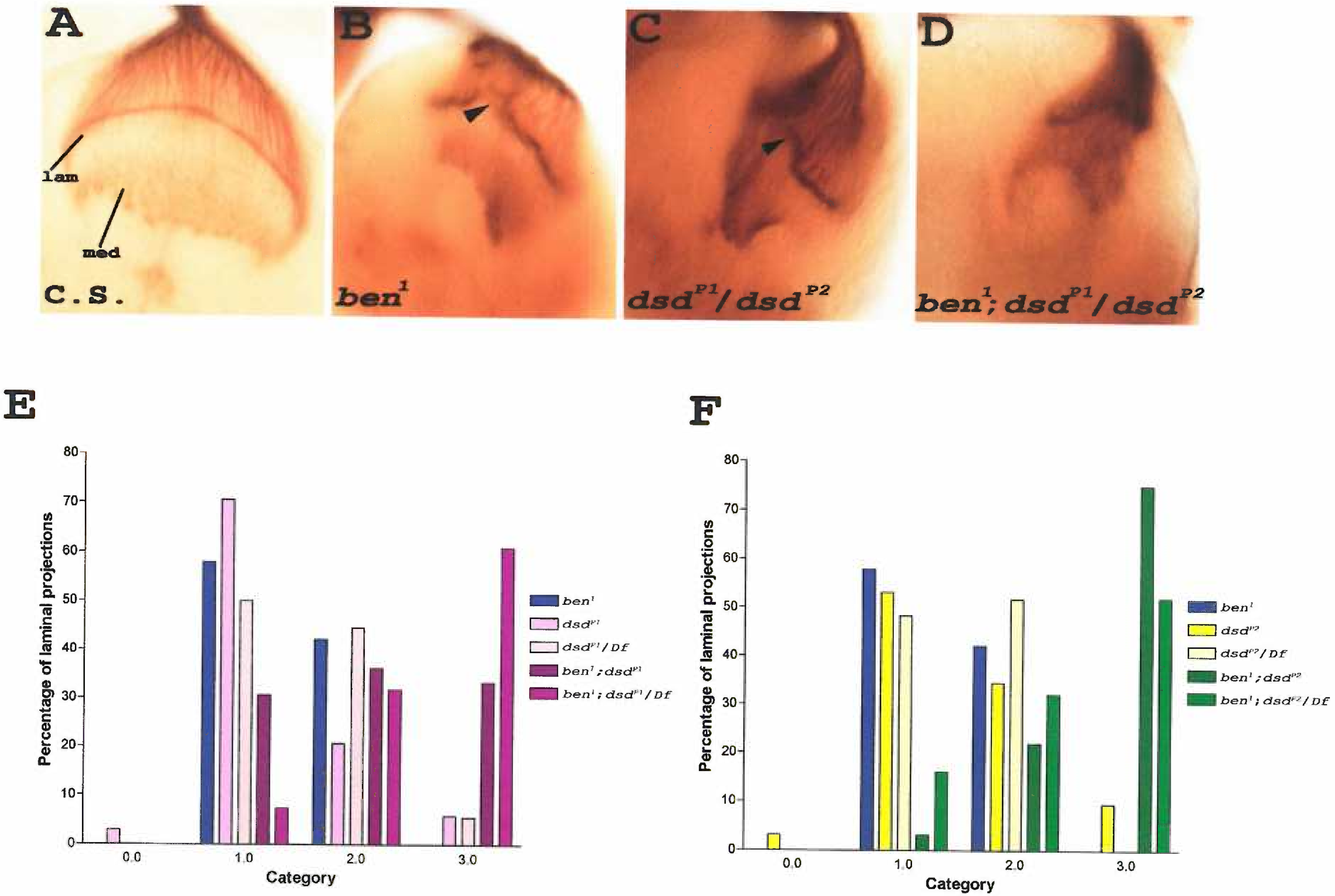
A
lam
med
C.S.
B
$ben^1$
C
$dsd^{P1}/dsd^{P2}$
D
$ben^1; dsd^{P1}/dsd^{P2}$
E
Percentage of laminal projections
80
70
60
50
40
30
20
10
0
0.0
1.0
2.0
3.0
Category
$ben^1$
$dsd^{P1}$
$dsd^{P1}/Df$
$ben^1;dsd^{P1}$
$ben^1;dsd^{P1}/Df$
F
Percentage of laminal projections
80
70
60
50
40
30
20
10
0
0.0
1.0
2.0
3.0
Category
$ben^1$
$dsd^{P2}$
$dsd^{P2}/Df$
$ben^1;dsd^{P2}$
$ben^1;dsd^{P2}/Df$

**Figure 3.** Failure of R2-R5 photoreceptor axons to respond to the lamina glia and terminate appropriately in mutants. *Ro-Tau-lacZ* was used to mark the R2-R5 axons (red) and anti-Repo (green) was used to stain mature glia. (A) No R2-R5 axons project past the lamina glia in control eye discs; R2-R5 axons stop between the two rows of glia. (B) In $ben^1$ mutants, some of the R2-R5 axons project past the lamina to the medulla (arrowhead). The lamina glia still form two layers though less organized. (C) R2-R5 axons in eye discs from $dsd^{P2}/Df(3R)ED6274$ larvae showed a similar phenotype to $ben^1$, the arrowhead indicating axons projecting into the medulla. Similarly, the lamina glia were layered but less organized compared to wild-type. (D) In $ben^1;dsd^{P2}/Df$, both the photoreceptors and glia were disorganized, though the glia were associated with the photoreceptors. Scale bar = 20 μm.

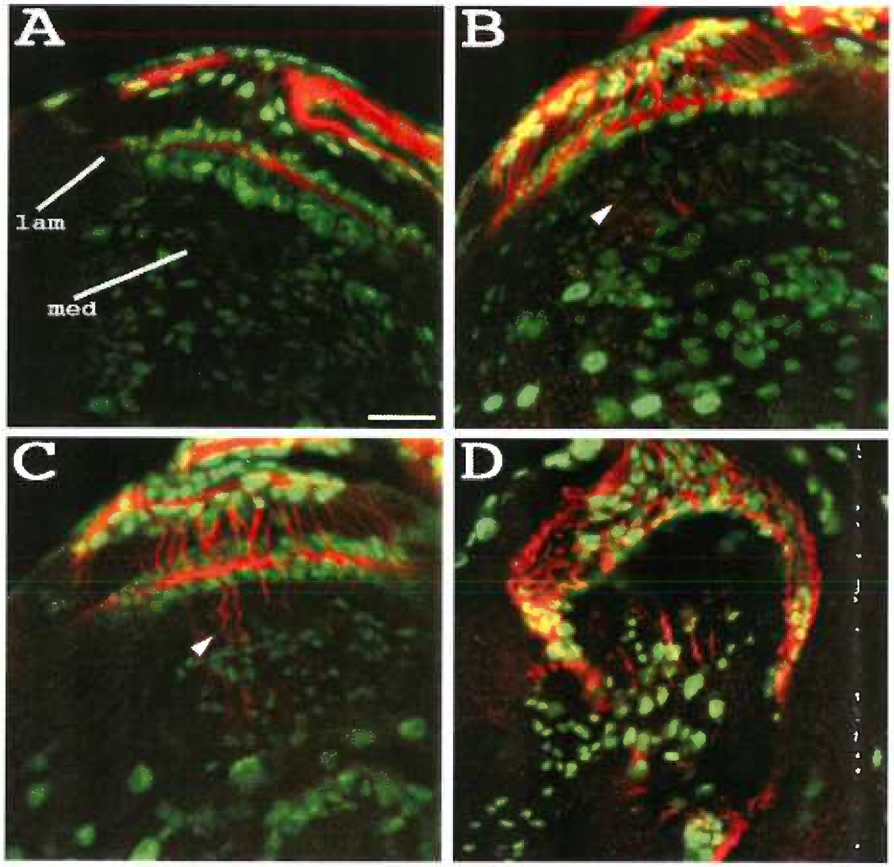
A
B
lam
med
C
D

**Figure 4.** The border of the Inner Proliferation Center (IPC) was not compromised in the mutants (B-D). *Ro-Tau-lacZ* was used to mark R2-R5 axons (red) and anti-Fasciclin III (Fas III; green) was used to stain the IPC cells. The orientation was shifted laterally compared to the more dorsal view in Figure 3. (A) The wild type R2-R5 projections were even and no intrusion of the Fas III staining of the IPC was seen in the lamina, where the R2-R5 terminate (arrow). (B, C) The *ben*$^{1}$ (B) and *dsd*$^{P2}$*/Df* (C) single mutants showed again uneven spacing of the photoreceptor axons but no intrusion of Fas III staining into the lamina. (D) The *ben*$^{1}$*;dsd*$^{P}$*/Df* double mutants showed no intrusion of Fas III IPC staining into the lamina either, despite the more seriously deranged R2-R5 axonal spacing (arrowhead). Scale bar = 20 µm.

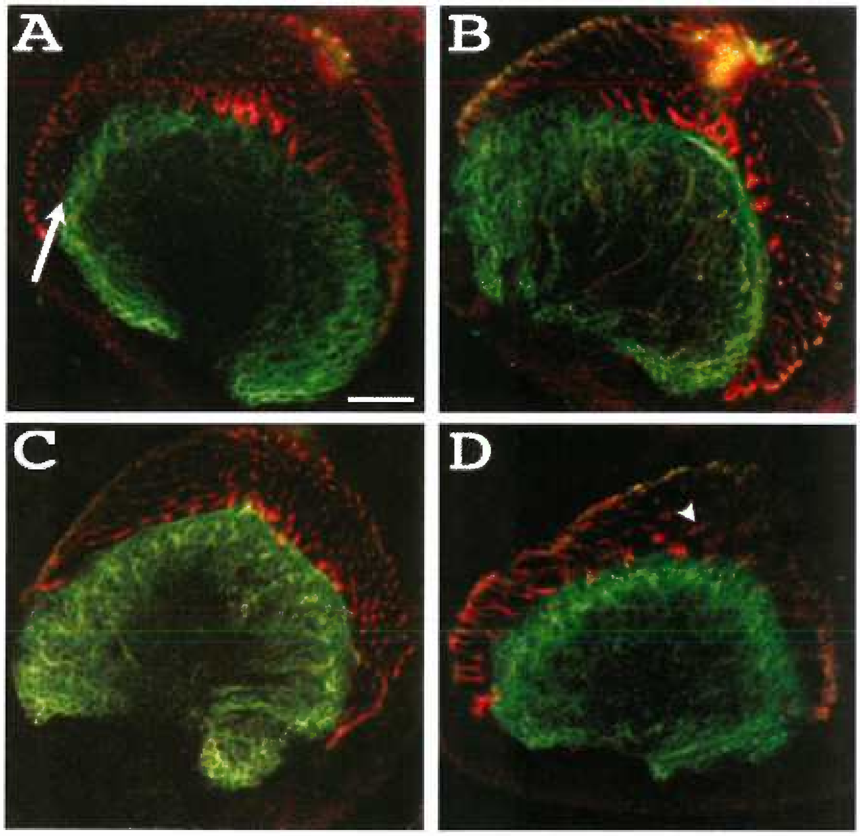
A
B
C
D

**Figure 5.** Adult brain architectural defects and age-dependent neural degeneration in adult flies. (A-D) Representative section from Day 1 flies. (A) C.S. (B) *ben*$^{1}$ (C) *dsd*$^{P1}$/*dsd*$^{P2}$ (D) *ben*$^{1}$; *dsd*$^{P1}$/*dsd*$^{P2}$ No vacuoles were seen on Days 1 though the neuronal architecture of the optic lobe was severely compromised in the double homozygous *ben*$^{1}$;*dsd*$^{P}$ animals, indicated by the arrow (D). (E-H) Representative sections from twelve-day-old flies with inset representing an enlargement of the antennal lobe. (E) C.S. (F) *ben*$^{1}$ (G) *dsd*$^{P1}$/*dsd*$^{P2}$ (H) *ben*$^{1}$;*dsd*$^{P1}$/*dsd*$^{P2}$. Day 12 antennal lobe of the single mutants contained reduced numbers of vacuoles compared to *ben*$^{1}$; *dsd*$^{P1}$/*dsd*$^{P2}$ adults (H). Lamina (lam), medulla (med), lobula (lob), lobula plate (lp) and antennal lobe (al) are indicated.

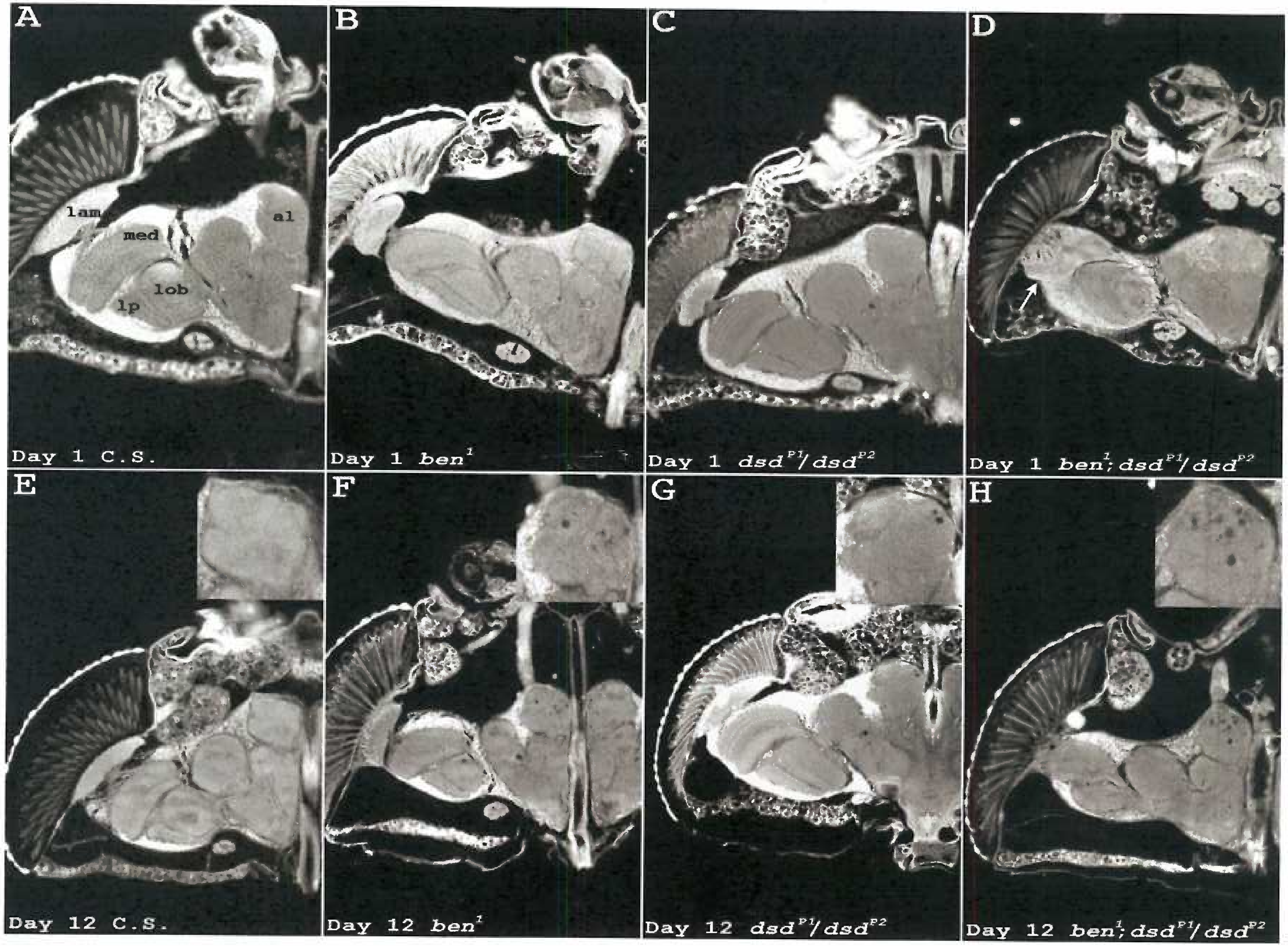
A
lam
med
al
lob
lp
Day 1 C.S.
B
Day 1 ben$^1$
C
Day 1 dsd$^{P1}$/dsd$^{P2}$
D
Day 1 ben$^1$;dsd$^{P1}$/dsd$^{P2}$
E
Day 12 C.S.
F
Day 12 ben$^1$
G
Day 12 dsd$^{P1}$/dsd$^{P2}$
H
Day 12 ben$^1$;dsd$^{P1}$/dsd$^{P2}$

**Figure 6.** Quantification of the antennal lobe vacuoles. (A) Age-dependent progressive degeneration of *ben*$^{1}$ and *ben*$^{1}$;*dsd*$^{P}$ antennal lobes showed that vacuole initially appeared on Day 3, increased on Day 6, and appeared to stabilize in number on Day 12. (B) Numbers of antennal lobe vacuoles present in *dsd*$^{P}$ mutants versus control C.S. on Day 12. Statistical analysis by student t-test. ** P< 0.01 *** P< 0.0001. (F) Numbers of antennal lobe vacuoles in *ben*$^{1}$;*dsd*$^{P}$ versus *ben*$^{1}$ adults on Day 12. *** P< 0.0001. C.S. (n=32), *ben*$^{1}$ (n=33), *dsd*$^{P1}$ (n=27), *dsd*$^{P2}$ (n=29), *dsd*$^{P1}$/*dsd*$^{P2}$ (n=29), *ben*$^{1}$;*dsd*$^{P1}$ (n=20), *ben*$^{1}$;*dsd*$^{P2}$ (n=28), *ben*$^{1}$;*dsd*$^{P1}$/*dsd*$^{P2}$ (n=26).

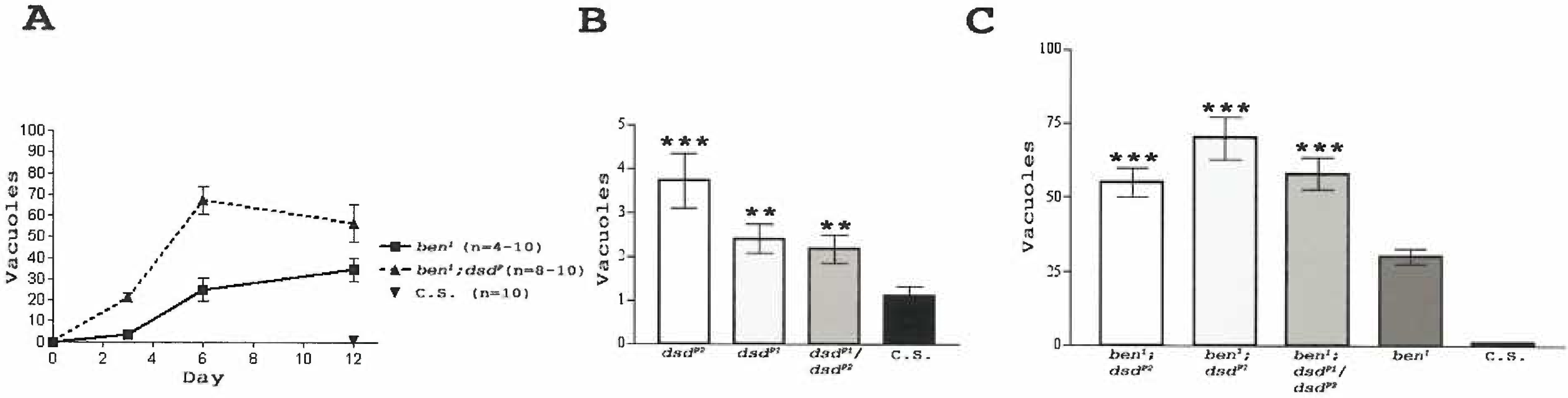
A
Vacuoles
100
90
80
70
60
50
40
30
20
10
0
0
2
4
6
8
10
12
Day
ben¹ (n=4-10)
ben¹;dsdᴾ(n=8-10)
C.S. (n=10)
B
Vacuoles
5
4
3
2
1
0
***
**
**
dsdᴾ²
dsdᴾ¹
dsdᴾ¹/dsdᴾ²
C.S.
C
Vacuoles
100
75
50
25
0
***
***
***
ben¹; dsdᴾ²
ben¹; dsdᴾ¹
ben¹; dsdᴾ¹/dsdᴾ²
ben¹
C.S.

# SUMMARY AND CONCLUSIONS

Attractin (Atrn) is a single pass transmembrane protein that affects pigmentation, energy homeostasis, neurodegeneration, myelination and immune cell interaction (49, 54). The *Drosophila* homologue of Atrn, Distracted (Dsd) has the same domain structure as Atrn, though, like the *C. elegans* homologue, lacks the C-lectin domain. Expression of the *dsd* transcript is found early during *Drosophila* embryogenesis and then again during the third instar larval stage, pupation and adulthood, particularly in the adult head. Examination of the expression of the Dsd protein in the third instar larval brain shows Dsd is expressed in the eye-antennal disc of the third instar larvae and at lower levels in the optic lobe and ventral nerve cord. This broad expression of Dsd mirrors the broad expression of Atrn in the central nervous system and in peripheral tissues (37, 60).

Inserts of transposable P-elements just upstream of the *dsd* start codon results in hypomorphic expression of *dsd*, as quantified by real time RT-PCR. Photoreceptor axon pathfinding has been examined in these $dsd^P$ mutants. In the $dsd^P$ mutants, the photoreceptors exit the optic stalk unevenly and the R1-R6 axons have gaps and dips in the laminar formation and project past the lamina to the medulla. Dsd expression, seen in the eye disc and optic lobe at the third instar larval stage, is also seen in the antennal disc. As adults, the $dsd^P$ mutants show a slight but significant increase in the vacuolization of the antennal lobe. This neurodegeneration suggests that Dsd and Atrn are functionally conserved since one major phenotype of *Atrn* mutants is neurodegeneration (10, 36, 54).

While the statistical difference between wild-type C.S. and the single $dsd^{P1}$ and $dsd^{P2}$ alleles supports the conclusion that there is a difference in the strength of the disruption in *dsd* expression, one limitation of our data is that we have not yet rescued the phenotype of the *dsd* mutants following reintroduction of wild-type Dsd, thereby demonstrating that the disruption in photoreceptor pathfinding or the appearance of antennal lobe vacuoles is strictly due to the disruption of *dsd* expression caused by the insertion of P-element. The increased $P$ values when the $dsd^P$ alleles are over the deficiency are suggestive that the P-element insertions do generate photoreceptor pathfinding defects and neuronal vacuolization specifically due to hypomorphic reduction in the levels of Dsd. However, since we have not assessed photoreceptor pathfinding in flies heterozygous for the deficiency alone, we cannot formally exclude the possibility that a 50% reduction in the levels of *dsd* might also generate pathfinding defects, or that the P-elements may also affect the expression of nearby genes that might be responsible for the phenotypes observed. The confirmation of the sole need for *dsd* disruption to cause these phenotypes awaits the characterization of *dsd* null alleles or the rescue of mutant phenotype by specific reintroduction of wild-type *dsd* into mutant flies. As the $dsd^P$ mutants are presumably hypomorphic, it will be interesting to see if the neurodegeneration is more severe in *dsd* null adults.

Using the Atrn C-terminal tail as bait, ubiquitin conjugating enzyme 13 (UBC13) has been identified from a mammalian yeast two-hybrid screen as an interacting partner. Using two different assays, we confirm that, like their mammalian homologues Atrn and UBC13, the *Drosophila* homologues, Dsd and Bendless (Ben) can interact. By both GST pulldown and yeast two-hybrid assays, the C-terminus of Dsd and the N-terminus of Ben are shown to interact physically. To test whether this interaction would be relevant in vivo, the $ben^1$ hypomorphic mutants were crossed to the $dsd^P$ mutants and the phenotypes examined for enhancement. Indeed, the photoreceptor pathfinding defects seen in $ben^1$

and *dsd*$^{P}$ single mutants became significantly more severe when both mutations are present. Additionally, the vacuolization of the antennal lobe is significantly higher in the *ben*$^{1}$;*dsd*$^{P}$ double homozygous than either *ben*$^{1}$ or *dsd*$^{P}$ alone. The *ben*$^{1}$ mutation did cause higher vacuolization alone than did the *dsd*$^{P}$ mutations. This result could simply indicate Ben has other upstream partners, besides Dsd, that are also important to antennal lobe vacuolization. The finding that a UBC13 homologue affects neurodegeneration is new and may indicate a direction for study of UBC13 in mammals.

Photoreceptor pathfinding in *Drosophila* depends on glial migration (97). Glial migration is induced by the innervation of photoreceptors into the optic lobe (20). In turn, however, the lamina glia signal the R1-R6 axons to stop. In the *ben*$^{1}$ and *dsd*$^{P}$ single mutants, the glia appear to migrate normally to the lamina but some of the axons that should stop do not. Similarly, in the *ben*$^{1}$;*dsd*$^{P}$ double homozygous mutants, the glia migrate but seem to follow the deranged pattern of the photoreceptor axons rather than the normal glial pattern. Given the high expression of Dsd in eye discs and the relatively normal glial migration in the single mutants, it seems likely that the photoreceptors are the site of Dsd and Ben action though this remains to be tested to determined whether the defects seen are due to *dsd* and *ben* in the photoreceptors or in the optic lobe. By making genetic mosaics where either the eye or optic lobe is mutant for *dsd* or *ben*, these questions can be addressed (74).

Projection of the R1-R6 photoreceptor axons past the lamina can be caused by disruption of the compartmental boundary between the lamina and the Inner Proliferation Center (IPC) as seen in *slit*$^{dui}$ mutants (98). In the *ben*$^{1}$ and *dsd*$^{P}$ mutants however, the IPC boundary appears to be intact, even in the double homozygous *ben*$^{1}$; *dsd*$^{P}$ mutants.

While the compartmental boundary between the lamina and IPC appears normal in the double homozygous mutants at the third instar stage, by the time they reach adulthood the lamina, medulla, and sometimes lobula became morphogenetically deranged in shape in the double homozygous *ben*$^{1}$;*dsd*$^{P}$ mutants, a phenotype not seen in the single *ben*$^{1}$ or *dsd*$^{P}$ mutants.

As the adult structure has only been examined at the gross level, this can explain why the single *ben*$^{1}$ and *dsd*$^{P}$ mutants show relatively normal optic lobes despite the photoreceptor pathfinding defects seen at the third instar stage. In the initial description of the *bendless* phenotype, the defect in photoreceptor pathfinding in *ben*$^{1}$ mutants persist into the adult but could only be visualized by staining of the axonal tracts, which are fewer and disorganized in the mutants (69, 78). Therefore, in the single *ben*$^{1}$ and *dsd*$^{P}$ mutants, it would be expected that the gross morphology would appear normal unless the photoreceptor tracts were stained or the brains examined at the electron microscopic level for the formation of the optic cartridges in the lamina, which are severely disrupted in the *ben*$^{1}$ mutants (78). In the double homozygous *ben*$^{1}$;*dsd*$^{P}$ mutants, the morphogenesis of the optic lobe appears to fail; the *ben*$^{1}$;*dsd*$^{P}$ mutants appear unable to make the laminal twist as normal. This result suggests there is a failure of correct morphogenetic movement during pupation in the double homozygous *ben*$^{1}$;*dsd*$^{P}$ mutants rather than a loss of compartmental boundaries.

The neurodegeneration seen in antennal lobes of both the single *ben*$^{1}$ and *dsd*$^{P}$ and double homozygous *ben*$^{1}$;*dsd*$^{P}$ animals is reminiscent of the vacuolization seen in the *futsch*$^{olk}$ mutants (19). Futsch is the *Drosophila* homologue of microtubule associated protein 1B (MAPIB). Atrn has been reported to interact with the MAPIA light chain 2

(LC2) (21) and our yeast two hybrid screen identifies both MAPIB LC1 and MAPIA LC2 as potential interacting partners for Atrn. Since both MAPs are involved in neurite outgrowth (7, 61, 76, 80) and *futsch* mutants show specific antennal lobe vacuolization (19), it is tempting to speculate that Dsd/Atrn and Ben/UBC13 interact with and possibly modify Futsch/MAPIB with K63 polyubiquitin chains. Another MAP, tau, has been shown to be K63 polyubiquitinated and the accumulation of this ubiquitinated form is associated with neurodegeneration (2, 56). Another link between UBC13/Ben K63 polyubiquitination and neurodegeneration comes from one of the familial Parkinson's disease proteins parkin, an E3 ligase, which facilitates the K63-linked polyubiquitination of $\alpha$-synphilin, leading to $\alpha$-synphilin's accumulation and possibly formation of inclusion bodies (58). These studies of K63 polyubiquitination seem to indicate that misregulation of UBC13 activity would lead to neurodegeneration. *Drosophila*, having proved itself a good model system for other neurodegenerative diseases (4, 90), provides an excellent model for further studies of neurodegeneration involving Dsd and Ben.

Innate and adaptive immunity has been implicated in the progression of such neurodegenerative diseases as Alzheimer's disease, Parkinson's disease, Huntington's disease, multiple sclerosis and amyotrophic lateral sclerosis (75). Both Atrn and UBC13 have been shown to be important to immunity. Atrn has a probable role in modulating immune cell interactions and generating of sufficient immune response (25, 85). It has been observed that patients with common variable immune deficiency (CVID) that present inadequate T-cell proliferation do not up regulate Atrn in response to T-cell activation. UBC13 is necessary for both innate and adaptive immune signaling pathways and Ben has been shown to be involved in *Drosophila* innate immunity (89, 103, 110, 111). The activation of NF-κB, which is neuroprotective when activated in neurons (32), is downstream of UBC13 action in these signaling pathways and it would therefore be interesting to see if NF-κB or a homologue is downstream of the Atrn/Dsd and UBC13/Ben interaction.

The roles for both Atrn and UBC13 in immune function (25, 111) point to the possibility that defects in innate immunity may underlie the neurodegeneration seen in *Atrn* mutants and the *Drosophila* $ben^1$, $dsd^P$, and $ben^1;dsd^P$ mutants; defects in innate immunity have been implicated in other neurodegenerative diseases such as Alzheimer's and Parkinson's (75). Defects in innate immunity could also explain the hypersensitivity to oxidative stress seen in cells derived from Atrn deficient rats (70). Future studies could elucidate the potential role of the Atrn family and its interaction with UBC13/Ben in the process of innate immunity and for innate immunity's role in the neurodegeneration seen with mutants in the Atrn family.

Although the described functions of UBC13/Ben fits well into the role of the molecule downstream of Atrn/Dsd, this does not exclude other molecules such as Pin1 or JIP3, potential Atrn interactors identified in our yeast two-hybrid screen, from contributing to Atrn/Dsd signaling. Pin1 has important roles in activating MAP kinase cascades (48), which have already been implicated in Atrn action as shown by the reduced activation of ERK in *Atrn* mutants and in Atrn-deficient cells when exposed to oxidative stress (70). Reduction in Pin1 activity also has links to neurodegeneration (59) and could then contribute to the appearance of this phenotype in *Atrn* mutants. JIP3, besides being involved in JNK activation (62) as is UBC13, also is involved in vesicle trafficking and axonal response to damage in *Drosophila* (14). So, Atrn could use JIP3 for JNK activation and for transport during nerve injury, which potential fits with the observed upregulation of Atrn after spinal cord injury (21). Pin1 and JIP3 are simply two additional examples of potential proteins that may be important players in the molecular function of Atrn.

The discovery of the functional interaction between Dsd and Ben leads to a model whereby Dsd/Atrn activates Ben/UBC13 to polyubiquitinate, through K63, some downstream target to mediate both axonal pathfinding and neurodegeneration. A potential E3 ubiquitin ligase downstream of the Atrn/UBC13 interaction in Mahogunin, which is the protein mutated in the *mahoganoid* (*md*) animals which have essentially the same phenotype as Atrn deficient animals (42, 44, 67, 82). The *md* animals have darker pigmentation and the *md* mutation blocks the yellow pigmentation and obesity of $A^y$ mice. The null $md^{nc}$ allele also causes neurodegeneration similar to that seen in *Atrn* mutants. The identification of Mahogunin as an E3 ubiquitin ligase strengthens ubiquitination as important to Atrn molecular function. The link between UBC13 and Atrn does not explain the pigmentation phenotype of *Atrn* mutants however as UBC13 has yet to be implicated in the control of pigmentation though UBC13 has been shown to be involved in the response to DNA damage both in yeast and mammals (1, 46). DNA damage has been implicated in causing increases in pigmentation (88). Further study should reveal how much of Atrn/Dsd action is dependent on UBC13/Ben and what other molecules and pathways are also important.

The interaction between Atrn/Dsd and UBC13/Ben is the first direct insight into a molecular mechanism for Atrn action and the *Drosophila* model system provides a means by which to further explore the importance of this interaction to neurodegeneration and to the potential importance of K63-linked polyubiquitin to the signaling of the Atrn family.

# REFERENCES

1. **Andersen, P. L., H. Zhou, L. Pastushok, T. Moraes, S. McKenna, B. Ziola, M. J. Ellison, V. M. Dixit, and W. Xiao.** 2005. Distinct regulation of Ubc13 functions by the two ubiquitin-conjugating enzyme variants Mms2 and Uev1A. J Cell Biol **170:**745-55.
2. **Babu, J. R., T. Geetha, and M. W. Wooten.** 2005. Sequestosome 1/p62 shuttles polyubiquitinated tau for proteasomal degradation. J Neurochem **94:**192-203.
3. **Barsh, G. S., L. He, and T. M. Gunn.** 2002. Genetic and biochemical studies of the Agouti-attractin system. J Recept Signal Transduct Res **22:**63-77.
4. **Bier, E.** 2005. Drosophila, the golden bug, emerges as a tool for human genetics. Nat Rev Genet **6:**9-23.
5. **Bork, P., and G. Beckmann.** 1993. The CUB domain. A widespread module in developmentally regulated proteins. J Mol Biol **231:**539-45.
6. **Bossard, C., H. Laurell, L. Van den Berghe, S. Meunier, C. Zanibellato, and H. Prats.** 2003. Translokin is an intracellular mediator of FGF-2 trafficking. Nat Cell Biol **5:**433-9.
7. **Bouquet, C., S. Soares, Y. von Boxberg, M. Ravaille-Veron, F. Propst, and F. Nothias.** 2004. Microtubule-associated protein 1B controls directionality of growth cone migration and axonal branching in regeneration of adult dorsal root ganglia neurons. J Neurosci **24:**7204-13.
8. **Bowman, A. B., A. Kamal, B. W. Ritchings, A. V. Philp, M. McGrail, J. G. Gindhart, and L. S. Goldstein.** 2000. Kinesin-dependent axonal transport is mediated by the sunday driver (SYD) protein. Cell **103:**583-94.
9. **Brent, R., and R. L. Finley, Jr.** 1997. Understanding gene and allele function with two-hybrid methods. Annu Rev Genet **31:**663-704.
10. **Bronson, R. T., L. R. Donahue, R. Samples, J. H. Kim, and J. K. Naggert.** 2001. Mice with mutations in the mahogany gene Atrn have cerebral spongiform changes. J Neuropathol Exp Neurol **60:**724-30.
11. **Brusky, J., Y. Zhu, and W. Xiao.** 2000. UBC13, a DNA-damage-inducible gene, is a member of the error-free postreplication repair pathway in Saccharomyces cerevisiae. Curr Genet **37:**168-74.
12. **Cafferty, P., L. Yu, and Y. Rao.** 2004. The receptor tyrosine kinase Off-track is required for layer-specific neuronal connectivity in Drosophila. Development **131:**5287-95.
13. **Campos-Ortega, J. A., Hartenstein, V.** 1985. The Embryonic development of Drosophila melanogaster. Springer Verlag, Berlin, Heidelberg.
14. **Cavalli, V., P. Kujala, J. Klumperman, and L. S. Goldstein.** 2005. Sunday Driver links axonal transport to damage signaling. J Cell Biol **168:**775-87.
15. **Chien, C. L., K. S. Lu, Y. S. Lin, C. J. Hsieh, and N. Hirokawa.** 2005. The functional cooperation of MAP1A heavy chain and light chain 2 in the binding of microtubules. Exp Cell Res **308:**446-58.
16. **Chotard, C., and I. Salecker.** 2004. Neurons and glia: team players in axon guidance. Trends Neurosci **27:**655-61.

17. **Clandinin, T. R., and S. L. Zipursky.** 2000. Afferent growth cone interactions control synaptic specificity in the Drosophila visual system. Neuron **28:**427-36.
18. **Cope, G. A., and R. J. Deshaies.** 2003. COP9 signalosome: a multifunctional regulator of SCF and other cullin-based ubiquitin ligases. Cell **114:**663-71.
19. **da Cruz, A. B., M. Schwarzel, S. Schulze, M. Niyyati, M. Heisenberg, and D. Kretzschmar.** 2005. Disruption of the MAP1B-related Protein FUTSCH Leads to Changes in the Neuronal Cytoskeleton, Axonal Transport Defects, and Progressive Neurodegeneration in Drosophila. Mol Biol Cell **16:**2433-42.
20. **Dearborn, R., Jr., and S. Kunes.** 2004. An axon scaffold induced by retinal axons directs glia to destinations in the Drosophila optic lobe. Development **131:**2291-303.
21. **Di Giovanni, S., A. I. Faden, A. Yakovlev, J. S. Duke-Cohan, T. Finn, M. Thouin, S. Knoblach, A. De Biase, B. S. Bregman, and E. P. Hoffman.** 2005. Neuronal plasticity after spinal cord injury: identification of a gene cluster driving neurite outgrowth. Faseb J **19:**153-4.
22. **Dinulescu, D. M., and R. D. Cone.** 2000. Agouti and agouti-related protein: analogies and contrasts. J Biol Chem **275:**6695-8.
23. **Dinulescu, D. M., W. Fan, B. A. Boston, K. McCall, M. L. Lamoreux, K. J. Moore, J. Montagno, and R. D. Cone.** 1998. Mahogany (mg) stimulates feeding and increases basal metabolic rate independent of its suppression of agouti. Proc Natl Acad Sci U S A **95:**12707-12.
24. **Dominguez, M., and F. Casares.** 2005. Organ specification-growth control connection: new in-sights from the Drosophila eye-antennal disc. Dev Dyn **232:**673-84.
25. **Duke-Cohan, J. S., J. Gu, D. F. McLaughlin, Y. Xu, G. J. Freeman, and S. F. Schlossman.** 1998. Attractin (DPPT-L), a member of the CUB family of cell adhesion and guidance proteins, is secreted by activated human T lymphocytes and modulates immune cell interactions. Proc Natl Acad Sci U S A **95:**11336-41.
26. **Duke-Cohan, J. S., C. Morimoto, J. A. Rocker, and S. F. Schlossman.** 1996. Serum high molecular weight dipeptidyl peptidase IV (CD26) is similar to a novel antigen DPPT-L released from activated T cells. J Immunol **156:**1714-21.
27. **Duke-Cohan, J. S., W. Tang, and S. F. Schlossman.** 2000. Attractin: a cub-family protease involved in T cell-monocyte/macrophage interactions. Adv Exp Med Biol **477:**173-85.
28. **Ea, C. K., L. Sun, J. Inoue, and Z. J. Chen.** 2004. TIFA activates IkappaB kinase (IKK) by promoting oligomerization and ubiquitination of TRAF6. Proc Natl Acad Sci U S A **101:**15318-23.
29. **Fan, W., B. A. Boston, R. A. Kesterson, V. J. Hruby, and R. D. Cone.** 1997. Role of melanocortinergic neurons in feeding and the agouti obesity syndrome. Nature **385:**165-8.
30. **Feng, Y., and C. A. Walsh.** 2004. The many faces of filamin: a versatile molecular scaffold for cell motility and signalling. Nat Cell Biol **6:**1034-8.
31. **Fischbach, K. F., and G. Technau.** 1984. Cell degeneration in the developing optic lobes of the sine oculis and small-optic-lobes mutants of Drosophila melanogaster. Dev Biol **104:**219-39.

32. **Fridmacher, V., B. Kaltschmidt, B. Goudeau, D. Ndiaye, F. M. Rossi, J. Pfeiffer, C. Kaltschmidt, A. Israel, and S. Memet.** 2003. Forebrain-specific neuronal inhibition of nuclear factor-kappaB activity leads to loss of neuroprotection. J Neurosci **23:**9403-8.
33. **Glynne, P. A., and T. J. Evans.** 2002. Role of the PDZ scaffolding protein in tubule cells in maintenance of polarised function. Exp Nephrol **10:**307-12.
34. **Gomi, H., T. Ikeda, T. Kunieda, S. Itohara, S. B. Prusiner, and K. Yamanouchi.** 1994. Prion protein (PrP) is not involved in the pathogenesis of spongiform encephalopathy in zitter rats. Neurosci Lett **166:**171-4.
35. **Gu, C., B. J. Limberg, G. B. Whitaker, B. Perman, D. J. Leahy, J. S. Rosenbaum, D. D. Ginty, and A. L. Kolodkin.** 2002. Characterization of neuropilin-1 structural features that confer binding to semaphorin 3A and vascular endothelial growth factor 165. J Biol Chem **277:**18069-76.
36. **Gunn, T. M., T. Inui, K. Kitada, S. Ito, K. Wakamatsu, L. He, D. M. Bouley, T. Serikawa, and G. S. Barsh.** 2001. Molecular and phenotypic analysis of Attractin mutant mice. Genetics **158:**1683-95.
37. **Gunn, T. M., K. A. Miller, L. He, R. W. Hyman, R. W. Davis, A. Azarani, S. F. Schlossman, J. S. Duke-Cohan, and G. S. Barsh.** 1999. The mouse mahogany locus encodes a transmembrane form of human attractin. Nature **398:**152-6.
38. **Habelhah, H., S. Takahashi, S. G. Cho, T. Kadoya, T. Watanabe, and Z. Ronai.** 2004. Ubiquitination and translocation of TRAF2 is required for activation of JNK but not of p38 or NF-kappaB. Embo J **23:**322-32.
39. **Hamdane, M., C. Smet, A. V. Sambo, A. Leroy, J. M. Wieruszeski, P. Delobel, C. A. Maurage, A. Ghestem, R. Wintjens, S. Begard, N. Sergeant, A. Delacourte, D. Horvath, I. Landrieu, G. Lippens, and L. Buee.** 2002. Pin1: a therapeutic target in Alzheimer neurodegeneration. J Mol Neurosci **19:**275-87.
40. **Haqq, A. M., P. Rene, T. Kishi, K. Khong, C. E. Lee, H. Liu, J. M. Friedman, J. K. Elmquist, and R. D. Cone.** 2003. Characterization of a novel binding partner of the melanocortin-4 receptor: attractin-like protein. Biochem J **376:**595-605.
41. **Hartenstein, V.** 1993. Atlas of Drosophila Developmenet. Cold Spring Harbor Laboratory Press.
42. **He, L., A. G. Eldridge, P. K. Jackson, T. M. Gunn, and G. S. Barsh.** 2003. Accessory proteins for melanocortin signaling: attractin and mahogunin. Ann N Y Acad Sci **994:**288-98.
43. **He, L., T. M. Gunn, D. M. Bouley, X. Y. Lu, S. J. Watson, S. F. Schlossman, J. S. Duke-Cohan, and G. S. Barsh.** 2001. A biochemical function for attractin in agouti-induced pigmentation and obesity. Nat Genet **27:**40-7.
44. **He, L., X. Y. Lu, A. F. Jolly, A. G. Eldridge, S. J. Watson, P. K. Jackson, G. S. Barsh, and T. M. Gunn.** 2003. Spongiform degeneration in mahoganoid mutant mice. Science **299:**710-2.
45. **Hoege, C., B. Pfander, G. L. Moldovan, G. Pyrowolakis, and S. Jentsch.** 2002. RAD6-dependent DNA repair is linked to modification of PCNA by ubiquitin and SUMO. Nature **419:**135-41.

46. **Hofmann, R. M., and C. M. Pickart.** 2001. In vitro assembly and recognition of Lys-63 polyubiquitin chains. J Biol Chem **276:**27936-43.

47. **Holmes, A. L., R. N. Raper, and J. S. Heilig.** 1998. Genetic analysis of Drosophila larval optic nerve development. Genetics **148:**1189-201.

48. **Hsu, T., D. McRackan, T. S. Vincent, and H. Gert de Couet.** 2001. Drosophila Pin1 prolyl isomerase Dodo is a MAP kinase signal responder during oogenesis. Nat Cell Biol **3:**538-43.

49. **Jackson, I. J.** 1999. The mahogany mouse mutation: further links between pigmentation, obesity and the immune system. Trends Genet **15:**429-31.

50. **Jackson, P. K., A. G. Eldridge, E. Freed, L. Furstenthal, J. Y. Hsu, B. K. Kaiser, and J. D. Reimann.** 2000. The lore of the RINGs: substrate recognition and catalysis by ubiquitin ligases. Trends Cell Biol **10:**429-39.

51. **Kim, J. C., J. L. Badano, S. Sibold, M. A. Esmail, J. Hill, B. E. Hoskins, C. C. Leitch, K. Venner, S. J. Ansley, A. J. Ross, M. R. Leroux, N. Katsanis, and P. L. Beales.** 2004. The Bardet-Biedl protein BBS4 targets cargo to the pericentriolar region and is required for microtubule anchoring and cell cycle progression. Nat Genet **36:**462-70.

52. **Krakow, D., S. P. Robertson, L. M. King, T. Morgan, E. T. Sebald, C. Bertolotto, S. Wachsmann-Hogiu, D. Acuna, S. S. Shapiro, T. Takafuta, S. Aftimos, C. A. Kim, H. Firth, C. E. Steiner, V. Cormier-Daire, A. Superti-Furga, L. Bonafe, J. M. Graham, Jr., A. Grix, C. A. Bacino, J. Allanson, M. G. Bialer, R. S. Lachman, D. L. Rimoin, and D. H. Cohn.** 2004. Mutations in the gene encoding filamin B disrupt vertebral segmentation, joint formation and skeletogenesis. Nat Genet **36:**405-10.

53. **Krendel, M., F. T. Zenke, and G. M. Bokoch.** 2002. Nucleotide exchange factor GEF-H1 mediates cross-talk between microtubules and the actin cytoskeleton. Nat Cell Biol **4:**294-301.

54. **Kuramoto, T., K. Kitada, T. Inui, Y. Sasaki, K. Ito, T. Hase, S. Kawagachi, Y. Ogawa, K. Nakao, G. S. Barsh, M. Nagao, T. Ushijima, and T. Serikawa.** 2001. Attractin/mahogany/zitter plays a critical role in myelination of the central nervous system. Proc Natl Acad Sci U S A **98:**559-64.

55. **Kuramoto, T., T. Nomoto, A. Fujiwara, M. Mizutani, T. Sugimura, and T. Ushijima.** 2002. Insertional mutation of the Attractin gene in the black tremor hamster. Mamm Genome **13:**36-40.

56. **Kuusisto, E., A. Salminen, and I. Alafuzoff.** 2001. Ubiquitin-binding protein p62 is present in neuronal and glial inclusions in human tauopathies and synucleinopathies. Neuroreport **12:**2085-90.

57. **Kuwamura, M., M. Maeda, T. Kuramoto, K. Kitada, T. Kanehara, M. Moriyama, Y. Nakane, J. Yamate, T. Ushijima, T. Kotani, and T. Serikawa.** 2002. The myelin vacuolation (mv) rat with a null mutation in the attractin gene. Lab Invest **82:**1279-86.

58. **Lim, K. L., K. C. Chew, J. M. Tan, C. Wang, K. K. Chung, Y. Zhang, Y. Tanaka, W. Smith, S. Engelender, C. A. Ross, V. L. Dawson, and T. M. Dawson.** 2005. Parkin mediates nonclassical, proteasomal-independent ubiquitination of synphilin-1: implications for Lewy body formation. J Neurosci **25:**2002-9.

59. **Lu, K. P.** 2004. Pinning down cell signaling, cancer and Alzheimer's disease. Trends Biochem Sci **29:**200-9.

60. **Lu, X., T. M. Gunn, K. Shieh, G. S. Barsh, H. Akil, and S. J. Watson.** 1999. Distribution of Mahogany/Attractin mRNA in the rat central nervous system. FEBS Lett **462:**101-7.

61. **Mack, T. G., M. P. Koester, and G. E. Pollerberg.** 2000. The microtubule-associated protein MAP1B is involved in local stabilization of turning growth cones. Mol Cell Neurosci **15:**51-65.

62. **Matsuguchi, T., A. Masuda, K. Sugimoto, Y. Nagai, and Y. Yoshikai.** 2003. JNK-interacting protein 3 associates with Toll-like receptor 4 and is involved in LPS-mediated JNK activation. Embo J **22:**4455-64.

63. **McKenna, S., T. Moraes, L. Pastushok, C. Ptak, W. Xiao, L. Spyracopoulos, and M. J. Ellison.** 2003. An NMR-based model of the ubiquitin-bound human ubiquitin conjugation complex Mms2.Ubc13. The structural basis for lysine 63 chain catalysis. J Biol Chem **278:**13151-8.

64. **McKenna, S., L. Spyracopoulos, T. Moraes, L. Pastushok, C. Ptak, W. Xiao, and M. J. Ellison.** 2001. Noncovalent interaction between ubiquitin and the human DNA repair protein Mms2 is required for Ubc13-mediated polyubiquitination. J Biol Chem **276:**40120-6.

65. **Mehler, M. F., P. C. Mabie, D. Zhang, and J. A. Kessler.** 1997. Bone morphogenetic proteins in the nervous system. Trends Neurosci **20:**309-17.

66. **Meinertzhagen, I. A.** 2000. Wiring the fly's eye. Neuron **28:**310-3.

67. **Miller, K. A., T. M. Gunn, M. M. Carrasquillo, M. L. Lamoreux, D. B. Galbraith, and G. S. Barsh.** 1997. Genetic studies of the mouse mutations mahogany and mahoganoid. Genetics **146:**1407-15.

68. **Moraes, T. F., R. A. Edwards, S. McKenna, L. Pastushok, W. Xiao, J. N. Glover, and M. J. Ellison.** 2001. Crystal structure of the human ubiquitin conjugating enzyme complex, hMms2-hUbc13. Nat Struct Biol **8:**669-73.

69. **Muralidhar, M. G., and J. B. Thomas.** 1993. The Drosophila bendless gene encodes a neural protein related to ubiquitin-conjugating enzymes. Neuron **11:**253-66.

70. **Muto, Y., and K. Sato.** 2003. Pivotal role of attractin in cell survival under oxidative stress in the zitter rat brain with genetic spongiform encephalopathy. Brain Res Mol Brain Res **111:**111-22.

71. **Nagle, D. L., S. H. McGrail, J. Vitale, E. A. Woolf, B. J. Dussault, Jr., L. DiRocco, L. Holmgren, J. Montagno, P. Bork, D. Huszar, V. Fairchild-Huntress, P. Ge, J. Keilty, C. Ebeling, L. Baldini, J. Gilchrist, P. Burn, G. A. Carlson, and K. J. Moore.** 1999. The mahogany protein is a receptor involved in suppression of obesity. Nature **398:**148-52.

72. **Nakayama, M., D. Nakajima, T. Nagase, N. Nomura, N. Seki, and O. Ohara.** 1998. Identification of high-molecular-weight proteins with multiple EGF-like motifs by motif-trap screening. Genomics **51:**27-34.

73. **Negishi, M., I. Oinuma, and H. Katoh.** 2005. Plexins: axon guidance and signal transduction. Cell Mol Life Sci **62:**1363-71.

74. **Newsome, T. P., B. Asling, and B. J. Dickson.** 2000. Analysis of Drosophila photoreceptor axon guidance in eye-specific mosaics. Development **127:**851-60.

75. **Nguyen, M. D., J. P. Julien, and S. Rivest.** 2002. Innate immunity: the missing link in neuroprotection and neurodegeneration? Nat Rev Neurosci **3:**216-27.

76. **Noiges, R., R. Eichinger, W. Kutschera, I. Fischer, Z. Nemeth, G. Wiche, and F. Propst.** 2002. Microtubule-associated protein 1A (MAP1A) and MAP1B: light chains determine distinct functional properties. J Neurosci **22:**2106-14.

77. **Nordgard, O., O. Dahle, T. O. Andersen, and O. S. Gabrielsen.** 2001. JAB1/CSN5 interacts with the GAL4 DNA binding domain: a note of caution about two-hybrid interactions. Biochimie **83:**969-71.

78. **Oh, C. E., R. McMahon, S. Benzer, and M. A. Tanouye.** 1994. bendless, a Drosophila gene affecting neuronal connectivity, encodes a ubiquitin-conjugating enzyme homolog. J Neurosci **14:**3166-79.

79. **Ollmann, M. M., B. D. Wilson, Y. K. Yang, J. A. Kerns, Y. Chen, I. Gantz, and G. S. Barsh.** 1997. Antagonism of central melanocortin receptors in vitro and in vivo by agouti-related protein. Science **278:**135-8.

80. **Oudega, M., F. Touri, M. G. Deenen, B. M. Riederer, and E. Marani.** 1998. Microtubule-associated protein 1a is involved in the early development of the rat spinal cord. Neurosci Lett **246:**81-4.

81. **Petrucelli, L., and T. M. Dawson.** 2004. Mechanism of neurodegenerative disease: role of the ubiquitin proteasome system. Ann Med **36:**315-20.

82. **Phan, L. K., F. Lin, C. A. LeDuc, W. K. Chung, and R. L. Leibel.** 2002. The mouse mahoganoid coat color mutation disrupts a novel C3HC4 RING domain protein. J Clin Invest **110:**1449-59.

83. **Pickart, C. M.** 2001. Mechanisms underlying ubiquitination. Annu Rev Biochem **70:**503-33.

84. **Pickart, C. M., and D. Fushman.** 2004. Polyubiquitin chains: polymeric protein signals. Curr Opin Chem Biol **8:**610-6.

85. **Pozzi, N., L. Gaetaniello, B. Martire, D. De Mattia, B. Balestrieri, E. Cosentini, S. F. Schlossman, J. S. Duke-Cohan, and C. Pignata.** 2001. Defective surface expression of attractin on T cells in patients with common variable immunodeficiency (CVID). Clin Exp Immunol **123:**99-104.

86. **Rao, Y., P. Pang, W. Ruan, D. Gunning, and S. L. Zipursky.** 2000. brakeless is required for photoreceptor growth-cone targeting in Drosophila. Proc Natl Acad Sci U S A **97:**5966-71.

87. **Ravid, T., and M. Hochstrasser.** 2004. NF-kappaB signaling: flipping the switch with polyubiquitin chains. Curr Biol **14:**R898-900.

88. **Rouzaud, F., A. L. Kadekaro, Z. A. Abdel-Malek, and V. J. Hearing.** 2005. MC1R and the response of melanocytes to ultraviolet radiation. Mutat Res **571:**133-52.

89. **Shi, C. S., and J. H. Kehrl.** 2003. Tumor necrosis factor (TNF)-induced germinal center kinase-related (GCKR) and stress-activated protein kinase (SAPK) activation depends upon the E2/E3 complex Ubc13-Uev1A/TNF receptor-associated factor 2 (TRAF2). J Biol Chem **278:**15429-34.

90. **Shulman, J. M., and M. B. Feany.** 2003. Genetic modifiers of tauopathy in Drosophila. Genetics **165:**1233-42.

91. **Suh, G. S., B. Poeck, T. Chouard, E. Oron, D. Segal, D. A. Chamovitz, and S. L. Zipursky.** 2002. Drosophila JAB1/CSN5 acts in photoreceptor cells to induce glial cells. Neuron **33:**35-46.

92. **Sun, L., L. Deng, C. K. Ea, Z. P. Xia, and Z. J. Chen.** 2004. The TRAF6 ubiquitin ligase and TAK1 kinase mediate IKK activation by BCL10 and MALT1 in T lymphocytes. Mol Cell **14:**289-301.

93. **Tang, W., and J. S. Duke-Cohan.** 2002. Human secreted attractin disrupts neurite formation in differentiating cortical neural cells in vitro. J Neuropathol Exp Neurol **61:**767-77.

94. **Tang, W., T. M. Gunn, D. F. McLaughlin, G. S. Barsh, S. F. Schlossman, and J. S. Duke-Cohan.** 2000. Secreted and membrane attractin result from alternative splicing of the human ATRN gene. Proc Natl Acad Sci U S A **97:**6025-30.

95. **Tanji, T., and Y. T. Ip.** 2005. Regulators of the Toll and Imd pathways in the Drosophila innate immune response. Trends Immunol **26:**193-8.

96. **Tautz, D., and C. Pfeifle.** 1989. A non-radioactive in situ hybridization method for the localization of specific RNAs in Drosophila embryos reveals translational control of the segmentation gene hunchback. Chromosoma **98:**81-5.

97. **Tayler, T. D., and P. A. Garrity.** 2003. Axon targeting in the Drosophila visual system. Curr Opin Neurobiol **13:**90-5.

98. **Tayler, T. D., M. B. Robichaux, and P. A. Garrity.** 2004. Compartmentalization of visual centers in the Drosophila brain requires Slit and Robo proteins. Development **131:**5935-45.

99. **Tessier-Lavigne, M., and C. S. Goodman.** 1996. The molecular biology of axon guidance. Science **274:**1123-33.

100. **Todorovic, A., and C. Haskell-Luevano.** 2005. A review of melanocortin receptor small molecule ligands. Peptides.

101. **Tsui, C., A. Raguraj, and C. M. Pickart.** 2005. Ubiquitin binding site of the ubiquitin E2 variant (UEV) protein Mms2 is required for DNA damage tolerance in the yeast RAD6 pathway. J Biol Chem **280:**19829-35.

102. **Varadan, R., M. Assfalg, A. Haririnia, S. Raasi, C. Pickart, and D. Fushman.** 2004. Solution conformation of Lys63-linked di-ubiquitin chain provides clues to functional diversity of polyubiquitin signaling. J Biol Chem **279:**7055-63.

103. **Wang, C., L. Deng, M. Hong, G. R. Akkaraju, J. Inoue, and Z. J. Chen.** 2001. TAK1 is a ubiquitin-dependent kinase of MKK and IKK. Nature **412:**346-51.

104. **Weis, W. I., and K. Drickamer.** 1996. Structural basis of lectin-carbohydrate recognition. Annu Rev Biochem **65:**441-73.

105. **Wooff, J., L. Pastushok, M. Hanna, Y. Fu, and W. Xiao.** 2004. The TRAF6 RING finger domain mediates physical interaction with Ubc13. FEBS Lett **566:**229-33.

106. **Wu, H., and J. R. Arron.** 2003. TRAF6, a molecular bridge spanning adaptive immunity, innate immunity and osteoimmunology. Bioessays **25:**1096-105.

107. **Xiong, W. C., H. Okano, N. H. Patel, J. A. Blendy, and C. Montell.** 1994. repo encodes a glial-specific homeo domain protein required in the Drosophila nervous system. Genes Dev **8:**981-94.

108. **Yeh, W. C., A. Shahinian, D. Speiser, J. Kraunus, F. Billia, A. Wakeham, J. L. de la Pompa, D. Ferrick, B. Hum, N. Iscove, P. Ohashi, M. Rothe, D. V.**

**Goeddel, and T. W. Mak.** 1997. Early lethality, functional NF-kappaB activation, and increased sensitivity to TNF-induced cell death in TRAF2-deficient mice. Immunity **7:**715-25.

109. **Zhong, J., and J. M. Kyriakis.** 2004. Germinal center kinase is required for optimal Jun N-terminal kinase activation by Toll-like receptor agonists and is regulated by the ubiquitin proteasome system and agonist-induced, TRAF6-dependent stabilization. Mol Cell Biol **24:**9165-75.
110. **Zhou, H., I. Wertz, K. O'Rourke, M. Ultsch, S. Seshagiri, M. Eby, W. Xiao, and V. M. Dixit.** 2004. Bcl10 activates the NF-kappaB pathway through ubiquitination of NEMO. Nature **427:**167-71.
111. **Zhou, R., N. Silverman, M. Hong, D. S. Liao, Y. Chung, Z. J. Chen, and T. Maniatis.** 2005. The role of ubiquitnation in Drosophila innate immunity. J Biol Chem.
112. **Zhu, Y. Y., E. M. Machleder, A. Chenchik, R. Li, and P. D. Siebert.** 2001. Reverse transcriptase template switching: a SMART approach for full-length cDNA library construction. Biotechniques **30:**892-7.

# APPENDIX

## A1. *ATTRACTIN* TISSUE AND DEVELOPMENTAL RT-PCR.

**Figure A1**. The expression of mouse *Attractin* (*Atrn*) in multiple tissues and at different embryonic stages was determined by RT-PCR using the Multiple Tissue mouse cDNA panel from Clontech, which comes normalized to four housekeeping genes. The RT-PCR was performed with primers specific to the intracellular tail-encoding portion of the *Atrn* mRNA. Expression of *Atrn* was seen as early as embryonic day 7 and continued throughout the other embryonic days represented.

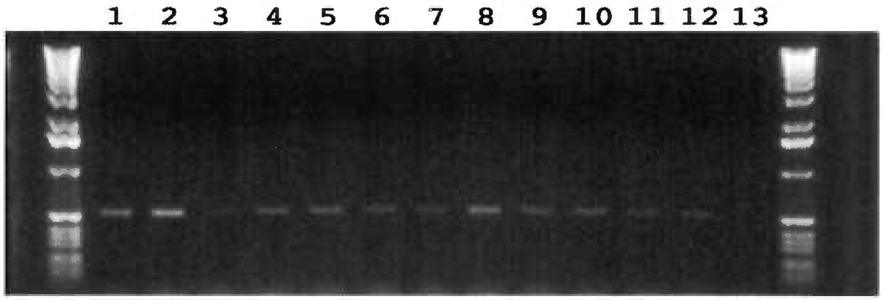
1 2 3 4 5 6 7 8 9 10 11 12 13

1. Heart
2. Brain
3. Spleen
4. Lung
5. Liver
6. Skeletal muscle
7. Kidney
8. Testis
9. Embryonic day 7
10. Embryonic day 11
11. Embryonic day 15
12. Embryonic day 17
13. Negative control

## A2. CREATION OF *DSD* DELETION ALLELES

Mobilization of the P-elements in *dsd*$^{P1}$ and *dsd*$^{P2}$ flies failed to produce imprecise excisions, which would result in a *dsd* null allele. Therefore, a new P-element insertion line, EY05482 was obtained. In this stock the P-element was 1.1 kb upstream of the *dsd* start codon. Mobilization of this P-element produced imprecise excisions, causing the deletion of the beginning of *dsd*. The imprecise excisions of EY05482 were identified by Southern. All of the 5 *dsd* deletion alleles were viable so *dsd* may not to be essential zygotically to life but, as seen with the *dsd*$^{P}$ hypomorphic mutations, may be necessary for the correct pattern of photoreceptor pathfinding. Further characterization will reveal whether *dsd* is needed in the eyes or in the optic lobe to affect photoreceptor pathfinding.

### Materials and Methods

To create *dsd* null alleles the *EY05482* stock, which carries the EY P-element 1.1 kb upstream of the *dsd* start codon, was crossed to transposase source, *delta 2-3, Sb/TM6, Tb*. Single male stubble progeny were crossed to *TM3, Sb/TM6, Dr* females. Single white-eyed progeny from these crosses were used to create at least 150 lines of independent hopout events. These lines were screened for deletions in the *dsd* gene by Southern blot (Roche Non-radioactive Southern kit) using a probe to the first part of the *dsd* gene. Lack of a band in the hopout lane would indicate that the first part of *dsd* had been deleted. PCR was then performed to confirm the deletion of the start of the *dsd* gene and sequencing will be done to determine the extent of the deletions. Credit for the Southern screening and subsequent PCR analysis goes to Jacqueline Parker.

# A3. MELANOCORTIN 5 RECEPTOR PAPERS

## A3.1 Melanocortin 5 receptor deficiency promotes defensive behavior in male mice.

ELSEVIER

Available online at www.sciencedirect.com
SCIENCE @ DIRECT®

Hormones and Behavior 45 (2004) 58–63

Hormones and Behavior

www.elsevier.com/locate/yhbeh

# Melanocortin-5 receptor deficiency promotes defensive behavior in male mice

Caurnel Morgan,* Ruth E. Thomas, and Roger D. Cone

*Vollum Institute for Advanced Biomedical Research, Oregon Health and Science University, Portland, OR, 97239 USA*

Received 1 February 2003; revised 12 August 2003; accepted 19 August 2003

**Abstract**

The endogenous melanocortin, alpha-melanocyte-stimulating hormone (alpha-MSH), is a neurohormone secreted by the neurointermediate lobe of the pituitary. Alpha-MSH promotes intermale aggression in mice by influencing pheromone secretion, but the role of specific melanocortin receptors has not been determined. We assessed mice made deficient in the gene for the melanocortin-5 receptor (MC5R) to determine its role in pheromone-regulated behavior. In heterotypic pairs assessed in the social interaction test (SIT), MC5R-deficient mice exhibited less aggressive behavior and more defensive behavior than their wild-type opponents. By contrast, when assessed in homotypic pairs and against stimulus animals in the SIT, MC5R-deficient and wild-type mice behaved similarly. Moreover, urine from MC5R deficient mice stimulated more aggression than did urine from wild-type mice. The results suggest that MC5R deficiency disinhibits an aggression-suppressing pheromonal signal.

© 2003 Elsevier Inc. All rights reserved.

*Keywords:* Melanocortin; MC5R; Aggression; Pheromone; Alpha-MSH; NDP-MSH; Urine; Social interaction test; Exocrine; Neuroendocrine

## Introduction

Alpha-melanocyte-stimulating hormone (alpha-MSH) and adrenocorticotropic hormone (ACTH) are circulating melanocortins that are secreted from arcuate neurons of the hypothalamus (O'Donohue and Dorsa, 1982; O'Donohue and Jacobowitz, 1980; Watson and Akil, 1980) and from the pituitary's neurointermediate lobe and anterior lobe, respectively (Kraicer et al., 1985; Mains and Eipper, 1979). Alpha-MSH influences rodent behavior through central and peripheral actions. Central injection of alpha-MSH has been shown to stimulate aggression in female rats (Gonzalez et al., 1996) and circulating alpha-MSH stimulates the growth of pheromone-producing exocrine glands (Chen et al., 1997; Nowell et al., 1980; van der Kraan et al., 1998). ACTH stimulates biosynthesis and secretion of adrenal corticosteroids (Cammas et al., 1995), which promote aggressive behavior in rodents (Leshner et al., 1973) via central effects (Hayden-Hixson and Ferris, 1991). ACTH may also regulate rodent behavior independently of corticosteroids (Delbende et al., 1985).

Chronic melanocortin administration stimulates lipogenesis, hypertrophy, hyperplasia, and pheromone secretion in the exocrine glands of rodents (Cooper et al., 1975; Ozegovic and Milkovic, 1972; Thody and Shuster, 1975), and repeated alpha-MSH injection increases the aggression-promoting activity of dominant male urine (Nowell and Wouters, 1975). Therefore, elevated melanocortin levels may stimulate biosynthesis or release of a dominance pheromone. Previous studies have shown that alpha-MSH releases pheromones that elicit aggression (Nowell and Wouters, 1975; Nowell et al., 1980), but none have shown evidence of a dominance pheromone.

Five receptors are known to mediate behavioral and physiological effects of melanocortins (Cone et al., 1996). Melanocortin-1 receptor (MC1R) is expressed in epidermal and follicular melanocytes (Chhajlani and Wikberg, 1992), and stimulates melanogenesis (Hadley et al., 1981; Levine et al., 1987). MC2R, in the adrenal cortex, mediates the effects of ACTH on corticosteroid secretion (Desarnaud et al., 1994; Penhoat et al., 2000). MC3R (Gantz et al., 1993a; Roselli-Rehfuss et al., 1993), MC4R (Gantz et al., 1993b), and MC5R (Labbe et al., 1994) all are found in the brain. Central MC3R (Butler et al., 2000; Chen et al., 2000) and

---

* Corresponding author. Bourne Behavioral Research Laboratory, New York-Presbyterian Hospital, 21 Bloomingdale Road, White Plains, NY 10605. Fax: +1-914-682-3793.

*E-mail address:* cam2025@med.cornell.edu (C. Morgan).

0018-506X/$ - see front matter © 2003 Elsevier Inc. All rights reserved.
doi:10.1016/j.yhbeh.2003.08.004

MC4R (Fan et al., 1997; Heisler et al., 2002) are important for body weight regulation. A clear function for the central MC5R has not been determined, but there is evidence that it may be involved in the control of luteinizing hormone secretion (Murray et al., 2000).

Peripherally, the MC5R is expressed abundantly in pheromone-producing exocrine glands, including sebaceous, lachrymal, Harderian, sex accessory, and preputial glands (Chen et al., 1997; van der Kraan et al., 1998). Mice that are genetically engineered to be MC5R-deficient (MC5R−/−) have defective sebaceous and Harderian glands (Chen et al., 1997), but little is known about their pheromonal signaling and pheromone-regulated behavior. A previous study has shown that urine from MC5R−/− mice elicits aggression toward stimulus mice (Caldwell and Lepri, 2002). In the present study, we assess the social behavior of these mutant mice.

## Materials and methods

### *Experiment 1*

*Animals and housing*

Male wild-type (MC5R+/+) and MC5R-deficient (MC5R−/−) mice on a C57BL/J6 genetic background (Chen et al., 1997) were maintained in group-housed conditions (3–5 per cage). Room temperature was maintained at 22 ± 2°C on a standard light–dark cycle (12-h light: 12-h darkness, lights on from 0600–1800 h) with food and water provided ad libitum. At 8 weeks of age, mice were individually housed for at least 4 weeks before behavioral testing. Mice were housed in filter-top cages within a Maxi-Miser System (Thoren Caging Systems; Hazelton, PA) that provides positive ventilation and air exhaust from each cage. During handling, individual cages of mice were transferred to a fume hood supplied with negative ventilation. Thus, the exchange of olfactory signals (i.e., pheromones, odorants, and dander) between mice was minimized. Procedures used in this study were approved by Institutional Animal Care and Use Committee.

*Experimental design*

Heterotypic (i.e., MC5R+/+ vs. MC5R−/−) pairs of mice were matched by body weight and assessed in the social interaction test during the middle of the light phase or the middle of the dark phase. Before testing, the tail of one opponent was marked with a black marker pen to distinguish it. At the time of testing, pairs of mice were placed in neutral cages with fresh bedding. Tests lasting 10 min were videotaped under normal room illumination in the light phase or infrared light in the dark phase. The infrared light source was provided by the TR-V65 Hi8 video camera (Sony; New York, NY). Behaviors were scored from videotapes by trained observers who were blind to the treatments. Aggressive behavior consisted of the combination of offensive behavior (biting and striking) and dominant behavior (dominant posturing, chasing, and tail rattling). Defensive behavior consisted of reactive aggression (responses to the opponent's approach or attack) and subordinate behavior (subordinate posturing, fleeing, vocalizing, and avoidance). Social behavior consisted of approaching, frontal investigation, and anogenital investigation. Nonsocial behavior consisted of self-grooming and rearing. Each mouse was scored for each occurrence of these behaviors.

Data were analyzed with SigmaStat 2.0 statistical software (SPSS; Chicago, IL). For behavioral data that were not normally distributed or that contained unequal variance, the Mann–Whitney rank sum test was used. All other data were analyzed using Student's *t* test.

### *Experiment 2*

*Animals and housing*

Male MC5R+/+ and MC5R−/− mice were housed as above. Wild-type stimulus mice were gonadectomized by the supplier (Taconic Farms; Germantown, NY), group housed upon arrival, and permitted 3 weeks for postsurgical recovery, before testing.

*Experimental design*

MC5R+/+ and MC5R−/− test mice were assessed with gonadectomized (GDX) stimulus mice in the social interaction test during the middle of the light phase, as described above. Tests lasting 5 min were videotaped, scored, and statistically analyzed as above.

### *Experiment 3*

*Animals and housing*

Male MC5R+/+, MC5R−/−, and GDX mice were housed as above.

*Experimental design*

MC5R+/+ and MC5R−/− urine donors were injected intraperitoneally every 48 h for 2 weeks with 500 ng of [Nle$^4$, d-Phe$^7$]-alpha-MSH (NDP-MSH) (Peninsula Laboratories; Belmont, CA) or vehicle (0.9% saline, 0.1 ml). Urine was collected on dry ice 48 h following each injection and stored at −20°C. Urine was swabbed onto the perineal region of stimulus mice. Responses of intact MC5R+/+ test mice toward the stimulus mice were assessed in the light phase, as above. Tests lasting 5 min were videotaped, scored, and statistically analyzed as above.

## Results

### *Experiment 1*

When paired with male MC5R+/+ mice, male MC5R−/− mice were less aggressive and much more defensive than were their wild-type opponents (Fig. 1). Social and nonsocial behaviors were unaltered (data not shown). Compared to light phase testing (Fig. 1, upper), dark phase testing (Fig. 1 lower) elevated aggression ($P < 0.05$) in MC5R+/+ mice and elevated defense ($P < 0.01$) in MC5R+/+ and MC5R−/− mice. Compared to MC5R+/+ mice, MC5R−/− mice exhibited less aggression and more defense in the dark phase (Fig. 1c). Dark phase testing elevated social behavior ($P < 0.05$) in MC5R+/+ and MC5R−/− mice, but there were no effects of MC5R deficiency on social and nonsocial behaviors (data not shown).

*Experiment 2*

When paired with GDX opponents, MC5R−/− mice showed levels of aggression and defense that were similar to their wild-type littermates (Fig. 2, upper). MC5R+/+ and MC5R−/− individuals were assessed against GDX stimulus mice. Under these conditions, MC5R deficiency did not alter aggressive or defensive behaviors (Fig. 2, upper). MC5R deficiency also failed to alter social and nonsocial behaviors (data not shown). It should be noted that aggressive behavior of wild-type mice toward GDX mice was reduced, compared to MC5R−/− (Fig. 2, upper vs. Fig. 1, upper) and MC5R+/+ (Fig. 2, upper vs. Fig. 2, lower) opponents. Mice were also tested in homotypic (MC5R+/+ vs. MC5R+/+ and MC5R−/− vs. MC5R−/−) pairs. Under these conditions, MC5R deficiency did not alter aggressive or defensive behaviors in individuals that emerged as dominant (Fig. 2, lower). MC5R deficiency also failed to alter aggressive and defensive behaviors in individuals that emerged as subordinate (data not shown).

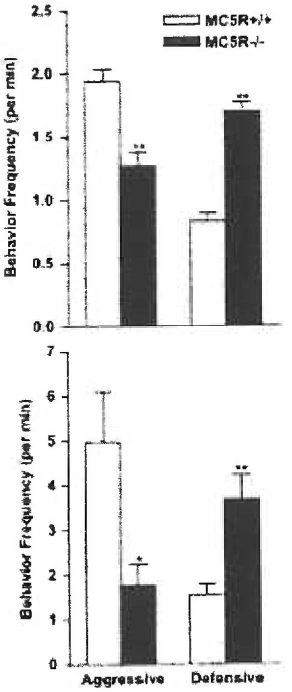

Fig. 1. Behaviors toward heterotypic opponents. In 10-min social interaction tests MC5R+/+ vs. MC5R−/− pairs ($n = 8$) were assessed in the light phase. Upper panel: In the light phase, aggressive behavior was reduced and defensive behavior was elevated in MC5R−/− mice. Lower panel: In the dark phase, aggressive behavior was reduced and defensive behavior was elevated in MC5R−/− mice. Means (± SEM) are shown (*$P < 0.05$, **$P < 0.01$).

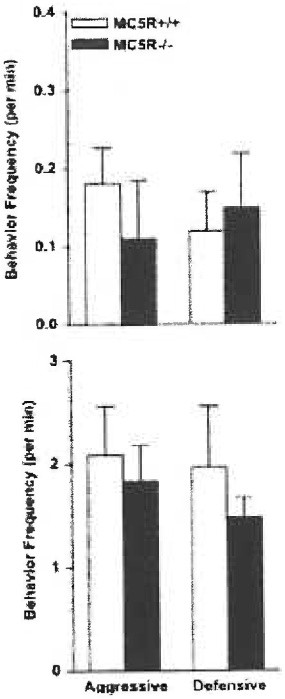

Fig. 2. Behaviors toward stimulus and homotypic opponents. In 10-min social interaction tests MC5R+/+ and MC5R−/− test mice ($n = 6$) were paired with GDX stimulus mice in the light phase. Upper panel: Aggressive and defensive behaviors were similar in MC5R+/+ and MC5R−/− mice. Lower panel: In 10-min social interaction tests MC5R+/+ vs. MC5R+/+ mice ($n = 8$) and MC5R−/− vs. MC5R−/− mice ($n = 14$) were assessed in the light phase. Aggressive and defensive behaviors were similar in MC5R+/+ and MC5R−/− mice that emerged from homotypic pairings as socially dominant. Means (± SEM) are shown.

### *Experiment 3*

When urine from NDP-MSH-injected MC5R−/− and MC5R−/− mice was swabbed onto GDX mice that were subsequently paired with intact test mice, MC5R−/− urine promoted more aggressive behavior than did urine from MC5R+/+ mice, and the effect was increased by NDP-MSH treatment (Fig. 3, upper). Urine from both groups of NDP-MSH-treated mice reduced defense in the test mice (Fig. 3, lower), but there were no statistically significant effects of genotype on defensive (Fig. 3, lower), or on social and nonsocial behaviors (data not shown). Urine from MC5R−/− mice reduced the attack latency by 1.7 min ($P < 0.05$) in vehicle-treated mice (data not shown). Attack latency was reduced in both groups by NDP-MSH treatment ($P < 0.05$), but there was no effect of genotype (data not shown).

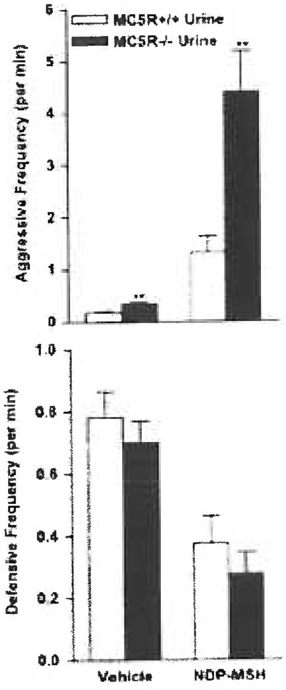

Fig. 3. Behaviors toward urine-swabbed stimulus mice. In 5-min social interaction tests, MC5R+/+ test mice ($n = 6$) were tested in the light phase against stimulus mice subjected to gonadectomy (GDX). Stimulus mice were swabbed with urine from MC5R+/+ and MC5R−/− mice that were injected every 48 h for 2 weeks with NDP-MSH (500 ng ip) or vehicle (0.1 ml ip). Upper panel: Aggressive behavior was elevated in response to urine from MC5R−/− mice and urine from NDP-MSH-injected MC5R+/+ and MC5R−/− mice. Lower panel: Defensive behavior was unaltered in response to urine from MC5R−/− mice, and was reduced by urine from NDP-MSH-injected MC5R+/+ and MC5R−/− mice. Means (± SEM) are shown ($^{**}P < 0.01$).

## Discussion

In the present study, we have demonstrated that in heterotypic pairs MC5R deficiency reduces aggression and elevates defense in male mice. The differences are not due to a broad behavioral defect, because social and nonsocial behaviors are unaltered in the mutant mice. This finding is supported by the lack of obvious differences in the physical characteristics (i.e., body weight, size, lean mass, pigmentation, etc.) between MC5R+/+ and MC5R−/− mice (Chen et al., 1997). Abundant MC5R expression in pheromone-producing exocrine glands (Chen et al., 1997) suggests a role in pheromonal signaling.

Melanocortins, including alpha-MSH, are secreted from the neurointermediate lobe of the pituitary in a diurnal rhythm (Millington et al., 1986; Tanaka et al., 1978; Tilders and Smelik, 1975; Wilson and Morgan, 1979). Elevated secretion occurs during the active portion of the 24-h light–dark cycle (i.e., the dark phase for rodents). Aggressive behavior is elevated in MC5R+/+ mice, but MC5R−/− mice, during the dark phase. We find no evidence that the behavioral difference is due to a shift in circadian rhythmicity, because MC5R−/− and MC5R+/+ mice exhibit nocturnal increases in defensive and social behaviors. Moreover, assessment of nocturnal behavior under infrared illumination confirms that differences in visual signaling or physical appearance do not play a major role in the behavioral defects. Because MC5R is expressed in brain and peripheral tissues, behavioral effects of MC5R deficiency might be central and peripheral. The present findings do not permit us to rule out either possibility.

Heterotypic pairing permits rapid assessment of behavioral differences and determination that the differences are selective. The results do not point to the specific nature of the behavioral defect caused by MC5R deficiency. However, pairing against stimulus and homotypic opponents demonstrates a context dependency of the behavioral defect, and suggests that normal dominant–subordinate relationships may be established among groups of mutant mice. In the latter two tests, MC5R deficiency does not significantly alter any of the behaviors measured. Taken together, the results suggest that behavior of either the wild-type or mutant mice is altered in the heterotypic pairing. Given the importance of olfaction in the social interactions of mice and the abundant expression of the MC5R in pheromone-producing glands (Chen et al., 1997; van der Kraan et al., 1998), it is plausible that MC5R deficiency alters an aspect of pheromonal signaling.

The experiment involving urine taken from NDP-MSH- and vehicle-injected MC5R+/+ and MC5R−/− mice suggests that melanocortins may stimulate an aggression-eliciting pheromone, which is greater in the absence of the

MC5R. The effect is consistent with studies demonstrating that alpha-MSH injection acutely releases such a signal in male mice and rats (Nowell and Wouters, 1975, Nowell et al., 1980), and it reveals that (a) the MC5R is not involved in the stimulation of an aggression-eliciting pheromone; and (b) MC5R activation attenuates this stimulatory effect of alpha-MSH, perhaps by stimulating an aggression-suppressing pheromone. The present study further demonstrates that basal and melanocortin-induced control of the pheromonal signal is altered by MC5R deficiency.

A previous study has shown that urine from MC5R−/− mice stimulates aggression toward stimulus mice by reducing attack latencies (Caldwell and Lepri, 2002). The authors of that study interpret their findings to suggest that the mutant mice have reduced levels of aggression-suppressing pheromones, but the findings do not exclude the possibility of elevated levels of aggression-eliciting pheromones. If, however, elevation of an aggression-eliciting signal were the principal defect, homotypic pairs of mutant mice would be expected to exhibit very high levels of aggression. Because that is not the case, reduction of an aggression-suppressing signal is plausible.

Melanocortins elevate aggression in opponents, as shown in the present study, and central injection of melanocortins elevates aggression in test animals (Gonzalez et al., 1996). Taken together, these findings suggest that the melanocortin system plays a role in coordinating central and peripheral signals for aggression. In the present study, gonadectomy reduced attacks from opponents. Therefore, gonadal steroids also might stimulate aggression in opponents, independently of MC5R activation. Both sets of hormones stimulate aggression when administered to the ventromedial hypothalamus and medial preoptic area (Gonzalez et al., 1996; Nyby et al., 1992). In addition, melanocortins and testosterone act synergistically to increase activity of pheromone-producing glands (Cooper et al., 1975; Ebling et al., 1975). Behaviors of the MC5R-deficient mice in homotypic pairs may indicate a balance between the reduction of an aggression-suppressing pheromonal signal and the elevation of an aggression-stimulating signal in the brain. In future studies, it would be interesting to determine whether activation of the MC5R and sex steroid receptors coordinates central and peripheral signals for aggression.

Male mice use aggression to establish and maintain social hierarchies. Even modest reductions in normal aggressive behavior could have a negative impact on survival. Therefore, behavioral defects of MC5R−/− mice observed in the laboratory suggest that the MC5R is critical for survival of male mice in their natural habitat. Furthermore, we have provided evidence for a peripheral melanocortin pathway being involved: Alpha-MSH release exerts neuroendocrine effects to elicit aggression from opponents. It is interesting to speculate that the MC5R may control complementary aspects of melanocortin-regulated aggression, and, thus, plays a role in the coordinate regulation of aggression. Additional components of the pathway may be identified by future studies, but our findings in the present study suggest that the MC5R regulates intermale aggression in mice.

## Acknowledgments

We thank Jeanie Zhou for technical assistance. National Institutes of Health Grants to CM (T32 DK07680) and RDC (DK51730) supported this work.

## References

Butler, A.A., Kesterson, R.A., Khong, K., Cullen, M.J., Pelleymounter, M.A., Dekoning, J., Baetscher, M., Cone, R.D., 2000. A unique metabolic syndrome causes obesity in the melanocortin-3 receptor-deficient mouse. Endocrinology 141 (9), 3518–3521.

Caldwell, H.K., Lepri, J.J., 2002. Disruption of the fifth melanocortin receptor alters the urinary excretion of aggression-modifying pheromones in male house mice. Chem. Senses 27 (1), 91–94.

Cammas, F.M., Kapas, S., Barker, S., Clark, A.J., 1995. Cloning, characterization and expression of a functional mouse ACTH receptor. Biochem. Biophys. Res. Commun. 212 (3), 912–918.

Chen, W., Kelly, M.A., Opitz-Araya, X., Thomas, R.E., Low, M.J., Cone, R.D., 1997. Exocrine gland dysfunction in MC5-R-deficient mice: evidence for coordinated regulation of exocrine gland function by melanocortin peptides. Cell 91 (6), 789–798.

Chen, A.S., Marsh, D.J., Trumbauer, M.E., Frazier, E.G., Guan, X.M., Yu, H., Rosenblum, C.I., Vongs, A., Feng, Y., Cao, L., Metzger, J.M., Strack, A.M., Camacho, R.E., Mellin, T.N., Nunes, C.N., Min, W., Fisher, J., Gopal-Truter, S., MacIntyre, D.E., Chen, H.Y., Van der Ploeg, L.H., 2000. Inactivation of the mouse melanocortin-3 receptor results in increased fat mass and reduced lean body mass. Nat. Genet. 26 (1), 97–102.

Chhajlani, V., Wikberg, J.E., 1992. Molecular cloning and expression of the human melanocyte stimulating hormone receptor cDNA. FEBS Lett. 309 (3), 417–420.

Cone, R.D., Lu, D., Koppula, S., Vage, D.I., Klungland, H., Boston, B., Chen, W., Orth, D.N., Pouton, C., Kesterson, R.A., 1996. The melanocortin receptors: agonists, antagonists, and the hormonal control of pigmentation. Recent Prog. Horm. Res. 51 (318), 287–317.

Cooper, M.F., Bowden, P.E., Thody, A.J., Shuster, S., 1975. Proceedings: synergistic effects of testosterone and alpha-melanocyte-stimulating hormone on lipogenesis in rat preputial gland. J. Endocrinol. 64 (3), 61P.

Delbende, C., Jegou, S., Tranchand-Bunel, D., Leroux, P., Tonon, M.C., Mocaer, E., Pelletier, G., Vaudry, H., 1985. Role of alpha-MSH and related peptides in the central nervous system. Rev. Neurol. (Paris) 141 (6–7), 429–439.

Desarnaud, F., Labbe, O., Eggerickx, D., Vassart, G., Parmentier, M., 1994. Molecular cloning, functional expression and pharmacological characterization of a mouse melanocortin receptor gene. Biochem. J. 299 (Pt 2), 367–373.

Ebling, F.J., Ebling, E., Randall, V., Skinner, J., 1975. The synergistic action of alpha-melanocyte-stimulating hormone and testosterone of the sebaceous, prostate, preputial, Harderian and lachrymal glands, seminal vesicles and brown adipose tissue in the hypophysectomized-castrated rat. J. Endocrinol. 66 (3), 407–412.

Fan, W., Boston, B.A., Kesterson, R.A., Hruby, V.J., Cone, R.D., 1997. Role of melanocortinergic neurons in feeding and the agouti obesity syndrome. Nature 385 (6612), 165–168.

Gantz, I., Konda, Y., Tashiro, T., Shimoto, Y., Miwa, H., Munzert, G., Watson, S.J., DelValle, J., Yamada, T., 1993a. Molecular cloning of a novel melanocortin receptor. J. Biol. Chem. 268 (11), 8246–8250.

Gantz, I., Miwa, H., Konda, Y., Shimoto, Y., Tashiro, T., Watson, S.J., DelValle, J., Yamada, T., 1993b. Molecular cloning, expression, and gene localization of a fourth melanocortin receptor. J. Biol. Chem. 268 (20), 15174–15179.

Gonzalez, M.I., Vaziri, S., Wilson, C.A., 1996. Behavioral effects of alpha-MSH and MCH after central administration in the female rat. Peptides 17 (1), 171–177.

Hadley, M.E., Heward, C.B., Hruby, V.J., Sawyer, T.K., Yang, Y.C., 1981. Biological actions of melanocyte-stimulating hormone. Ciba Found. Symp. 81, 244–262.

Hayden-Hixson, D.M., Ferris, C.F., 1991. Steroid-specific regulation of agonistic responding in the anterior hypothalamus of male hamsters. Physiol. Behav. 50 (4), 793–799.

Heisler, L.K., Cowley, M.A., Tecott, L.H., Fan, W., Low, M.J., Smart, J.L., Rubinstein, M., Tatro, J.B., Marcus, J.N., Holstege, H., Lee, C.E., Cone, R.D., Elmquist, J.K., 2002. Activation of central melanocortin pathways by fenfluramine. Science 297 (5581), 609–611.

Kraicer, J., Gajewski, T.C., Moor, B.C., 1985. Release of pro-opiomelanocortin-derived peptides from the pars intermedia and pars distalis of the rat pituitary: effect of corticotrophin-releasing factor and somatostatin. Neuroendocrinology 41 (5), 363–373.

Labbe, O., Desarnaud, F., Eggerickx, D., Vassart, G., Parmentier, M., 1994. Molecular cloning of a mouse melanocortin 5 receptor gene widely expressed in peripheral tissues. Biochemistry 33 (15), 4543–4549.

Leshner, A.I., Walker, W.A., Johnson, A.E., Kelling, J.S., Kreisler, S.J., Svare, B.B., 1973. Pituitary–adrenocortical activity and intermale aggressiveness in isolated mice. Physiol. Behav. 11 (5), 705–711.

Levine, N., Lemus-Wilson, A., Wood, S.H., Abdel Malek, Z.A., Al-Obeidi, F., Hruby, V.J., Hadley, M.E., 1987. Stimulation of follicular melanogenesis in the mouse by topical and injected melanotropins. J. Invest. Dermatol. 89 (3), 269–273.

Mains, R.E., Eipper, B.A., 1979. Synthesis and secretion of corticotropins, melanotropins, and endorphins by rat intermediate pituitary cells. J. Biol. Chem. 254 (16), 7885–7894.

Millington, W.R., Blum, M., Knight, R., Mueller, G.P., Roberts, J.L., O'Donohue, T.L., 1986. A diurnal rhythm in proopiomelanocortin messenger ribonucleic acid that varies concomitantly with the content and secretion of beta-endorphin in the intermediate lobe of the rat pituitary. Endocrinology 118 (2), 829–834.

Murray, J.F., Adan, R.A., Walker, R., Baker, B.I., Thody, A.J., Nijenhuis, W.A., Yukitake, J., Wilson, C.A., 2000. Melanin-concentrating hormone, melanocortin receptors and regulation of luteinizing hormone release. J. Neuroendocrinol. 12 (3), 217–223.

Nowell, N.W., Wouters, A., 1975. Proceedings: release of aggression-promoting pheromone by male mice treated with alpha-melanocyte-stimulating hormone. J. Endocrinol. 65 (3), 36P–37P.

Nowell, N.W., Thody, A.J., Woodley, R., 1980. The source of an aggression-promoting olfactory cue, released by alpha-melanocyte stimulating hormone, in the male mouse. Peptides 1 (1), 69–72.

Nyby, J., Matochik, J.A., Barfield, R.J., 1992. Intracranial androgenic and estrogenic stimulation of male-typical behaviors in house mice (*Mus domesticus*). Horm. Behav. 26 (1), 24–45.

O'Donohue, T.L., Dorsa, D.M., 1982. The opiomelanotropinergic neuronal and endocrine systems. Peptides 3 (3), 353–395.

O'Donohue, T.L., Jacobowitz, D.M., 1980. Studies of alpha-MSH-containing nerves in the brain. Prog. Biochem. Pharmacol. 16, 69–83.

Ozegovic, B., Milkovic, S., 1972. Effects of adrenocorticotropic hormone, growth hormone, prolactin, adrenalectomy and corticoids upon the weight, protein and nucleic acid content of the female rat preputial glands. Endocrinology 90 (4), 903–908.

Penhoat, A., Naville, D., El Mourabit, H., Buronfosse, A., Durand, P., Begeot, M., 2000. Functional expression of the human ACTH receptor gene. Endocr. Res. 26 (4), 549–557.

Roselli-Rehfuss, L., Mountjoy, K.G., Robbins, L.S., Mortrud, M.T., Low, M.J., Tatro, J.B., Entwistle, M.L., Simerly, R.B., Cone, R.D., 1993. Identification of a receptor for gamma melanotropin and other proopiomelanocortin peptides in the hypothalamus and limbic system. Proc. Natl. Acad. Sci. U.S.A. 90 (19), 8856–8860.

Tanaka, K., Nicholson, W.E., Orth, D.N., 1978. Diurnal rhythm and disappearance half-time of endogenous plasma immunoreactive beta-MSH (LPH) and ACTH in man. J. Clin. Endocrinol. Metab. 46 (6), 883–890.

Thody, A.J., Shuster, S., 1975. Control of sebaceous gland function in the rat by alpha-melanocyte-stimulating hormone. J. Endocrinol. 64 (3), 503–510.

Tilders, F.J., Smelik, P.G., 1975. A diurnal rhythm in melanocyte-stimulating hormone content of the rat pituitary gland and its independence from the pineal gland. Neuroendocrinology 17 (4), 296–308.

van der Kraan, M., Adan, R.A., Entwistle, M.L., Gispen, W.H., Burbach, J.P., Tatro, J.B., 1998. Expression of melanocortin-5 receptor in secretory epithelia supports a functional role in exocrine and endocrine glands. Endocrinology 139 (5), 2348–2355.

Watson, S.J., Akil, H., 1980. Alpha-MSH in rat brain: occurrence within and outside of beta-endorphin neurons. Brain Res. 182 (1), 217–223.

Wilson, J.F., Morgan, M.A., 1979. Cyclical changes in concentrations of alpha-melanotrophin in the plasma of male and female rats. J. Endocrinol. 82 (3), 361–366.

## A3.2 Melanocortin 5 receptor deficiency reduces a pheromonal signal for aggression in male mice.

Chem. Senses 29: 111–115, 2004

DOI: 10.1093/chemse/bjh011

# Melanocortin-5 Receptor Deficiency Reduces a Pheromonal Signal for Aggression in Male Mice

**Caurnel Morgan**[1], **Ruth E. Thomas**[1], **Weidong Ma**[2], **Milos V. Novotny**[2] **and Roger D. Cone**[1]

[1]Vollum Institute for Advanced Biomedical Research, Oregon Health and Science University, Portland, OR 97239, USA and [2]Department of Chemistry and Institute for Pheromone Research, Indiana University, Bloomington, IN 47405, USA

*Correspondence to be sent to: Caurnel Morgan, Bourne Behavioral Research Laboratory, Weill Medical College of Cornell University (Westchester Division), 21 Bloomingdale Road, White Plains, NY 10605, USA. e-mail: cam2025@med.cornell.edu*

### Abstract

Mice lacking the melanocortin-5 receptor (MC5R) exhibit decreased sensitivity to the stimulatory effects of systemic melanocortin injections on aggressive behavior. Because the pheromone-producing preputial gland expresses the MC5R, we tested the hypothesis that decreases in preputial pheromones underlie the behavioral deficit. Here we show that MC5R deficiency decreases preputial and urine levels of the sex pheromones, alpha- and beta-farnesene, relative to wild-type mice. We also demonstrate that farnesenes potently stimulate aggression in mice. Moreover, farnesene-stimulated aggression is reduced in MC5R-deficient mice, relative to wild-type mice. Our results suggest that activation of the MC5R promotes aggression by increasing farnesene signaling.

**Key words:** aggression, farnesene, gas chromatography–mass spectrometry, gene knockout, melanocortin-5 receptor, pheromones

### Introduction

In male mice, social dominance is acquired during aggressive encounters that are influenced by pheromonal signals. The male rodent preputial gland releases aggression-promoting pheromones to the urine (Jones and Nowell, 1973; Novotny *et al.*, 1985; Ingersoll *et al.*, 1986). Additionally, preputial hypertrophy in dominant males (Hucklebridge *et al.*, 1972) and the correlation between induced preputial atrophy and subordinate behavior (Brain *et al.*, 1991) suggest that preputial pheromones may promote the acquisition and maintenance of social status. However, these relationships are poorly understood.

Preputial activity depends on the circulating melanocortin, alpha-melanocyte-stimulating hormone (α-MSH) (Cooper *et al.*, 1975; Ebling *et al.*, 1975), and chronic melanocortin administration stimulates preputial lipogenesis, hypertrophy, hyperplasia, and pheromone secretion in rodents (Ozegovic and Milkovic, 1972; Thody and Shuster, 1975; C. Morgan and R.D. Cone, submitted for publication). In this regard, melanocortins act synergistically with androgens (Cooper *et al.*, 1975; Ebling *et al.*, 1975; Thody and Shuster, 1975). Therefore, endogenous melanocortins may stimulate biosynthesis of aggression-promoting pheromones in the preputial gland.

Of the five known melanocortin receptors (MC1R–MC5R) (Cone *et al.*, 1996), the MC5R is most abundantly expressed in the preputial gland (Chen *et al.*, 1997; van der Kraan *et al.*, 1998). Melanocortin injection releases into the urine of male mice an unidentified chemical signal that stimulates attacking behavior from test mice when swabbed onto stimulus mice (Nowell and Wouters, 1975; Nowell *et al.*, 1980), and we and others have shown that MC5R deficiency increases the release of this signal (Caldwell *et al.*, 2001; Caldwell and Lepri, 2002; Morgan *et al.*, 2004). We have also shown that MC5R knockout (KO) mice exhibit reduced aggression and elevated defense toward wild-type (WT) opponents (Morgan *et al.*, 2004), and that these mutant mice are less sensitive to melanocortin stimulation of aggression and preputial growth (C. Morgan and R.D. Cone, submitted for publication). In the present study, we tested the hypothesis that decreased preputial pheromones contribute to the decreased aggressive responses of MC5R KO mice.

Chemical Senses vol. 29 no. 2 © Oxford University Press 2004; all rights reserved.

## Materials and methods

### Animals and housing

Male wild-type (WT) and MC5R knockout (KO) mice on a C57BL/J6 genetic background (Chen *et al.*, 1997) were maintained in group-housed conditions (3–5/cage). Room temperature was maintained at 22 ± 2°C on a standard light-dark cycle (12 h light: 12 h darkness; lights on from 06.00 to 18.00 h) with food and water provided *ad libitum*. At 8 weeks of age, mice were individually housed for at least 4 weeks prior to behavioral testing. Mice were housed in filter-top cages within a Maxi-Miser System (Thoren Caging Systems; Hazelton, PA) that provides positive ventilation and air exhaust from each cage. During handling, individual cages of mice were transferred to a fume hood supplied with negative ventilation. Thus, the exchange of olfactory signals between mice was minimized. All animal experiments were approved by the Institutional Animal Care and Use Committee.

### Surgical procedures

#### *Preputialectomy (PPX)*

Mice were anesthetized with an intraperitoneal injection of 100 mg/kg ketamine and 10 mg/kg xylazine. A transverse incision was made through the skin of the lower abdominal region. Subcutaneous fat and connective tissue were removed, and the preputial gland was excised at the base and placed on dry ice until weighed.

#### *Gonadectomy (GDX)*

The supplier (Taconic Farms; Germantown, NY) performed the gonadectomies. Surgically altered mice were individually housed (following PPX) or socially housed (following GDX), and permitted at least three weeks for post surgical recovery, before being used in behavioral tests.

### Behavior

Test mice were paired with GDX stimulus mice in neutral cages with fresh bedding during the light phase. Prior to testing, the tail the stimulus mouse was marked with a black marker to distinguish it. Encounters lasting 5 min were videotaped and behaviors were scored from the videotapes by trained observers who were blind to the treatments. Aggressive behavior consisted of offensive (biting and striking) and dominant (dominant posturing, chasing, and tail rattling) behaviors. Each mouse was scored for each occurrence of these behaviors.

### Gas chromatography–mass spectrometry

Analysis by gas chromatography coupled to mass spectrometry (GC–MS) of volatile compounds was performed as previously described (Novotny *et al.*, 1974). Preputial extracts or pooled 10 ml aliquots of urine from wild-type and MC5R-deficient mice were homogenized in 1 ml of distilled water, 200 mg of ammonium sulfate and 4 μl of internal standard (200 p.p.m. 7-tridecanone in methanol). Samples were extracted at 50°C with purified helium at 70 ml/min for 30 min. The upper phase was passed through a water-chilled condenser then a pre-column packed with 4 mg of Tenax GC adsorbent (Applied Science Laboratories' State College, PA). Compounds trapped on the pre-column were desorbed in the heated injection port (250°C) of a Finnegan MAT Magnum GC/MS Instrument (San Jose, CA) and trapped in a liquid nitrogen-cooled capillary column. The analytical column was a 30 mm × 0.25 mm (ID) DB-5 (J & W Scientific, Folsum, CA). Helium was used as the carrier at an inlet pressure of 12 PSI. The oven temperature was maintained at 30°C for 5 min, and elevated to 200°C at a rate of 2°C/min. Transfer line temperature was 290°C. Peak areas of compounds were normalized to peak area of the internal standard.

### Farnesene treatment

Mice were permitted to inhale a 250 or 500 p.p.m. solution of α- and β-farnesene or vehicle (distilled water) from a cotton swab for 1 min in their home cages. The test animals were maintained in their home cages for 60 min before behavioral testing.

### Statistical analyses

Data were analyzed with SigmaStat 2.0 statistical software (SPSS, Inc. Chicago, IL). Because behavioral data from farnesene-stimulated mice (Figure 2B) were not normally distributed or contained unequal variance, the Mann-Whitney rank sum test was used. All other data were analyzed using Student's *t*-test. GC–MS data were log-transformed before statistical analysis.

## Results

GC–MS analysis of preputial extracts revealed smaller peaks corresponding to the sesquiterpenes, α-farnesene and β-farnesene, as well as an unidentified sesquiterpene and ethyl nonanoate in the KO mice, relative to WT littermates (Figure 1A, upper panel). Statistical analysis of log-transformed data, by Student's *t*-test, confirmed that in WT mice the levels of α-farnesene, β-farnesene, uncharacterized sesquiterpene and ethyl nonanoate exceeded those of the KO mice by 39, 27, 207 and 185%, respectively (Figure 1B, upper panel).

GC–MS analysis of pooled urine samples revealed reduced peaks corresponding to farnesenes in the KO mice (Figure 1B, lower panel), relative to WT mice. Quantitative analysis of the urine data suggested that in WT mice the levels of α- and β-farnesene exceeded those of KO mice by as much as 62 and 92%, respectively (Figure 1B, lower panel). Sample pooling (10 ml from 8–10 mice per treatment group) prevented statistical analysis. Under our experimental conditions, the uncharacterized sesquiterpene and ethyl nonanoate were not detected.

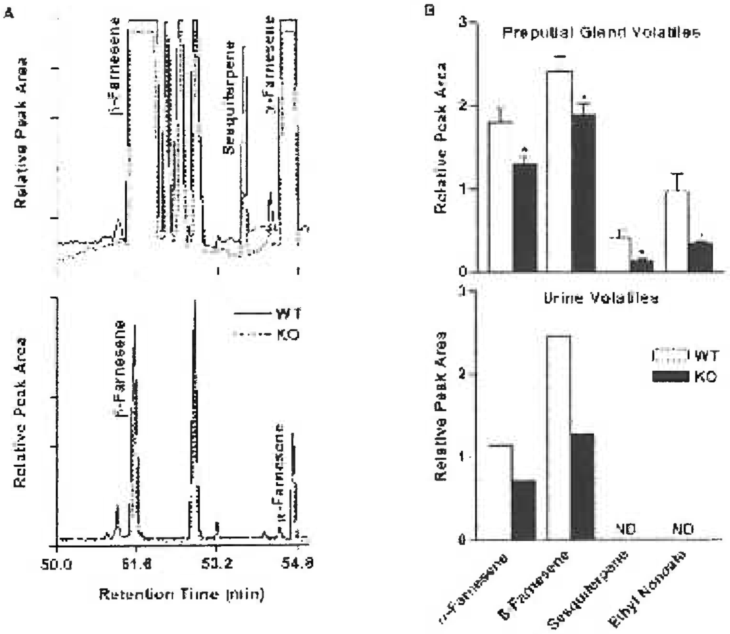

**Figure 1** Gas chromatography-mass spectrometry analysis of volatile compounds of preputial origin. (A) Upper panel: partial chromatogram of volatile compounds extracted from the preputial gland of a wild-type (WT) mouse and an MC5R-deficient (KO) mouse. Peaks corresponding to sex pheromones (α- and β-farnesene) and an uncharacterized, but structurally related compound (a sesquiterpene) are shown. Lower panel: partial chromatogram of volatile compounds extracted from the urine of a WT mouse and a KO mouse. Peaks corresponding to α- and β-farnesene are shown. Preputial and urine peaks for ethyl nonanoate are not shown. (B) Upper panel: preputial levels of α- and β-farnesene, the uncharacterized sesquiterpene, and ethyl nonanoate were reduced in KO mice ($n = 6$), relative to WT mice ($n = 10$). Lower panel: urine levels of α- and β-farnesene were reduced in a 10 ml sample pooled from eight KO mice, relative to a 10 ml sample pooled from 10 WT mice. The uncharacterized sesquiterpene and ethyl nonanoate were not detected (ND) under these experimental conditions. Means (± SEM) are shown. (*$P < 0.05$)

To determine the effects of farnesenes on aggression in WT and KO mice, we tested vehicle-treated and farnesene-treated mice against stimulus mice. We also tested preputialectomized (PPX) mice because we have shown previously that PPX and KO mice are insensitive to stimulatory effects of melanocortins on aggression (C. Morgan and R.D. Cone, submitted for publication). Sixty min following a one-minute inhalation of a low (250 p.p.m.) dose, farnesenes increased aggression 18-fold in WT mice (Figure 2A). Analysis by Student's $t$-test revealed that farnesene-stimulated aggression was reduced in the KO mice ($P < 0.05$) and PPX mice ($P < 0.01$), relative to the WT mice.

Analysis by Mann–Whitney rank sum test revealed that 60 min following exposure to a high (500 p.p.m.) dose of farnesenes, WT and KO mice displayed similar increases in aggression (Figure 2B). The aggression-stimulating effects of the high-dose farnesene treatment were transient, as the levels of aggressive behavior in WT and KO mice returned to basal 7 and 14 days, respectively, after single exposures (Figure 2B).

## Discussion

The results of the present study demonstrate that MC5R deficiency in mice reduces preputial gland and urine levels of α- and β-farnesene. In addition to their actions as sex pheromones (Ma *et al.*, 1999; Novotny *et al.*, 1999), we show that farnesenes are potent aggression-promoting pheromones. Although statistical analysis was not performed on the urine data because of pooling, we collectively analyzed by GC–MS samples from 8–10 mice per genotype. Because the reduction in urine farnesenes (and other compounds) was accompanied by decreases in preputial farnesenes, we conclude that decreased biosynthesis and secretion occur in MC5R KO mice. Therefore, the reduction of endogenous

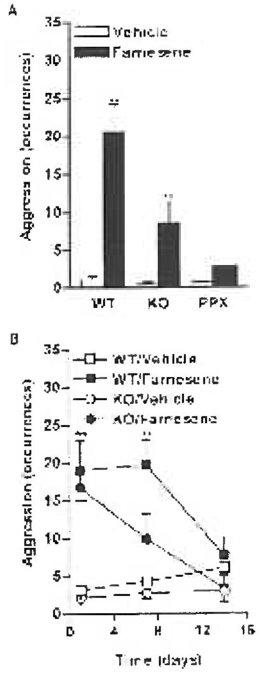

**Figure 2** Farnesene effects on aggressive behavior. **(A)** Brief inhalation of 250 p.p.m. α- and β-farnesene for 1 min in the home cage stimulated aggression in wild-type (WT), MC5R-deficient (KO), but not preputialectomized (PPX), mice during 5 min interactions with stimulus mice. **(B)** On day 1, brief inhalation of 500 p.p.m. farnesenes stimulated the aggressive behavior of WT and KO mice toward stimulus mice. WT mice, but not KO mice, exhibited farnesene-stimulated aggression on day 7. WT and KO mice exhibited basal levels of aggression on day 14. Means (± SEM) are shown ($n = 6$; $^{**}P < 0.01$).

farnesene levels may contribute to the reduction of aggressive behavior in the mutant mice toward WT opponents (Morgan *et al.*, 2004).

At a low dose, farnesenes stimulate less aggression in the KO mice, relative to WT mice. The diminished response might be partly due to reductions in the levels of preputial and urine farnesenes of the KO mice. Consistent with this idea, farnesene-stimulated aggression is markedly reduced in PPX mice. The preputial gland is the only exocrine gland known to secrete aggression-promoting pheromones downstream of the urinary bladder (Ingersoll *et al.*, 1986), and bladder urine does not contain farnesenes (Novotny *et al.*, 1990). Therefore, our finding that farnesenes stimulate aggression confirms that the preputial gland is the principal source of farnesenes in the urine. Thus, the responsiveness of WT, KO, and PPX mice to exogenous farnesenes correlated with their endogenous farnesene levels.

Inhalation of a high dose of farnesenes transiently increases aggression similarly in WT and KO mice. This finding demonstrates that, at the high dose, farnesenes are sufficient to overcome behavioral defects in the KO mice. Moreover, it suggests that a fifty-percent difference in exogenous farnesene concentration (500 versus 250 p.p.m.) is detectable and has important behavioral consequences for the KO mice. Presumably, prolonged decreases in self-exposure to farnesenes might negatively affect responsiveness to these same pheromones. Therefore, it is plausible that the observed deficits in urine farnesenes contribute to the decrease of farnesene-stimulated aggression in the mutant mice.

Even at the high dose, farnesene-stimulated aggression diminished more rapidly in the KO mice, relative to WT mice. The reduced farnesene release might have contributed to the more rapid return to basal levels of aggressive behavior in the KO mice. Additionally, because the MC5R is thought to be expressed in the olfactory bulbs and brain (Griffon *et al.*, 1994; Chen *et al.*, 1997), reduced farnesene responsiveness in the KO mice might have been due to decreased olfactory detection and central processing of the farnesene signal.

It is unlikely that the KO mice exhibit a universal defect in pheromone detection. Untreated MC5R KO mice in homotypic pairs do not exhibit decreased aggression (Morgan *et al.*, 2004), demonstrating that the behavioral responses of these mice are context-dependent. Furthermore, MC5R-deficiency does not reduce responsiveness to an aggression-promoting pheromonal signal that is released by melanocortin injection (C. Morgan and R.D. Cone, submitted for publication). Future studies should be able to determine the specific role of the MC5R in farnesene release and farnesene processing.

Taken together, the requirement for long-term preputial stimulation in melanocortin-stimulated aggression and preputial hypertrophy (C. Morgan and R.D. Cone, submitted for publication), and abundant preputial MC5R expression (Chen *et al.*, 1997; van der Kraan *et al.*, 1998), suggest that MC5R-deficiency may reduce biosynthesis and secretion of preputial pheromones that stimulate aggression. This view is supported by the present finding that MC5R-deficient mice exhibit deficits in farnesenes and other volatile compounds that originate in the preputial gland and are secreted into the urine.

Farnesenes are male pheromones that induce estrus in female mice (Ma *et al.*, 1999), and they are aversive olfactory signals that discourage territorial urine marking in male mice (Jemiolo *et al.*, 1992). Furthermore, the preputial gland is the only known source of farnesenes in the urine of male mice (Ingersoll *et al.*, 1986; Novotny *et al.*, 1990). Therefore, MC5R-deficiency and preputialectomy appear to produce a common physiological defect (i.e. reduced endogenous farnesene levels), as well as a common behavioral defect (i.e. reduced aggression).

We have shown previously that melanocortin-stimulated aggression, following repeated systemic injection, requires preputial hypertrophy, and that MC5R KO mice are deficient in the preputial and behavioral responses to melanocortin treatment (C. Morgan and R.D. Cone, submitted for publication). We have also shown previously that following surgical removal of the testes preputial atrophy accompanies decreased aggressive behavior in WT mice (C. Morgan and R.D. Cone, submitted for publication). Our present findings suggest that the behavioral insensitivity to melanocortin treatment might be due to deficits in a pheromonal pathway involving preputial farnesenes. Because melanocortin treatment, in the previous study did not involve the exchange of male pheromonal signals between opponents, it is plausible that the farnesene signal promotes aggression in a self-stimulatory manner.

## Acknowledgements

We thank Jeanie Zhou and Rebecca Morgan for technical assistance. This work was supported by National Institutes of Health Grants to C.M. (T32 DK07680), R.D.C. (DK51730) and M.V.N. (DC02418).

## References

**Brain, P.F., Simon, V.M.** and **Martinez, M.** (1991) *Ethopharmacological studies on the effects of antihormones on rodent agonistic behavior with especial emphasis on progesterone.* Neurosci. Biobehav. Rev., 15, 521–526.

**Caldwell, H.K.** and **Lepri, J.J.** (2002) *Disruption of the fifth melanocortin receptor alters the urinary excretion of aggression-modifying pheromones in male house mice.* Chem. Senses, 27, 91–94.

**Caldwell, H.K., Wang, L.** and **Lepri, J.J.** (2001) *Simplified tests of aggression chemosignals in male house mice suggest that a melanocortin-dependent product of the preputial gland reduces attacks.* In Marchlewska-Koj, A., Lepri, J.J. and Muller-Schwarze, D. (eds), Chemical Signals in Vertebrates. Kluwer/Academic Press, New York, vol. 27, pp. 445–452.

**Chen, W., Kelly, M.A., Opitz-Araya, X., Thomas, R.E., Low, M.J.** and **Cone, R.D.** (1997) *Exocrine gland dysfunction in MC5-R-deficient mice: evidence for coordinated regulation of exocrine gland function by melanocortin peptides.* Cell, 91, 789–798.

**Cone, R.D., Lu, D., Koppula, S., Vage, D.I., Klungland, H., Boston, B., Chen, W., Orth, D.N., Pouton, C.** and **Kesterson, R.A.** (1996) *The melanocortin receptors: agonists, antagonists, and the hormonal control of pigmentation.* Recent Prog. Horm. Res., 51, 287–317; discussion 318.

**Cooper, M.F., Bowden, P.E., Thody, A.J.** and **Shuster, S.** (1975) *Proceedings: synergistic effects of testosterone and alpha-melanocyte-stimulating hormone on lipogenesis in rat preputial gland.* J. Endocrinol., 64, 63P.

**Ebling, F.J., Ebling, E., Randall, V.** and **Skinner, J.** (1975) *The synergistic action of alpha-melanocyte-stimulating hormone and testosterone of the sebaceous, prostate, preputial, Harderian and lachrymal glands, seminal vesicles and brown adipose tissue in the hypophysectomized-castrated rat.* J. Endocrinol., 66, 407–412.

**Griffon, N., Mignon, V., Facchinetti, P., Diaz, J., Schwartz, J.C.** and **Sokoloff, P.** (1994) *Molecular cloning and characterization of the rat fifth melanocortin receptor.* Biochem. Biophys. Res. Commun., 200, 1007–1014.

**Hucklebridge, F.H., Nowell, N.W.** and **Wouters, A.** (1972) *A relationship between social experience and preputial gland function in the albino mouse.* J. Endocrinol., 55, 449–450.

**Ingersoll, D.W., Morley, K.T., Benvenga, M.** and **Hands, C.** (1986) *An accessory sex gland aggression-promoting chemosignal in male mice.* Behav. Neurosci., 100, 777–782.

**Jemiolo, B., Xie, T.M.** and **Novotny, M.** (1992) *Urine marking in male mice: responses to natural and synthetic chemosignals.* Physiol. Behav., 52, 521–526.

**Jones, R.B.** and **Nowell, N.W.** (1973) *Effects of preputial and coagulating gland secretions upon aggressive behaviour in male mice: a confirmation.* J. Endocrinol., and, 203–204.

**Ma, W., Miao, Z. and Novotny, M.V.** (1999) *Induction of estrus in grouped female mice (Mus domesticus) by synthetic analogues of preputial gland constituents.* Chem. Senses, 24, 289–293.

**Morgan, C., Thomas, R.E.** and **Cone, R.D.** (2004) *Melanocortin-5 receptor deficiency promotes defensive behavior in male mice.* Hormone Behav., 45, 58–63.

**Novotny, M., Harvey, S.** and **Jemiolo, B.** (1990) *Chemistry of male dominance in the house mouse, Mus domesticus.* Experientia, 46, 109–113.

**Novotny, M., Harvey, S., Jemiolo, B.** and **Alberts, J.** (1985) *Synthetic pheromones that promote inter-male aggression in mice.* Proc. Natl Acad. Sci. USA, 82, 2059–2061.

**Novotny, M., McConnell, M.L.** and **Lee, M.L.** (1974) *Some aspects of high-resolution gas chromatographic analysis of complex volatile samples.* J. Agric. Food Chem., 22, 765–770.

**Novotny, M.V., Ma, W., Wiesler, D.** and **Zidek, L.** (1999) *Positive identification of the puberty-accelerating pheromone of the house mouse: the volatile ligands associating with the major urinary protein.* Proc. R. Soc. Lond. B Biol. Sci., 266, 2017–2022.

**Nowell, N.W., Thody, A.J.** and **Woodley, R.** (1980) *The source of an aggression-promoting olfactory cue, released by alpha-melanocyte stimulating hormone, in the male mouse.* Peptides, 1, 69–72.

**Nowell, N.W.** and **Wouters, A.** (1975) *Proceedings: release of aggression-promoting pheromone by male mice treated with alpha-melanocyte-stimulating hormone.* J. Endocrinol., 65, 36P–37P.

**Ozegovic, B.** and **Milkovic, S.** (1972) *Effects of adrenocorticotropic hormone, growth hormone, prolactin, adrenalectomy and corticoids upon the weight, protein and nucleic acid content of the female rat preputial glands.* Endocrinology, 90, 903–908.

**Thody, A.J.** and **Shuster, S.** (1975) *Control of sebaceous gland function in the rat by alpha-melanocyte-stimulating hormone.* J. Endocrinol., 64, 503–510.

**van der Kraan, M., Adan, R.A., Entwistle, M.L., Gispen, W.H., Burbach, J.P.** and **Tatro, J.B.** (1998) *Expression of melanocortin-5 receptor in secretory epithelia supports a functional role in exocrine and endocrine glands.* Endocrinology, 139, 2348–2355.

*Accepted November 25, 2003*